NAS CR-134481
TRW ER-7648

C.3

GENERATION OF LONG TIME CREEP DATA ON REFRACTORY ALLOYS AT ELEVATED TEMPERATURES

FINAL REPORT

Prepared for

NATIONAL AERONAUTICS AND SPACE ADMINISTRATION
LEWIS RESEARCH CENTER
UNDER CONTRACT NAS 3-15554

TRW MATERIALS TECHNOLOGY LABORATORIES
CLEVELAND, OHIO

Request for copies of this report should be referred to

National Aeronautics and Space Administration
Office of Scientific and Technical Information
Attention: AFSS-A
Washington, D. C. 20546

FOREWORD

The work described herein was performed by TRW Inc. under the sponsorship of the National Aeronautics and Space Administration under Contract NAS-3-15554. This contract involved work similar to that conducted under Contracts NAS-3-13469, NAS-3-9439, and NAS-3-2545. The purpose of this study is to obtain design creep data on refractory metal alloys for use in advanced space power systems. A listing of all reports presented to date on this program is included in Appendix 1.

The program is administered for TRW Inc. by H. E. Collins, Program Manager; K. D. Sheffler is the Principal Investigator with R. R. Ebert supervising the experimental program. The NASA Technical Managers were Robert H. Titran and Paul E. Moorhead. The period of performance for this program was 3 June 1971 through 2 June 1972.

Prepared by: K. D. Sheffler
K. D. Sheffler
Principal Engineer

R. R. Ebert
Laboratory Supervisor

Reviewed by: H. E. Collins
H. E. Collins
Principal Engineer

Approved by: J. A. Alexander
J. A. Alexander
Manager
Materials Research Department

TABLE OF CONTENTS

TABLE OF CONTENTS (continued)

LIST OF TABLES

LIST OF ILLUSTRATIONS

LIST OF ILLUSTRATIONS (CONTINUED)

LIST OF ILLUSTRATIONS (CONTINUED)

SUMMARY

The purpose of this program was the development of design creep data on refractory alloys in ultrahigh vacuum. The study was divided into four topical areas involving investigations of the tantalum alloys T-111 and ASTAR 811C and pure CVD tungsten. The first and second parts of the study involved two separate investigations of the creep behavior of T-111 alloy. One of these involved an investigation of the influence of pre-exposure to vacuum or to liquid lithium in the temperature range of 1800 to 2400°F (1255 to 1589°K) on the subsequent 1% creep life. This study showed that pre-exposure to either environment in the 1800 to 1900°F (1255 to 1311°K) temperature range caused large decreases in the 1% creep life as compared to unexposed material. These decreases were more severe in the creep test temperature range of 1650 to 2000°F (1172 to 1366°K) than at higher test temperatures. As an extreme example of this effect, a specimen exposed to lithium for 1000 hours at 1800°F (1255°K) plus 4000 hours at 1900°F (1310°K) exhibited a 1% creep life of 2 hours at 1650°F (1172°K) and 50 ksi (344 MN/m^2) as compared to a life of 938 hours for an unexposed specimen tested at the same conditions. Exposure to vacuum or lithium at 2400°F (1589°K) also influenced the creep life of T-111, although the life variations were not nearly so large as those observed with the lower temperature exposures. An explanation was developed for the observed creep life variations which involved two separate effects of long time exposure on T-111 alloy. The first of these was grain growth, which occurred only at the highest exposure temperature (2400°F; 1589°K), and which tended to increase the creep life in the creep test temperature range above 2000°F (1366°K). The second effect was depletion of residual oxygen from solid solution, either by direct loss to the environment or by precipitation in the form of hafnium oxide. This effect was observed at all of the exposure temperatures studied. The depletion of oxygen from solid solution caused large creep life decreases at the creep test temperature of 1650°F (1172°K), where an oxygen related dynamic strain age strengthening mechanism is operative in T-111 alloy. Above this test temperature, life decreases caused by the oxygen depletion became progressively smaller. At a test temperature of 2400°F (1589°K) no significant creep life changes were observed as a result of the oxygen loss.

The second investigation of T-111 alloy involved characterization of the creep behavior under conditions of continuously increasing stress and decreasing temperature which simulated the conditions anticipated in radioisotope capsule service. Results of this study showed that such test conditions produced creep curves having a highly unusual shape. The most unusual characteristic of these curves was that creep strain did not increase continuously to rupture as in normal creep tests, but instead reached a maximum strain value past which creep ceased to be significant. Since none of the usual creep design parameters, such as rupture life or minimum creep rate, applied to this unusual creep curve shape, the variable temperature-variable stress (VTVS) curves were characterized for design purposes by the maximum strain achieved at a given set of service conditions, which was

designated as the "stall strain." Analytical methods involving both calculation of VTVS behavior from conventional (isostatic, isothermal) creep results and parametric extrapolation of experimental VTVS data were developed to predict long time VTVS creep behavior from short time results. The parametric extrapolation method showed good promise for this purpose, although additional experimental data will be required before actual design specifications can be established.

The third investigation was directed toward characterization of the vacuum creep behavior of ASTAR 811C alloy in two different conditions of heat treatment (1/2 hour at 3600°F; 2255°K and 1 hour at 3000°F; 1922°K) and concluded with an investigation to define a third heat treatment which maximized the advantages and minimized the disadvantages of the first two. Results of this study established tentative design data for ASTAR 811C in the two conditions of heat treatment. Metallographic examinations showed that the higher temperature annealing cycle produced relatively large grained carbide free microstructure (average grain size of 0.1μm) while the lower temperature produced a finer grained microstructure (average grain size of 0.01μm) containing numerous undissolved carbides. However, additional examinations showed that extensive reprecipitation occurred in the solutioned specimens during heating to the creep test temperature, so that the carbide structures associated with the two treatments were quite similar during creep testing. Examination of both pre- and post-test specimens indicated that the carbides were located primarily in the grain boundaries during testing, although numerous intragranular carbides were also observed. The creep test results showed that the higher annealing temperature provided significantly longer creep lives in the test temperature range above 2200°F (1478°K) but that the two annealing treatments produced roughly equivalent creep life results below that temperature range. Metallographic examination of creep tested specimens showed that grain growth occurred during testing at temperatures above 2800°F (1881°K) which will effectively limit the use of this alloy to lower temperatures except in applications where excessive grain growth would not degrade the usefulness of the material. Specimens tested above 2800°F (1811°K) were also shown to be carbide free, indicating that the near equilibrium carbide solvus temperature was below 2800°F (1811°K) for this alloy. The presence of undissolved carbides in the 1 hour at 3000°F (1922°K) annealed microstructure thus indicates that an equilibrium structure is not achieved with this annealing treatment. Analysis of the stress and temperature dependence of the minimum creep rate showed that the pretest annealing treatment had very little influence on the activation energy for creep of ASTAR 811C alloy. The observed activation energies varied with test temperature from a value approximately equal to the activation energy for self diffusion (100K cal/mole; 3420 J/mole) in the 1800-2000°F (1255 to 1366°K) temperature range to values on the order of 150K cal/mole (5130 J/mole) in the range of 2400-2600°F (1589-1700°K). Based on the above observations, a hypothesis was developed which suggested that the primary role of the carbide is strengthening the ASTAR 811C alloy was to act as a grain boundary pinning agent, rather than in a true dispersion hardening role. This hypothesis led to the conclusion that the increased creep life provided by the higher annealing temperature was probably the result of the difference in grain size rather than the difference in pretest carbide structure. Because of the fact that the 3600°F (2255°K) annealing treatment

was judged to be somewhat impractical for commercial applications, additional studies were conducted to determine if an alternate heat treatment cycle could be defined which retained the improved creep properties developed by the higher temperature heat treatment, but offered more commercial promise. The results of these studies showed that a heat treatment of 100 hours at 3000°F (1922°K), which is within the range of present commercial capabilities, produced creep lives as good as those obtained with the higher temperature anneal.

The fourth investigation performed on this program involved a small number of tests on CVD tungsten. Results of these tests showed that possible differences existed between the creep life of this material obtained from two different sources. However, sufficient data was not generated on this program to determine if these differences were significant.

INTRODUCTION

The purpose of this program was to study the creep behavior of several refractory metal alloys which are candidates for application in space electric power system design at the NASA Lewis Research Center. Because of the sensitivity of refractory metals to interstitial contamination, the anticipated service environment was simulated by testing in an ultrahigh vacuum at pressures of less than 1×10^{-8} torr.

The specific alloys studies in this program were T-111 (Ta-8%W-2%Hf), ASTAR 811C (Ta-8%W-1%Hf-1%Re-0.025%C) and pure CVD tungsten. The overall program involved four separate investigations into various aspects of the vacuum creep behavior of the three alloys. The first and second parts of the program involved two separate investigations of the creep behavior of T-111 alloy. One of these involved an evaluation of the effects of elevated temperature exposure to liquid lithium on the 1% creep life of T-111. This was a cooperative program between TRW, NASA and the NSP Division of the General Electric Co., Cincinnatti, Ohio. Overall program direction and specimen procurement were performed at NASA. The exposures were made at G.E. while the creep testing and data interpretation were performed at TRW. This investigation was prompted by previous studies at TRW which had shown that long time elevated temperature exposure to ultrahigh vacuum significantly reduced the residual oxygen content of T-111, which in turn caused an unstable creep rate transition to occur during vacuum creep testing. This instability was observed in the 1200 to 2000°F (922 to 1366°K) temperature range where an oxygen-related dynamic strain aging phenomenon occurred. This dynamic aging behavior and its influence on creep of T-111 were well characterized in a previous paper (1). The occurrence of this deoxidation related creep instability created some concern regarding the proposed use of T-111 for the containment of liquid lithium, which is known to be a powerful deoxidant for tantalum alloys, and thus led to the present study.

The other investigation of T-111 creep behavior involved the problems associated with the use of T-111 alloy for structural containment in radioisotope capsule design. These problems result from the fact that a number of the proposed isotope fuels generate helium as a decay product, which causes the capsule liner to operate at elevated temperatures under conditions of simultaneously increasing stress and decreasing temperature. It was thus necessary to characterize the creep behavior of T-111 under conditions which simulated those anticipated in capsule service*. The characterization of

- - - - - - - - - - - - - - -

* While it is possible to design a vented capsule, it is still necessary to anticipate the unvented configuration as a safety precaution in case the vent should become plugged.

T-111 for capsule design was complicated by the safety requirement that the integrity of the capsule should be maintained for at least 10 half-lives in the event of accidental system re-entry and impact at a random uncontrolled location (2,3). The most extreme case of this general requirement occurs for the PU^{238} fuel, which has half life of 87.5 years. Thus, while the anticipated service life of a capsule fueled power system may be no more than five or ten years, the problem of predicting and/or experimentally characterizing the liner creep resistance was complicated by the need to develop techniques for extrapolating the observed creep behavior to extremely long times. A twofold approach involving both analytical and experimental methods was used to study this problem. The purpose of the analytical portion of the program was to develop mathematical procedures to predict long time variable temperature - variable stress (VTVS) creep behavior from conventional (isostatic, isothermal) creep data. The purpose of the experimental part of the program was to develop experimental techniques for creep testing with stress and temperature variations which simulated those anticipated in capsule service and to compare the results of such tests with the analytical predictions.

The third study which was conducted as a part of this program involved an investigation of the influence of heat treatment on the creep behavior of ASTAR 811C alloy. ASTAR 811C is a Westinghouse developed alloy having a unique balance of creep strength, low temperature ductility, and weldability which is superior to any other tantalum alloy presently available on a commercial basis. This unique balance of properties was achieved through a combination of solid solution strengthening provided by tungsten and rhenium with dispersed phase strengthening provided by the addition of carbon (4)*. Preliminary studies at the Westinghouse Astronuclear Laboratory showed that the creep strength of ASTAR 811C could be enhanced by annealing in the 3600°F (2255°K) temperature range, rather than at the 3000°F (1922°K) temperature more commonly used for the present generation of tantalum alloys. Unfortunately, the 3600°F (2255°K) annealing temperature is not highly practical because it exceeds the capability of the most commercially available vacuum annealing facilities. It also suffers the disadvantage that time at temperature and cooling rate are difficult to control for thick section sizes. The investigation described in this paper was therefore undertaken to characterize the microstructure and creep behavior of ASTAR 811C at both annealing temperatures and to determine if a third annealing treatment could be defined which would be commercially feasible and still provide the improved creep strength achieved at 3600°F (2255°K).

The fourth part of this program involved a small number of tests with CVD tungsten which were directed toward measurement of the 1% creep life of this material as obtained from two different sources.

- - - - - - - - - - - - - - -

* Hafnium is added to ASTAR 811C primarily for liquid metal corrosion resistance.

EXPERIMENTAL DETAILS

Materials

T-111 test material for the lithium exposure program was obtained from the Wah Chang Co. in the form of 0.020 in. (0.51mm) cold rolled sheel (Wah Chang Heat 650050) having the composition shown in Table 1. Standard one inch (2.54cm) gage length sheet type tension test specimens were machined from this material. All of these specimens were given a duplex heat treatment consisting of 1 hour at 3000°F (1922°K) plus 1 hour at 2400°F (1589°K) using a diffusion pumped vacuum system operating at pressures on the order of 10^{-7} torr. The 3000°F (1922°K) anneal provided a completely recrystallized, equiaxed, single phase microstructure which is shown in Figure 1. The additional 2400°F (1589°K) heat treatment was used to simulate the post weld stress relief treatment which would be applied to a fabricated hardware item. Previous testing had shown that this additional heat treatment has essentially no effect on the creep properties of T-111 alloy (5).

Exposure of these specimens to lithium or vacuum was accomplished by incorporating a portion of the specimens in lithium capsules and then attaching the remainder of the specimens to the exterior of the capsules. The capsules were than exposed at various temperatures for various times in ion pumped ultrahigh vacuum chambers at pressures below 1×10^{-9} torr according to the schedule in Table II. Detailed exposure procedures may be found in Reference 6.

Test material for the T-111 VTVStests was also obtained from Wah Chang in the form of 0.030 inch (0.76mm) cold rolled sheet (Heat 650028). Chemical analysis of the as-received material is shown in Table 1. Standard pin loaded sheet type tension test specimens having a 2 1/4 inch long x 1/2 inch wide (5.72 x 1.27cm) gage section were machined from the as-received sheet and were vacuum annealed 1 hour at 3000°F (1922°K) at a pressure of less than 1×10^{-6} torr prior to testing. This annealing treatment provided a completely recrystallized equiaxed microstructure which is shown in Figure 2.

The ASTAR 811C test material for this investigation was obtained from the Wah Chang Co. (Heat 650056) in the form of 0.030 inch (0.76mm) cold rolled sheet having the composition shown in Table 1. Test specimens were obtained from this sheet using procedures which were identical to those described above for the T-111 VTVS specimens. The various annealing treatments and resulting microstructures for this material will be described in the results and discussion section of this report.

The CVD tungsten which was evaluated in this program was obtained from two sources. The first lot was obtained from the San Fernando Laboratories Division of Fansteel Inc. (SFL), and was in the form of 4 inches (10.2cm) long x .060 inch (1.52mm) thick sheet-type creep test specimens which were vapor deposited and machined to print by the vendor. Chemical analysis of a typical specimen is presented in Table I, while a typical photomicrograph appears in Figure 3. The specimens were of the duplex type with the cross-section containing approximately 45 mils (1.14mm) of a structure typical of the fluoride deposition process, and approximately 15 mils (.38mm) of a structure typical of the chloride deposition process. The annealing treatment for these specimens was 100 hours at 3272°F (2073°K). The second lot of CVD tungsten specimens was provided by the Oak Ridge National Laboratory (ORNL) through NASA, and were of the same general configuration as the first lot. Chemical analysis and metallographic samples were not made available for this test material. The pretest heat treatment for these specimens was also unknown.

Creep Test Procedures

The creep test procedures used for all four of the studies involved in this program were essentially identical, except for the VTVS tests where special modifications were necessary to achieve the desired programmed load and temperature variations. Both the construction and operation of the test chambers and the service instruments in the laboratory have been described in detail in previous reports (Appensix 1). Briefly, the creep test procedure involved initial evacuation of the test chamber to a pressure of less than 5×10^{-10} torr at room temperature, followed by heating of the test specimen at such a rate that the pressure never rose above 1×10^{-6} torr. With the exception of the specimens tested in the lithium exposure program, pretest heat treatments were performed in situ. Complete thermal equilibrium of the specimens was attained by a two-hour hold at the test temperature prior to load application. The pressure was always below 1×10^{-8} torr during the tests and generally fell into the 10^{-10} torr range as testing proceeded. Specimen extension was determined over a two inch gage length with an optical extensometer which measured the distance between two scribed reference marks to an accuracy of ±50 microinches (±1.3 μm).

Specimen temperature was established at the beginning of each test using a W-3%Re W-25%Re thermocouple. Since thermocouples of all types are subject to a time-dependent change in EMF output under isothermal conditions, the absolute temperature during test was maintained by an optical pyrometer. In practice the specimen was brought to the desired test temperature using a calibrated thermocouple attached to the specimen as a temperature standard. The use of this thermocouple was continued during the temperature stabilization period which lasted 50 to 100 hours. At this time, a new reference was established using an optical pyrometer having the ability to detect a temperature difference of ±1°F (±0.6°K) and this reference was used subsequently as the primary temperature standard.

Several modifications were made to the creep test equipment to provide the required variation of load and temperature for the VTVS tests. Load variation was accomplished by using a motor driven screw to continuously feed lead shot into a load pan attached directly to the specimen load train as described in a previous paper (7). An electromechanical device involving a system of resistors, stepping switches, cam timers, and patch boards was designed to program the rate of shot input as a function of time. Because the tests were conducted in vacuum and the load was applied externally through a metal bellows, it was possible to adjust the initial weight of shot in the load pan so that the total weight applied was just balanced by atmospheric pressure on the bellows, thereby providing a true condition of zero load on the specimen at the start of each test. The load train was instrumented with strain gage load cell for measurement of the applied load during testing. The results obtained with this sytems are shown in Figure 4a where the applied load for a typical test is compared with the loading profile anticipated in capsule service. Programmed temperature variation was accomplished using a similar electromechanical switching system to drive an electrical motor attached to the temperature controller. Typical results from this system are compared to the anticipated capsule temperature profile in Figure 4b.

RESULTS AND DISCUSSION

All of the creep results generated on the current contract are summarized in Appendix II together with similar data from the previous contracts which were noted in the Foreword. Discussion of these test results will be divided into four topical sections related to the four separate investigations described in the Introduction.

1. Influence of Pre-Exposure to Lithium or Vacuum on T-111 Creep Behavior

A. CHEMICAL ANALYSIS

Results of pre- and post-exposure chemical analyses for the interstitials oxygen, nitrogen, hydrogen, and carbon are presented in Table III. These results showed no significant variation of the nitrogen, hydrogen, and carbon levels between the as-received and the exposed specimens. The oxygen analyses in Table III show that the pre-exposure annealing treatments increased the oxygen level of the as-received material from 30 to 104 ppm. With the exception of the 5K-2400 exposure condition*, the vacuum exposures dropped the oxygen level back to the 25-30 ppm range. As anticipated, the lithium proved in most cases to be a more effective deoxidant than vacuum, with the residual oxygen levels for the lithium exposed specimens ranging between 3 and 12 ppm.

B. MICROSTRUCTURAL OBSERVATIONS

The influence of exposure on the microstructure of the T-111 alloy is shown in Figure 5. These photomicrographs show that the high temperature (2400°F; 1589°K) exposures caused significant grain growth, with the grain size increasing from 28 μm to approximately 40 μm in 1000 hours and to over 100 μm in 5000 hours. Approximately the same amount of grain growth occurred in both vacuum and lithium, indicating that the growth was not sensitive to environment. The micrographs in Figure 5 also showed significant variations in the amount of precipitate relative to that present in the unexposed specimen. This precipitate was typical of that seen in numerous other heats of T-111 and has been previously identified as a hafnium oxide. The short term vacuum exposed specimens showed essentially no change in precipitate concentration from the unexposed condition (Figures 5b and 5c), while the short term lithium exposures caused small increases in the amount of precipitate (Figures 5f and 5g). The duplex exposures caused large increases in the amount of precipitate, with the vacuum exposure causing a larger increase than the lithium (Figures 5d and 5h). Both of the long time high temperature specimens were essentially clean, with no precipitate visible at 1000X (Figures 5e and 5i).

- - - - - - - - - - - - - - -

* Refer to Table II for explanation of exposure references.

To confirm that the precipitate observed in the photomicrographs was indeed the hafnium oxide which has been previously observed in T-111 alloy, the specimen containing the largest amount of precipitate (duplex vacuum) was subjected to electron probe microanalysis. The results of this analysis are presented in Figures 6b and 6c, which show simultaneous hafnium and oxygen X-ray emission intensity scans for a beam traverse across the precipitate shown in Figure 6a. These traces definitely show the precipitate to be rich in both hafnium and oxygen, thereby supporting the previous identification.

A qualitative correlation of the observed residual oxygen levels with the amount of precipitate present in each specimen indicated that a significant portion of the residual oxygen remained in solid solution in some of the specimens. For example, the amount of precipitate present in the unexposed material was less than that normally seen in T-111 at the 100 ppm oxygen level (i.e., the specimen was "cleaner" than normal), which indicated a substantial proportion of the oxygen was in solid solution prior to exposure. Similarly, the short term exposure specimens contained less precipitate than the duplex samples, despite the fact that all three of the specimens exposed to each environment exhibited similar oxygen levels. This result indicates that some oxygen must be present in solid solution in the short term specimens, with substantially more being present in the vacuum than in the lithium exposed samples. Finally, the 5K-2400 specimens appeared completely clean and yet showed measurable oxygen levels, again indicating that these specimens contained at least a small amount of oxygen in solid solution. These observations are important for the interpretation of the subsequently observed mechanical behavior because it is the oxygen in solid solution, and not the total oxygen content, which controls the magnitude of the dynamic strain aging phenomena in T-111 alloy.

C. CREEP LIFE RESULTS

The initial creep test program for the exposed specimens was directed toward determination of the 1% creep life in the temperature range of 1650 to 2200°F (1172 to 1478°K), plus determination of the rupture life at 1650°F (1172°K). Four test conditions were chosen in this temperature range to obtain 1% creep lives on the order of 500 to 1000 hours for the unexposed material, as shown in Table IV. As testing proceeded it became evident that certain of the exposure conditions severely degraded life (by greater than two orders of magnitude) so that to obtain test lives on the exposed material which were of the same order as the unexposed specimens, supplementary test conditions were chosen which are also listed in Table IV. In addition, selected specimens were tested at 2400°F (1589°K) in this supplimentary program.

Creep curves obtained at each of the four basic creep test conditions are presented in Figures 7a through 7d, while creep curves obtained at the 2400°F (1589°K) supplimentary conditions are shown in Figure 7e. Curves obtained at the 2000 and 2200°F (1366 and 1478°K) supplimentary conditions are not shown as these curves had shapes similar to those presented in Figure 7 at

the corresponding temperature in the basic set. The 1% creep and rupture life data for each exposure condition are presented in tabular form in Table V. The 1% life data are also presented in parametric form in Figure 8. These results show that the long time elevated temperature exposure of T-111 to either lithium or vacuum caused significant and in some cases even dramatic changes of creep life.

The observed 1% creep life variation showed systematic dependencies on both the exposure and the creep test conditions*. In almost all cases the low temperature exposures reduced the creep life (Figure 8a). The life reductions caused by the low temperature exposures were dependent on the creep test temperature, being largest at the lowest test temperature and diminishing as the test temperature increased. At the highest test temperature (2400°F; 1589°K) there appeared to be essentially no significant effect of exposure on creep life for the two duplex exposures, although these exposures caused the most severe life reductions at the lower test temperatures. For both the 1000 and 5000 hour low temperature exposures the lithium environment caused larger life reductions than the vacuum environment. For a given environment, the long time low temperature exposures caused larger life reductions than the short time low temperature exposures.

The creep life variations caused by the high temperature exposures were not as large as those produced by low temperature exposures (Figure 8) and it was therefore more difficult to separate significant effects of exposure from the data scatter inherent in creep testing. As with the low temperature exposures, the high temperature exposure effects were dependent on creep test temperature. At the lower creep test temperatures, most of the high temperature exposures caused life reductions; however, at the highest creep test temperature (2200°F; 1478°K) the high temperature exposures either caused no change or increased the creep life. Where life reductions occurred the effects of high temperature exposure time and environment tended to be consistent with those observed at the lower exposure temperatures; that is, lithium caused larger life reductions than vacuum and for a given environment the 5000 hour exposures tended to cause larger life reductions than the 1000 hour exposures.

- - - - - - - - - - - - - - - - -

* The influence of each of the exposures on rupture life at 1650°F (1172°K) was essentially the same as on the 1% creep life, and the rupture life data will therefore not be specifically discussed. All remarks concerning the 1% creep life behavior at 1650°F (1172°K) may be considered to apply to both 1% creep and rupture life.

D. RATIONALIZATION OF EXPOSURE EFFECTS

The effects of exposure on the creep life of T-111 alloy are rationalized on the basis of two competing mechanisms; grain growth and deoxidation. These two effects are separated on the basis of differences in the effect of creep test temperature on the operation of each mechanism. Grain boundary sliding is basically a high temperature creep deformation mode, and the effectiveness of grain growth in increasing the creep life therefore increases with test temperature. The deoxidation effect, on the other hand, is associated with the oxygen controlled dynamic strain aging behavior which is most pronounced in the temperature range of 1600 to 1700°F (1144 to 1200°K) and decreases with either increasing or decreasing temperature outside of this range. The creep life degredations caused by deoxidation should therefore become smaller with increasing creep test temperature.

Grain growth effects were limited to the high temperature exposure series since no grain growth occurred at the lower exposure temperatures. The grain growth effects were difficult to separate from deoxidation effects since both phenomenon occurred simultaneously at the high exposure temperature. The grain size effect was therefore evaluated at the 2200°F (1478°K) creep test temperature where this effect was expected to be the largest and the deoxidation effects were expected to be smallest.

At temperatures where grain boundary sliding contributes significantly to creep deformation, the creep rate should be proportional to the grain boundary surface area per unit volume of material. The surface area per unit volume of a polycrystalline material is inversely proportional to the mean intercept grain size, d. Thus, the creep rate $\dot{\varepsilon}$ should be inversely proportional to d; that is,

$$\dot{\varepsilon} \propto d^{-1}$$

Garofalo reports data which confirm this relationship for lead, tin, monel, and an Fe-Cr-Ni-Mn alloy tested at high homologous temperatures (8). Presuming that creep life is inversely related to creep rate, the measured creep life should be directly proportional to grain size. A plot of 1% creep life versus grain size is shown in Figure 9 for the unexposed and the four high temperature exposure specimens tested at 2200°F (1478°K). The five data points on this plot were divided into two categories for analysis; those representing specimens containing significant residual oxygen (the pre-exposed and the 1K-2400 vacuum specimens) and those representing specimens having relatively low residual oxygen levels (the 1K and 5K-2400 lithium and the 5K-2400 vacuum specimens). The two sets of data exhibited slopes of +.7 and +.8, indicating a significant contribution of grain boundary sliding to creep of both the oxygen containing and the deoxidized T-111 alloy.

The influence of deoxidation on the creep behavior of T-111 was evaluated by analysis of creep curve shape. The observed creep curves exhibited significant shape variations which depended on both exposure and creep test conditions. The changes resulting from variations in test temperature are illustrated in Figure 10, where the variation of creep rate with creep strain is plotted for the unexposed specimens. At the lowest test temperatures (1650 and 1800°F; 1172 and 1255°K) where the dynamic aging phenomenon was most pronounced, these curves exhibited an unusual shape characterized by a complete cessation of creep over a finite period at a low strain level, followed by a resumption of creep with a steadily increasing creep rate (Figures 10a and 10b). Previous studies have shown that the creep cessation in T-111 was associated with the dynamic strain aging phenomenon, and that the increase in creep rate subsequent to cessation was associated with vacuum indiced deoxidation which depleted the interstitial species associated with the dynamic aging (1). It was also observed in previous studies that after deoxidation the rate versus strain curve eventually became level over a finite strain interval, indicating the establishment of a steady state creep rate which was characteristic of the deoxidized alloy. This phenomenon did not occur in the present tests. This is probably a result of the fact that the stress levels employed in this program were much higher than those used previously.

The creep cessation phenomenon did not occur at the 2000 and 2200°F (1366 and 1478°K) test temperatures. However, these curves did exhibit basically the same shape as the lower temperature curves (Figure 10c and 10d) indicating that the dynamic aging phenomenon may continue to play a role in the creep deformation of the T-111 alloy up to 2200°F (1478°K). It was not until the test temperature was increased to 2400°F (1589°K) that the T-111 creep curve assumed what might be considered a "normal" shape (Figure 10e).

Analysis of the creep curves for the exposed specimens showed that the majority of the exposures substantially reduced or completely eliminated the creep cessation phenomenon which occurred in the unexposed material at the lower test temperatures. This reduction in the effect of dynamic aging on creep was assumed to be associated with the deoxidation caused by exposure. To document this association, the shapes of the creep curves obtained at 1650°F (1172°K), where the dynamic aging effect was most prominent, were examined in more detail on plots of creep rate versus creep strain (Figure 11). These curves showed that the only treatments which completely eliminated the dynamic aging effect were the two duplex exposures to lithium and vacuum (Figures 11c and 11g). This observation may at first seem anomalous in the case of the duplex vacuum exposure, where chemical analysis showed a residual oxygen level of 30 ppm. However, this apparent anomaly may be explained by noting that the dynamic aging phenomenon involves the oxygen in solid solution, and not the total oxygen content. It would thus appear that the duplex vacuum specimen has been deoxidized internally (in the sense of removing all of the oxygen from solid solution) by the precipitation of hafnium oxide. The two short term vacuum exposures, where substantial oxygen appeared to have remained in solid solution, continued to display the creep cessation phenomenon (Figures 11a and 11b). The

remaining four exposure conditions did not show a creep cessation, but did continue to exhibit slight dynamic aging effects, despite the low oxygen levels (Figures 11d, 11e, 11f, and 11h). This observation indicates that the dynamic strain aging in this alloy requires only a few ppm of residual oxygen in solution to be operative.

II. Creep Behavior of T-111 Under Conditions of Continuously Increasing Stress and Decreasing Temperature

A. ANALYTICAL INVESTIGATION

1. Characterization of Anticipated Service Conditions

Presuming that the capsule operates in an environment where heat extraction occurs primarily by conduction and/or convection, the difference between the capsule temperature T and the ambient temperature T_a will be directly proportional to the rate of isotope decay, which is in turn proportional to the amount of parent isotope present (N); that is,

$$T-T_a = \delta N \tag{1}$$

where δ is a proportionality constant. The ratio of the operating temperature difference to the initial temperature difference will thus be:

$$\frac{T-T_a}{T_o-T_a} = \frac{\delta N}{\delta N_o} = \frac{N}{N_o} \tag{2}$$

where N_o is the original amount of fuel in the capsule. The ratio of N/N_o decays exponentially with time according to the relationship

$$N/N_o = e^{-\lambda t} \tag{3}$$

where λ is the decay constant for the isotope involved. The capsule temperature will therefore decrease with time according to the equation:

$$T = T_a + (T_o-T_a)e^{-\lambda t} \tag{4}$$

in a conductive or convective thermal environment.

The effective stress σ in the capsule is proportional to P (the internal pressure), which is related to T (the absolute temperature) and n (the amount of helium gas present) through the universal gas law:

$$\sigma \propto \frac{nRT}{V} \tag{5}$$

The amount of helium gas in the capsule is proprotional to the difference between the initial amount of isotope and the amount remaining at time t:

$$n \propto (N_o-N) = N_o(1-N_o/N) = N_o(1-e^{-\lambda t}) \tag{6}$$

Incorporation of Equations (3) and (6) into Equation (5) provides an expression for the effective stress in the capsule liner:

$$\sigma = F(T_a+(T_o-T_a)e^{-\lambda t})(1-e^{-\lambda t}) \tag{7}$$

where the $N_o R/V$ term has been combined with a proportionality constant involving capsule dimensions and safety factors into a single effective proportionality constant F.

Figure 12 shows the variations of temperature and stress which are predicted by Equations (4) and (7) for operation in still air at 75°F (297°K). This is the type of environment that the capsule would encounter if an accidental re-entry occurred in a remote and inaccessible location, and was the assumed environment for all of the analytical and experimental work performed in this study. The exponential temperature decay shown in Figure 12 is straightforward and requires little discussion. However, the variation of stress with time is more complicated because of the counteracting effects of increasing helium concentration and decreasing temperature. These competing effects cause the stress to increase early in the capsule lifetime, with a subsequent decrease as the fuel becomes exhausted.

2. Predicted Creep Behavior

a) Specification of Stress Levels

For a given service application, the initial capsule temperature and decay constant will be fixed and the design parameter which must be adjusted to provide allowable loading is the stress proportionality constant F, which may be varied to suit the design requirements by proper selection of capsule dimensions. Presuming a fixed ambient temperature of 75°F (297°K), there is a maximum permissible value of F for each starting temperature which is determined by the approach of the operating stress to the material yield strength. Calculation of this maximum F value is complicated by the fact that the yield strength varies with temperature, as illustrated in Figure 13 for the T-111 alloy. Thus, it is not sufficient to adjust F to a value where the maximum stress achieved during capsule service will not exceed the yield strength (Curve A in Figure 13), because the applied stress will then exceed the yield strength at some point in the capsule life prior to the time at which the stress reaches its maximum (Area C in Figure 13). The proper adjustment of F for a yield criteria is the one used to generate Curve B, which is just tangent to the yield strength versus time curve.

Since the tangency calculation for F is made in terms of half life rather than real time, it is independent of decay constant and depends only on the initial temperature. Thus, for a specified starting temperature there is a unique F value for yield tangency which constitutes an upper limit on F for creep loading. The F values which will cause a yield tangency to occur in T-111 alloy have been calculated for a range of starting temperatures and the results of these calculations are presented in Table VI. The applied stress levels used for the subsequent analytical and experimental determinations of creep behavior will be specified in terms of the fraction of the maximum applicable F value for the chosen starting temperature. For example, at a starting temperature of 2600°F, a specified stress level of .65 indicates that the F factor used to calculate stress is 65% of 42.4 psi/°F (526 $MN/m^2/°K$) and that the stress at any point during the capsule lifetime will be 65% of the value in a situation where a yield tangency occurs.

b) Predicted Creep Curve Shape

The method used to calculate creep strain for T-111 alloy tested with the stress and temperature profiles illustrated in Figure 12 involved the integration of the steady state creep rate $\dot{\varepsilon}$ with respect to time:

$$\varepsilon = \int_0^t \dot{\varepsilon} dt \qquad (8)$$

The equation used to represent $\dot{\varepsilon}$ as a function of stress and temperature was the hyperbolic sine relationship developed for T-111 alloy by Sheffler et al (3):

$$\dot{\varepsilon} = 1.65 \times 10^9 [\sinh(6.6 \times 10^{-5}\sigma)]^{3.17} e^{-90,000/RT} \qquad (9)$$

This equation was based on a correlation of conventional (isostatic, isothermal) steady state creep rate data from five different heats of T-111 alloy, and may be expected to predict experimental creep rates of a specific heat within a factor of approximately ±3.

The use of Equation (9) for prediction of VTVS behavior involved substitution of the analytical expression for σ and T (Equations 7 and 4) into Equation (9) to provide an expression for $\dot{\varepsilon}$ which could be integrated with respect to time to determine the accumulated creep strain at any point in the capsule life. The repeated integration of this function over a range of successively increasing upper limits provides, in effect, a predicted creep curve for the chosen stress level, initial temperature, and decay constant. A set of hypothetical creep curves calculated in this fashion using computer assisted numerical integration techniques is presented in Figure 14. The program used to calculate these curves included adjustments to the calculated creep strain for both thermal contraction and elastic strain, so that the creep strain calculated for any given time represented the extension which would be physically measured in an experimental test.

c) Selection of a Creep Design Parameter

The most unusual characteristic of the postulated creep curves shown in Figure 14 was that the creep strain did not increase continuously to rupture, as normally observed in isostatic, isothermal tests, but instead reached a maximum strain value which was achieved at the point in time where the rate of change of mechancial strain was just equal to the rate of thermal

contraction. Beyond this point the calculated creep rate was smaller than the calculated thermal contraction so that the net observable rate of dimensional change became negative.

The selection of a creep design parameter for the rather unusual creep curves presented in Figure 14 was further complicated by the fact that the normally used parameters such as rupture life or minimum creep rate did not apply. While the time to a specified strain level (e.g., the 1% creep life) might have been used in selected cases, this parameter was not universally applicable to the VTVS curves since the specified strain level may not be reached during the course of the capsule life. Because of these shortcomings, an entirely new parameter was selected to characterize the VTVS creep curves. This parameter was the maximum strain achieved during the capsule lifetime and was designated as the "stall strain" since it represented the extension at which creep essentially "stalled" or ceased to be significant.

d) Predicted Influence of Service Variables on Stall Strain

To explore the influence of the capsule variables (initial temperature, stress level, and decay constant) on the stall strain, and also to provide a guide for the selection of test parameters for the experimental portion of the program, the stall strain was calculated over the range of each of these variables. The results of these calculations are presented in Figure 15, where the calculated stall strain is plotted versus half life (half life = ln 2/decay constant) for a range of stress levels and initial temperatures. Presuming that these predicted curves did indeed exactly represent the observed material behavior, the problem of capsule design for a specified starting temperature and isotope would reduce to a simple matter of selecting the stress level corresponding to the maximum allowable creep strain. For example, if the maximum allowable creep strain were determined to be 1% for a Pu^{238} capsule (decay constant = $.93 \times 10^{-7}$) which went into service at 2200°F (1478°K), the maximum allowable stress level (as determined from Figure 15) would be 0.3 (Point "A") and the capsule dimensions would be adjusted to provide an F value which was 30% of the yield limiting value of 53.7 psi/°F (666 $MN/m^2/°K$).

Unfortunately, the subsequently discussed experimental results showed systematic deviations from the predicted curves, which means that the problem of creep-limited capsule design will be considerably more complicated than indicated by the above example. However, the results of the calculations were highly useful in the design of the experimental program. The calculated creep curves served to define the creep curve shape which could be anticipated with VTVS loading, and permitted the critical design parameter (stall strain) to be identified in advance of the experimental effort. In addition, the calculated stall strain data were used to establish values of the experimental parameters (starting temperature, stress level, and decay constant) which allowed completion of the experimental effort in a reasonable time, and also provided data which could be used to explore methods for extrapolation of the short time stall strain values to longer service lives.

B. EXPERIMENTAL PROGRAM

1. Program Objectives

The objectives of the experimental program were twofold. The first objective was to characterize the creep behavior of T-111 alloy with the continuously varying stress and temperature profiles of the type shown in Figure 12, and to compare this observed behavior with the behavior predicted by Equation (8). The second objective was to generate limited short time stall strain data and to evaluate the usefulness of such data for the prediction of long time behavior.

The commonly used approaches for extrapolation of short time creep data are: (a) manual extrapolation of isothermal stress rupture curves or (b) analytical extrapolation using correlating parameters such as the Larson-Miller or the Manson-Halford (9, 10). With either approach, the primary concern with extrapolation is the potential occurrence of creep instabilities at times beyond the range of experimental investigation. While there is no infallible solution to the problem of predicting potential instabilities, one common approach is to examine the creep behavior at temperatures slightly above the anticipated service temperature with the hope that the occurrence of potential instabilities will be accelerated at the higher temperatures. In manual extrapolation this approach boils down to the use of a "judgment factor" which is developed by visual examination of the higher temperature stress rupture curves. In analytical extrapolation, the use of correlating parameters represents an effort to provide a mathematical basis for the characterization of temperature effects on rupture behavior.

While none of the conventional extrapolation methods were directly applicable to the capsule design problem, it was still possible to make use of the basic principles involved in these methods for design of the experimental program; that is, to run short tests at high temperatures which could be used to predict longer time behavior at lower temperatures. To implement this approach, experimental values of starting temperature, stress level, and decay constant were chosen which were significantly larger than the anticipated capsule service conditions (Table VII). Increasing these three independent test variables served to shorten the time required to reach the stall strain and thus allowed the objectives of the investigation to be fulfilled within a reasonable expenditure of experimental effort. The calculated results were used to select test parameters which would provide stall strains on the order of 1/2 to 5%. The ranges of the independent variables were selected to facilitate evaluation of the adaptability of such data to correlation methods. It must be emphasized that the tests conducted on this program were strictly exploratory in nature, and were not intended to be used directly for capsule design. However, the results of this study should be highly useful in the design of further experimental programs directed toward the generation of specific design data.

2. Experimental Results

An experimental creep curve having a typical shape is compared in Figure 16 with a predicted curve which was calculated using Equation (8). These curves were generated using the load and temperature profiles presented in Figure 4. While the observed and predicted curves did not coincide perfectly, the shape of the experimental curve was generally similar to the predicted shape. The experimental data also exhibited the predicted stall phenomenon. Furthermore, the predicted and experimental stall strains were quite close for this particular test. Unfortunately, the agreement between predicted and observed stall strain was not as good for the majority of the test results as for this particular example, as shown in Table VIII. The experimental stall strains exhibited consistent deviations from the predicted values, which were dependent on the applied test parameters as illustrated in Figure 17. At the .65 stress level, the observed stall strains were smaller than predicted, while at the 1.0 stress level the opposite was true. The observed curves of stall strain versus decay constant also exhibited a lower slope than predicted, so that the deviations between the observed and predicted values become larger with decreasing decay constant at the .65 stress level and become smaller at the 1.0 stress level.

In an effort to determine the cause of the observed deviations between the predicted and measured stall strains, creep rates were calculated as a function of time for each test and were compared with the creep rates predicted by Equation (9) to determine if consistent deviations between the observed and predicted rates were occurring. This comparison was performed by plotting the ratios of the observed to the predicted rates as a function of test time, as shown in Figure 18. In order to rationalize the data from the three tests performed at each starting temperature and stress level, the rate ratio data were plotted as a function of time in half lives, rather than real time. These data showed systematic deviations between predicted and observed rates which were consistent for all twelve tests. These deviations were characterized by a "U" shaped plot of the observed/predicted creep rate ratio versus test time. This behavior was presumed to be caused by the occurrence of primary and tertiary creep in the early and later stages of the experimental tests. During the intermediate stages of testing, where the material substructure was presumably stabilized to a configuration approximating the substructure which develops during conventional steady state creep, the experimental VTVS creep rates approached, and actually fell below the values predicted by Equation (9).

While the occurrence of primary and tertiary creep accounts for the large positive deviations between observed and predicted creep rates in the early and later stages of the VTVS tests, it does not account for the fact that the experimentally observed creep rates were consistently below the predicted rates (i.e., the rate ratios were consistently less than unity) during the intermediate stages of each test. Analysis of limited conventional (isostatic, isothermal) creep test data for the Heat 650028 indicated that the primary cause of this deviation was a difference between the creep properties

of Heat 650028 and the properties predicted by Equation (9), which represents an average of the measured creep behavior of five other heats of T-111 alloy. This difference is documented in Table IX, which shows the experimental versus observed creep rate ratios for five conventional vacuum creep tests on Heat 650028.

The rate ratio data presented in Figure 18 provide an explanation for the deviations between the observed and predicted stall strains. This explanation is based on the fact that the observed creep rates were different from the predicted values at the predicted stall time, as shown in Figure 18. For the two sets of tests at the .65 stress level (Figures 18a and 18b) the predicted stall times were within the range where the experimental creep rates were lower than predicted, so that the observed creep rate fell below the rate of thermal contraction sooner than predicted and stall occurred prematurely at a total strain level which was below the calculated value. For the two sets of tests at the 1.0 stress level, the predicted stall times fell in the range where the experimental creep rates were higher than predicted (Figures 18x and 18D) so that the observed stall times and stall strains were larger than predicted.

In order to provide a complete description of the observed VTVS creep behavior of T-111 alloy, there are two additional experimental observations which must be discussed. The first of these involved grain growth and deoxidation which occurred during certain of the VTVS tests. Oxygen levels after testing were about half of the pre-test value (Table X). As shown in Table XI the grain growth was confined to the longer time tests, and was not thought to have a major influence on the test results. However, it is noted here because it is a factor which must be considered in the organization of future test programs to generate specific capsule design data. The occurrence of grain growth at the higher test temperatures will limit the potential for trade-offs between time and temperature for the generation of such data.

Another unusual and somewhat disturbing phenomenon occurred in the two longest tests conducted at the 2400°F (1589°K) starting temperature (S-152 and 154). Both of these tests exhibited large discontinuous jumps in the creep curve after stall had occurred. This phenomenon is illustrated by the data in Figure 19, which show jumps over 1% for both tests. The temperature and stress at the time of these sudden strain increases were approximately 1050°F (839°K) and 41.7 ksi (287 MN/m^2) for test S-154 and 1230°F (939°K) and 40.5 ksi (279 MN/m^2) for test S-152. Comparison of the applied stress for tests S-152 and S-154 with 0.2% offset yield strength data for Heat 650028 showed that the yield tangency occurred at about 1400°F (760°K) for these two tests, which is well above the temperatures at which the jumps occurred (Figure 20). It would thus appear that no explanation can be given at the present time for this highly unusual phenomenon. Since the occurrence of the jumps was confined to these tests where the applied stress level was considerably higher than would be anticipated in actual capsule service, this phenomenon was not considered to be important with regard to capsule design.

3. Design Considerations

As previously mentioned, the primary objective of this program was characterization of the VTVS creep behavior of T-111 alloy, with emphasis on the problem of predicting creep behavior at extremely long times. Two approaches to this problem were studied in this program. The first was analytical calculation of VTVS behavior from conventional creep results, and the second was parametric extrapolation of short time VTVS experimental results. The experimental data indicated that the prediction of VTVS behavior from conventional minimum creep rates was not sufficiently accurate for design purposes, with deviations as large as 600% being observed between the predicted and observed stall strain values. Fortunately, the nonconservative deviations (observed stall strain> predicted stall strain) were confined to the 1.0 stress level, which is well above the stress levels which could presumably be considered for design purposes. At the lower stress level studied, the observed stall strains were all below the predicted values, meaning that a capsule designed on the basis of the calculated values would be over rather than under designed.

While the present method of analytical prediction was not sufficiently accurate for design purposes, the experimental data developed in this study indicated certain areas where the method could be improved to make it more accurate. The two primary causes of inaccurate predictions were deviations of the specific heat properties from the average values used for prediction and systematic deviation of the observed from the predicted creep rates as a result of primary and tertiary creep. Both of these deviations could easily be incorporated into the predicting equation to improve the accuracy of future predictions.

The second approach which was studied for the prediction of long time VTVS behavior was extrapolation of short time results. To implement this approach the following correlating parameter was developed using the calculated VTVS data:

$$\text{Parameter} = \log(HL) - \frac{35,200}{T+460} - .75 \log(SS) \qquad (10)$$

where HL is hypothetical isotope half life in hours, T is starting temperature in °F, and SS in stall strain in percent. The calculated stall strain data shown in Figure 15 are replotted in Figure 21 to illustrate the use of this parameter*. To test the ability of the parametric method for extrapolation of short time stall strain data, Equation 10 was used to correlate the four tests with half lives of 400 hours or less at each of the two stress levels investigated, and the resulting parameter values were used to predict the stall strains for the 1000 and 2000 hour tests. The results of these predictions are compared with the experimental data in Table XII. With the exception of test S-153, the extrapolated stall strains were all within 25% of the observed values, which is highly encouraging considering the very limited amount of experimental data which were available for the parametric extrapolation. These results indicate that as a larger data base becomes available, it should be possible to develop a parameter which can be used with reasonable confidence for extrapolation to the required design life times.

- - - - - - - - - - - - - - - -

* The data plotted in Figure 21 showed that the three terms parameter did not provide an exact fit of the calculated data, which deviated systematically with stall strain over a narrow band. Additional work indicated that a four term parameter involving a second order polynomial in stall strain would exactly fit the calculated data:

$$\text{Parameter} = \log(HL) - \frac{35,200}{T+460} + .73348 \log(SS) - .17861[\log(SS)]^2 \qquad (11)$$

However, the use of both of these parameters to correlate the test results showed that the three term parameter actually provided a better fit of the experimental stall strain data. As additional experimental results become available from possible future programs, it should be possible to further refine the correlating parameter for a more exact fit of real data.

III. Influence of Heat Treatment on the Microstructure and Creep Behavior of ASTAR 811C Alloy

A. SELECTION OF HEAT TREATMENTS

The two heat treatments studied in this program were 1/2 hour at 3600°F (2255°K) and 1 hour at 3000°F (1922°K). The former was used because it represents a standard heat treatment for commercial tantalum alloys. The latter was chosen more or less arbitrarily to provide the maximum possible creep strength while limiting grain size to the 100 to 120μm range. While combinations of longer time or higher temperature might have produced even greater improvements in creep strength, they would also have increased grain size to the point of limiting the engineering usefulness of the material.

B. MICROSTRUCTURAL OBSERVATIONS

The microstructures produced by each of the two heat treatments studied in this program are shown in Figures 22 and 23. The 3600°F (2255°K) anneal produced relatively large grained, single phase microstructure (average grain size 100μm) which was essentially free of carbides (Figure 22), while the 3000°F (1922°K) treatment yielded a finer grained structure (average grain size 10μm) containing a large amount of undissolved carbide (Figure 23). The size, snape, and distribution of carbides in the 3000°F (1922°K) specimens were quite complex. Within the grains both an acicular shaped (A) and a more rounded type of carbide (B) were found. The grain boundaries contained both rounded and elongated carbide particles (C) together with a larger carbide having a fine lamellar internal structure (D) reminiscent of a euctectoid mixture. The composition of these carbides was presumed to be the same as that determined by Buckman and Goodspeed who found only the dimetal carbide Ta_2C in their study of ASTAR 811C (4). No effort was made to confirm this composition in the present investigation.

C. CREEP RESULTS

Creep curves characteristic of the two structures discussed above are presented in Figures 24 and 25. Two curves are shown in each figure, one generated at a test temperature of 2400°F (1589°K) and the other at a lower temperature in the 1900 to 2000°F (1339 to 1366°K) range. The difference observed in the shapes of these four curves appeared to be associated with the difference in test temperature rather than with the difference in heat treatment. Both of the 2400°F (1589°K) curves showed no primary creep and exhibited a continuously increasing creep rate (Figures 24a and 25a), whereas the curves generated at the lower test temperatures exhibited both first and second stage creep (Figures 24b and 25b). The temperature range over which this change of creep curve shape occurred corresponded to the temperature range over which Harrod, Ammon, and Buckman observed a change in the grain size dependence of creep life in ASTAR 811C alloy (12). These authors showed that the creep life of this alloy was grain size dependent at 2400°F (1589°K), but not at 2000°F (1366°K), indicating that the temperature at which grain boundary sliding

becomes an important deformation mechanism (the equicohesive temperature) falls within this range. Thus, it would appear that the observed change in creep curve shape between 2000 and 2400°F (1366 to 1589°K) may be associated with this assumed change in the creep mechanism.

One percent creep life data for ASTAR 811C in both conditions of heat treatment are displayed in parametric form in Figure 26. The range of previously observed 1% creep life data for the commercially available T-111 tantalum alloy (1) is also shown in this figure to document the improved creep life achieved by the newer Westinghouse alloy. The ASTAR 811C data in Figure 26 clearly show the benefit to be obtained from the higher temperature annealing treatment. However, these data also show that this benefit is considerably diminished at the higher stresses and lower test temperatures, where the curves for the two different heat treatments tend to merge. All of the tests conducted at or below 2200°F (1378°K) have been indicated in Figure 26 to show that the temperature range over which the two curves merge coincides with the assumed equicohesive temperature range for ASTAR 811C. This coincidence suggests that the life improvement caused by the higher temperature anneal may be associated with the larger grain size rather than with the difference in carbide character between the two microstructures. While only limited data were available in the low stress-high temperature range, it appears from the limited results presented in Figure 26 that the creep life curves for the two heat treatments may also be merging in this stress and temperature range. This apparent tendency is attributed to changes occurring in the microstructure during creep testing, which are described below.

D. INFLUENCE OF CREEP ON MICROSTRUCTURE

Metallographic examination of specimens tested above 2800°F (1811°K) indicated that both grain growth and carbide dissolution occurred during creep testing in this temperature range. An example of this phenomenon is shown in Figure 27. The observed grain growth was assumed to be responsible for the apparent tendency of the two creep life curves in Figure 26 to merge at the lower stresses and higher temperatures. The grain growth phenomenon is significant with respect to design coinsideration for ASTAR 811C since it means that service temperatures for this material will probably be limited to values below 2800°F (1811°K) except in unusual circumstances where excessive grain growth will not degrade the usefulness of the material.

Metallographic examination of specimens creep tested at lower temperatures showed that the carbide structure in material tested at 2400°F (1589°K) was quite similar, regardless of the pre-test heat treatment. The creep tested structures were characterized by a tendency for carbides to be located preferentially at the grain boundaries, as shown in Figures 28 and 29. For the specimens annealed at 3000°F (1922°K), the average grain boundary carbide size appeared to be somewhat larger than before testing, indicating a tendency for carbide migration and agglomeration of the grain boundaries (Figure 28). For the specimens annealed 1/2 hour at 3600°F (2255°K), the carbide tended to reprecipitate preferentially at the grain boundaries

(Figure 29). An extreme example of this tendency was found in a specimen which tested for over 20,000 hours at 2600°F (1700°K) and 2 ksi (13.8 MN/m^2) Figure 30). This specimen exhibited a structure which was completely free of carbide in the interior of the grains, with an abundance of large, blocky carbides being located at the grain boundaries*.

E. PHENOMENOLOGICAL ANALYSIS

Another approach which was used to study the influence of annealing temperature on the creep behavior of ASTAR 811C involved phenomenological analysis of creep rate data to determine the stress and temperature dependence of the minimum creep rate for both conditions of heat treatment. At the lower test temperatures where primary creep occurred (Figures 24b and 25b), the minimum creep rates used for this analysis were measured in the usual way. At the higher test temperatures where primary creep did not occur (Figures 24a and 25a), the initial creep rate was used for analysis, since it represented the lowest creep rate exhibited by the material prior to the onset of tertiary creep.

The methods used to determine the stress (σ) and temperature (T) dependence of the minimum creep rate ($\dot{\varepsilon}$) involved a combination of manual plotting and computer assisted multiple linear regression analysis to fit the rate data to the equation

$$\dot{\varepsilon} = Af(\sigma)e^{-\Delta H/RT} \tag{12}$$

where A is a proportionality constant, ΔH is the activation energy for thermally activated deformation, and R is the universal gas constant (1.987 cal/mole°K). The three stress functions investigated were the exponential, the power, and the hyperbolic sine laws:

$$f(\sigma) = e^{B\sigma} \text{ (exponential law)} \tag{13}$$

$$f(\sigma) = \sigma^n \text{ (power law)} \tag{14}$$

$$f(\sigma) = [\sinh(\alpha\sigma)]^n \text{ (hyperbolic sine law)} \tag{15}$$

The B, n, and α terms in these expressions are arbitrary constants established by the best fit of the data. Results of a preliminary analysis showed that the power law did not fit the data as well as either the exponential or the hyperbolic sine functions, which both appeared to fit the data equally well. Since the hyperbolic sine law is a more complicated function generally reserved for cases where neither the exponential or the power law will fit the data adequately, the exponential function was arbitrarily chosen for the subsequent portion of the analysis.

- - - - - - - - - - - - - - -

* It should be noted that the specimen shown in Figure 30 was not from the same heat of material used for the rest of the study. However, the behavior is presumed to be typical of the alloy.

Activation energies for creep of ASTAR 811C in each of the two conditions of heat treatment were determined by graphical methods. Using expression (13) for $f(\sigma)$, Equation (12) was rearranged to the form

$$\ln \{\dot{\varepsilon} e^{-B\sigma}\} = \ln A - (\Delta H/R)(1/T) \quad (16)$$

or

$$\log \{\dot{\varepsilon} e^{-B\sigma}\} = \log A - (\Delta H/2.303R)(1/T) \quad (17)$$

so that the value of ΔH could be determined from the slope of a semilogarithmic plot of the stress modified creep rate parameter versus reciprocal temperature. Regression methods were used to determine the values of the stress constant (B) which are given below:

Annealing Treatment	Stress Constant (B) $(ksi)^{-1}$	$(MN/m^2)^{-1}$
1 hour 3000°F (1922°K)	.35	.051
1/2 hour 3600°F (2255°K)	.42	.061

Using these B values, the creep rate data for each heat treatment were plotted according to Equation (17) to determine ΔH values, as shown in Figures 31 and 32. The results presented in these figures indicated that the activation energy for creep of ASTAR 811C varied with creep test temperature, as illustrated in Figure 33. These data also showed that annealing temperature did not significantly influence the observed activation energy values, which was somewhat surprising in view of the significant differences in creep life caused by the two different annealing treatments.

The variation of ΔH with test temperature for both heat treatments was somewhat puzzling. At the lower test temperatures (below 2000°F; 1366°K) where the deformation mode was presumably intragranular, the measured activation energies for creep were in the range of the activation energy for self diffusion in tantalum (~100K cal/mole; 3420 J/mole). At the higher test temperatures, where grain boundary sliding, presumably contributed to creep deformation, the measured ΔH values for creep were significantly above the ΔH for self diffusion, which is characteristic of a dispersion strengthening mechanism. This observation would seem to indicate that the carbide strengthening in ASTAR 811C is effective only where grain boundary sliding is a contributing deformation mode. This point, coupled with the metallographic observation that the carbide tends to migrate to the grain boundaries during creep testing regardless of the pretest heat treatment, leads to the hypothesis that the primary role of the carbide in strengthening the ASTAR 811C alloy is to act as a grain boundary pinning agent.

The above hypothesis; that is, that the primary effect of the carbide in ASTAR 811C is to pin the grain boundaries, is consistent with all of the experimental observations developed in this program, and leads to the conclusion that the increased creep life provided by the high temperature annealing treatment is probably the result of grain growth rather than solutioning of the carbide. This conclusion is based on the assumption that the solutioned carbide reprecipitates on the grain boundaries either during the two hour temperature stabilization period prior to creep load application or at a very early point during creep testing of specimens annealed at 3600°F (2255°K), so that the carbide structure is similar for both heat treatments during testing. To test this assumption a creep test specimen was annealed 1/2 hour at 3600°F (2255°K), cooled to room temperature, and reheated to 2400°F (1589°K) for the two hour stabilization period. This specimen was then cooled to room temperature and examined metallographically. As shown in Figure 34, this specimen exhibited an extensive grain boundary carbide network, which confirms the hypothesis that the grain boundary carbide distribution is similar for both heat treatments during creep testing, despite the significant differences observed in the as-annealed condition. The confirmation of this hypothesis in turn lends additional support to the hypothesis that the difference in creep life caused by the two different annealing treatments is primarily a grain size effect.

F. DEFINITION OF ALTERNATE ANNEALING TREATMENTS

As mentioned in the introduction, one of the objectives of this study was to define an alternative to the two previously discussed annealing treatments. Based on the conclusion that grain size was the primary determinant in improving creep life, three alternative annealing treatments involving longer times at lower temperatures were selected to provide an annealed grain size on the same order as that produced by the 1/2 hour at 3600°F (2255°K) treatment. The three time-temperature combinations selected were 5 hours at 3450°F (2172°K), 24 hours at 3270°F (2072°K), and 100 hours at 3000°F (1589°K). The grain size and 1% creep life produced by each of these annealing treatments are compared in Table XIII with similar data from the two previously discussed annealing conditions. These data clearly show that the improved creep strength provided by the 1/2 hour at 3600°F (2255°K) anneal can be achieved by any of the three proposed alternates. The microstructure produced by the three alternative heat treatments were (except for grain size) identical to the 1/2 hour at 3600°F (2255°K) structure, with no carbides visible at 5000X magnification. Based on the fact that the temperature limits of most commercial sized vacuum annealing furnaces suitable for ASTAR 811C alloy are on the order of 3000°F (1922°K), the 100 hour at 3000°F (1922°K) annealing treatment was selected as the primary alternate to the 3600°F (2255°K) heat treatment. In addition to being within the range of presently available capabilities, the 100-hour heat treatment also avoids the previously noted difficulties anticipated in the application of a short time high temperature treatment to thick section sizes. However, it suffers from the disadvantage of higher costs associated with longer annealing time, so that the potential benefit of improved creep life must be carefully balanced against the increased cost prior to specification of the 100-hour heat treatment over the one-hour treatment at 3000°F (1922°K).

IV. CVD Tungsten Creep Results

The 1% creep life results obtained from the two lots of CVD tungsten investigated on this program are summarized on a Larson-Miller plot in Figure 35. These data show a definite break in the creep life behavior of this material which occurred at a stress level on the order of 2 ksi (13.8 MN/m^2). No explanation can be offered for this behavior at the present time. While two of the three test results on the material supplied by ORNL are clearly above the corresponding SFL results, the third ORNL point would appear to be equal to or below the SFL data. Based on the available results it is not possible to determine at the present time if there is a distinguishable difference between the creep life of the two materials, or if the observed differences are the result of experimental scatter.

CONCLUSIONS

1. T-111 Lithium Exposure Investigation

Long time elevated temperature exposure to vacuum and to liquid lithium caused large and in some cases even dramatic reductions in the creep life of T-111 alloy. As an extreme example of this effect, a specimen exposed to lithium for 1000 hours at 1800°F (1255°K) plus 4000 hours at 1900°F (1310°K) exhibited a 1% creep life of 2 hours at 1650°F (1172°K) and 50 ksi (344 MN/m^2), as compared to a life of 938 hours for an unexposed specimen. These results indicated that great caution must be exercised in the application of T-111 for the containment of liquid lithium in space electric power systems.

Metallographic and chemical analysis of exposed specimens revealed that two separate effects were responsible for the observed variations of creep life. The first of these was grain growth, which increased the creep life in the test temperature range where grain boundary sliding occurred. The second effect was depletion of residual oxygen from solid solution either by direct environmental deoxidation or by the precipitation of hafnium oxide, which reduced the creep life in the test temperature range where an oxygen-controlled dynamic strain aging phenemonon occurred.

The effects of exposure on creep life were grouped into two basic categories, depending on the exposure temperature. At the lower exposure temperatures (1800 and 1900°F; 1255 and 1310°K) only deoxidation occurred and large creep life reductions were observed. The magnitude of the life reductions was largest at the 1650°F (1172°K) creep test temperature, where the oxygen controlled dynamic aging effect was most prominent, and diminished as the test temperature was increased. At the highest creep test temperature investigated (2400°F; 1589°K) the low temperature exposures caused no significant change in creep life. The influence of the low temperature exposures on creep life was sensitive to both environment and exposure time. Lithium proved to be a more effective deoxidant than vacuum and therefore caused larger life reductions. For each exposure medium, the creep life reductions increased with increased exposure time. It was shown that the effect of deoxidation on the T-111 creep behavior correlated better with residual oxygen in solid solution than with total oxygen content.

At the high exposure temperature (2400°F; 1589°K), both grain growth and deoxidation occurred. The operation of these two competing effects caused the net creep life variations to be smaller than those observed for the low temperature exposures. As with the low temperature exposures, the effect of high temperature exposure on creep life varied with creep test temperature. At the lower test temperatures (1650, 1800, and 2000°F; 1172, 1255, and 1366°K) the deoxidation effect was more significant than the grain growth effect, and the net creep life change was therefore negative (life reduction). At the higher test temperature (2200°F; 1478°K), the grain growth effect predominated and the post-exposure lives tended to be longer than the pre-exposure lives. As with the low temperature exposures, the high temperature effects were sensitive to environment and exposure time, with larger effects being observed for the longer exposure times and the lithium environment.

II. T-111 Variable Temperature-Variable Stress Investigation

Vacuum creep tests conducted on T-111 alloy with continuously increasing stress and decreasing temperature variations which simulated the service conditions anticipated in radioisotope capsule service have shown that these test conditions produce creep curves having a highly unusual shape. The most unusual characteristic of these curves was that creep strain did not increase continuously to rupture, as in normal creep tests, but instead reached a maximum strain value where the rate of change of mechanical strain was just equal to the rate of thermal contraction. Beyond this point the creep rate was smaller than the rate of thermal contraction so that the net observable rate of dimensional change became negative as temperature decreased. Since none of the existing creep design parameters such as rupture life or minimum creep rate applied to this unusual creep curve shape, a new parameter designated "stall strain" was developed to characterize these curves for design purposes. This parameter was defined as the maximum creep strain achieved during the course of the variable temperature-variable stress (VTVS) tests.

In an effort to predict the VTVS creep behavior of T-111 at very long times, an analytical method was developed to calculate the VTVS stall strain from conventional (isostatic, isothermal) creep results. Comparison of the calculated stall strain values with the experimental results indicated that the analytical method was not sufficiently accurate for design application. However, the results of these calculations, which were performed prior to the creep tests, were highly useful in the design of the experimental program. Without these results it would have been impossible to establish a well organized program which maximized the information available from a given expenditure of experimental effort.

Analysis of the experimentally observed creep rates indicated two primary causes of deviations between the predicted and observed VTVS creep behavior. The first of these involved the occurrence of primary and tertiary creep, which were not accounted for in the model. The second was a difference between the creep properties of the specific heat tested and the average properties used for prediction. Based on these observations, suggestions were made for improvement of the model by tailoring the predicting equation to the specific type of creep behavior observed in the preliminary experimental tests conducted in this study. These suggested modifications would involve adjustments of the proportionality constant in Equation (9) to reflect the creep properties of the specific heat of material being tested, and the addition of a half life dependent modifying expression to adjust the creep rate for primary and tertiary creep.

A second approach to prediction of long time VTVS creep behavior involved parametric extrapolation of short time VTVS data. This approach showed a great deal of promise and indicated that it should be possible to predict long time behavior by extrapolation of short time results obtained at temperatures above the anticipated service range. The only major limitation to this approach appeared to be the tendency for grain growth to occur in the longer time tests at the higher temperatures. Future experimental programs aimed at the development of specific design data must be carefully designed to avoid confounding of the experimental results by this phenomenon.

One other unusual and somewhat disturbing phenomenon which was observed during the course of this investigation was the occurrence of discontinuous jumps in some of the VTVS creep curves. No explanation could be advanced for this phenomenon. Fortunately, the occurrence of the jumps was confined to tests where the applied stress levels were considerably in excess of those which could be anticipated in actual service, so that there should be no major problem so far as design is concerned.

III. ASTAR 811C

Annealing of ASTAR 811C alloy for 1/2 hour at 3600°F (2255°K) was shown to produce a carbide free microstructure with an average grain size on the order of 100 μm. Annealing for 1 hour at 3000°F (1922°K) provided a finer grained structure (average grain size 10 μm) containing a wide range of sizes and shapes of undissolved carbides located both within the grains and at the grain boundaries. Additional metallographic examinations showed that extensive reprecipitation occurred in the solutioned specimens during heating to the test temperature, so that the carbide structure was quite similar for both treatments during creep testing. Creep test results showed that the higher temperature annealing treatment caused a significant improvement in the 1% creep life of ASTAR 811C in the temperature range above 2200°F (1479°K). Below that temperature the 1% creep life data were roughly equivalent for both annealing treatments. While only limited data were available above 2800°F (1811°K), it appeared from a Larson-Miller plot that the creep life data for the two annealing treatments might also be tending to merge in this temperature range. Metallographic examination of specimens creep tested above 2800°F (1811°K) revealed that grain growth occurred during testing, which might explain the observed creep life behavior. These examinations also showed the tested specimens to be carbide free, indicating that the near equilibrium carbide solvus temperature for ASTAR 811C alloy is probably below 2800°F (1811°K). Metallographic examination of specimens creep tested at 2400°F (1589°K) showed that the carbide was located predominantly in the grain boundaries after testing. Examination of a specimen tested for an extremely long time (over 20,000 hours) at 2600°F (1700°K) showed a microstructure which was completely free of carbide within the grains and contained numerous large, blocky carbides at the grain boundaries.

Analysis of the stress and temperature dependence of the minimum creep rate of ASTAR 811C showed that the pretest annealing treatment did not significantly influence the activation energy for creep of this alloy. In the temperature range of 1800-2000°F (1255-1366°K) the ΔH values for creep were on the order of the ΔH for self diffusion in tantalum (100K cal/mole; 3420 J/mole), which indicates a normal diffusion controlled creep mechanism. Above this temperature ΔH rose gradually to values on the order of 150 K cal/mole (5130 J/mole) in the range of 2400-2600°F (1589-1700°K), which implied that dispersion strengthening was involved in creep of ASTAR 811C in this temperature range. These observations were considered somewhat puzzling in view of work performed at the Westinghouse Astronuclear Laboratory (where this

alloy was developed) which showed that the creep rate of ASTAR 811C was grain size dependent at 2400°F (1589°K) but not at 2000°F (1366°K). This observation, combined with the activation energies measured in this program, implied that dispersion hardening was effective in ASTAR 811C only in the temperature range where grain boundary sliding was an operative creep mechanism, and lead to the hypothesis that the primary effect of the carbide in the ASTAR 811C was to act as a grain boundary pinning agent. This hypothesis was supported by the previously discussed observation that the carbide was found to be located predominantly in the grain boundaries after creep testing, regardless of the pretest heat treatment.

The above observations lead to the conclusion that the improved creep life provided by the high temperature heat treatment was probably the result of the increased grain size rather than the solutioning of the carbides. This hypothesis would explain why the creep life improvement was observed only above 2200°F (1478°K) where grain boundary sliding was an operative creep mechanism.

Because the 3600°F (2255°K) annealing treatment was judged to be somewhat impractical on a commercial scale, additional studies were conducted to determine if an alternative heat treatment could be developed which retained the improved creep life but offered more commercial promise. To implement this study three lower temperature annealing cycles were selected to provide grain sizes which were roughly equivalent to that produced by the 1/2 hour at 3600°F (2255°K) treatment. The time-temperature combinations selected were 5 hours at 3450°F (2172°K), 24 hours at 3270°F (2072°K) and 100 hours at 3000°F (1922°K). All of these alternate treatments produced grain sizes and 1% creep lives which were equivalent to those provided by the high temperature heat treatment and would thus all be suitable for processing of ASTAR 811C to obtain the improved creep life. Based on the fact that the temperature limits of most commercial sized vacuum annealing furnaces are presently on the order of 3000°F (1422°K), the 100 hours at 3000°F (1922°K) treatment was selected as the prime alternative to the 1/2 hour at 3600°F (2255°K) heat treatment.

IV. CVD Tungsten

Preliminary 1% creep life data have been generated for CVD tungsten from two sources. The data obtained was insufficient to distinguish a significant difference in properties between the two sources.

REFERENCES

1. K. D. Sheffler, J. C. Sawyer, and E. A. Steigerwald, "Mechanical Behavior of Tantalum-Base T-111 Alloy at Elevated Temperature," Trans. ASM, Vol. 62, 1969, p. 749.

2. G. P. Dix, "Safety Considerations for Radioisotope Power Systems," Symposium on Materials for Radioisotope Heat Sources, D. E. Thomas, W. O. Harms, and R. T. Huntoon, Ed., 1969, AIME, N.Y., pp. 50-70.

3. S. McAlees, Jr., "Effects of Reentry Environment on Radioisotope Heat Sources," Symposium on Materials for Radiosiotope Heat Sources, D. E. Thomas, W. O. Harms, and R. T. Hunton, Ed., AIME, 1969, N.Y., pp. 280-297.

4. R. W. Buckman, Jr. and R. C. Goodspeed, "Considerations on the Development of Tantalum Base Alloys," Refractory Metal Alloys; Metallurgy and Technology, Plenum Press, New York, 1968, p. 373.

5. K. D. Sheffler, "Generation of Long Time Creep Data on Refractory Alloys at Elevated Temperatures," Semi-Annual Report. Contract NAS-3-13469, TRW ER-7506, NASA-CR-72871, 16 November 1970.

6. W. H. Hendrixson and E. E. Hoffman, "Exposure of T-111 Specimens in Lithium," Final Report, Contract NAS-3-13470, GESP-656, July 15, 1971.

7. K. D. Sheffler and J. C. Sawyer, "Creep Behavior of T-111 Alloy Under the Influence of Continuously Varying Stresses," ASTM Jl. of Mat., Vol. 5, 1970, pp. 384-395.

8. F. Garofalo, Fundamentals of Creep and Creep-Rupture in Metals, McMillan, New York, 1965, p. 27ff.

9. S. S. Manson, "Approaches to Life-Prediction Problems in Creep Rupture and Fatigue at High Temperatures," NASA SP-227, Aerospace Structural Materials Conference, Lewis Research Center, Cleveland, Ohio, November 1969.

10. S. S. Manson, "Time-Temperature Parameters - A Re-Evaluation and Some New Approaches, " Keynote Address, Symposium on Creep Behavior, ASM Congress and Metals Exposition, Detroit, October 1968.

11. K. D. Sheffler, "Influence of Vacuum Environment on the Composition, Structure, and Mechanical Behavior of the Tantalum Tungsten Hafnium Alloy T-111," Proceedings of the 1971 Vacuum Metallurgy Conference, R. C. Krutenat, Ed., American Vacuum Society, New York, 1971.

12. D. L. Harrod, R. L. Ammon, and R. W. Buckman, Jr., "Effect of Thermal-Mechanical Processing on the Creep Properties of Tantalum-Base Alloy ASTAR 811C," Paper presented at AIME Technical Session on Refractory Metals III - Mechanical Behavior, Cleveland, Ohio, October 22, 1970.

Table I

Chemical Composition of Alloys Being Evaluated in Creep Program

Material	Weight %					ppm				
	W	Re	Ta	Hf	C	F	Cl	N_2	O_2	H_2
CVD Tungsten	Bal.				.0029	5	7	3	12	2
T-111										
Heat 650050	7.9		Bal.	1.9	.0033			6	30	1
Heat 650028	8.3		Bal.	2.1	.0030			12	30	2
ASTAR 811C										
Heat 650056	7.9	1.2	Bal.	1.0	.0251			14	30	4

Table II

Heat Treatment and Exposure Conditions Applied to T-111

Exposure				
Time Hours	Temperature °F	°K	Environment	Exposure Code*
1000	1800	1255	Vacuum	1K-1800 Vacuum
1000	2400	1589	Vacuum	1K-2400 Vacuum
1000 + 4000	1800 1900	1255 1310	Vacuum	Duplex Vacuum
5000	2400	1589	Vacuum	5K-2400 Vacuum
1000	1800	1255	Lithium	1K-1800 Lithium
1000	2400	1589	Lithium	1K-2400 Lithium
1000 + 4000	1800 1900	1255 1310	Lithium	Duplex Lithium
5000	2400	1589	Lithium	5K-2400 Lithium

* Used for reference to exposure conditions in text and subsequent tables and figures refering to variable temperature-variable stress test results.

Table III

Chemical Analysis of T-111 Exposure Specimens

Exposure Code*	Concentration, ppm**			
	O	N	H	C
As-Received	30(6)	6(2)	1(2)	33(2)
Annealed 1 hour 3000°F (1922°K) plus 1 hour 2400°F (1589°K) (pre-exposure test condition)	104(3)	-	-	-
1K-1800 Vacuum	24(3)	6(2)	<1	36(2)
1K-2400 Vacuum	29(3)	6(2)	<1	36
Duplex Vacuum	30(2)	7(2)	<1	26
5K-2400 Vacuum	4(2)	14(2)	<1	24
1K-1800 Lithium	12(3)	6(2)	<1	25
1K-2400 Lithium	3(2)	6(2)	<1	38(2)
Duplex Lithium	4(2)	7(2)	<1	29
5K-2400 Lithium	6(2)	7(2)	<1	21

* See Table II

** O, N, and H determined by vacuum fusion method: C determined by combustion conductometric method; numbers in parenthesis refer to the number of replicate analyses performed to obtain the average figure reported. Analysis performed at NASA Lewis Research Center.

Table IV

Creep Test Conditions for T-111 Exposed Specimens

Temperature °F	Temperature °K	Stress ksi	Stress MN/m^2
	Basic Set		
1650	1172	50	344
1800	1255	35	241
2000	1366	24	165
2200	1478	16	110
	Supplementary Tests		
2000	1366	16	110
2200	1478	10.5	72
2400	1589	5	34

Table V

Influence of Long Time Elevated Temperature Exposure to 10^{-9} Torr Vacuum and to Lithium on the Creep Properties of T-111 Alloy

Exposure Code*	Pre-Exposure	1K-1800 Vacuum	1K-2400 Vacuum	Duplex Vacuum	5K-2400 Vacuum	1K-1800 Lithium	1K-2400 Lithium	Duplex Lithium	5K-2400 Lithium
Creep Test Conditions				One Percent Creep Life, Hours					
1650°F (1172°K) 50 ksi (344 MN/m^2)	938	262	1278	4	340	43	448	2	180
1800°F (1255°K) 35 ksi (241 MN/m^2)	528	227	465	10	745	87	323	5	350
2000°F (1366°K) 24 ksi (165 MN/m^2)	410	123	215	55	205	65	91	10	200
2200°F (1478°K) 16 ksi (110 MN/m^2)	435	429	546	155	885	110	440	73	1100
2000°F (1366°K) 16 ksi (110 MN/m^2)	-	-	-	2780	-	-	-	1530	-
2200°F (1478°K) 10.5 ksi (72 MN/m^2)	2330	-	-	1475	-	-	-	732	-
2400°F (1589°K) 5 ksi (34 MN/m^2)	600	-	-	570	-	-	-	463	-
				Rupture Life, Hours					
1650°F (1172°K) 50 ksi (344 MN/m^2)	1242	420	1886	48	655	165	700	34	204
				Rupture Elongation, Percent					
1650°F (1172°K) 50 ksi (344 MN/m^2)	20.8	25.8	27.0	30.0	13.8	25.3	17.9	26.6	19.6

* See Table II

Table VI

VTVS Stress Factors for a T-111 Yield Tangency for Various Starting Temperatures

Starting Temperature °F	Starting Temperature °K	Stress Factor (F) psi/F°	Stress Factor (F) $MN/m^2/K°$
1600	1144	78.3	971
1700	1200	73.4	911
1800	1255	68.9	854
1900	1311	64.7	802
2000	1366	60.7	753
2100	1422	57.1	708
2200	1478	53.7	666
2300	1533	50.6	630
2400	1589	47.6	591
2500	1644	44.9	557
2600	1700	42.4	526
2700	1755	40.2	598
2800	1811	38.1	472
2900	1866	36.1	448
3000	1922	34.3	426

Table VII

Test Conditions for T-111 Alloy Exponentially Varying Stress and Temperature Creep Tests

Test No.	Starting Temperature °F	Starting Temperature °K	Stress Level (Dimensionless)	Half Life Hours	Decay Constant (λ) $hour^{-1}$
S-145	2400	1589	1.00	400	1.73×10^{-3}
S-152	2400	1589	1.00	1000	6.93×10^{-4}
S-154	2400	1589	1.00	2000	3.47×10^{-4}
S-110	2600	1700	1.00	100	6.93×10^{-3}
S-111	2600	1700	1.00	170	4.08×10^{-3}
S-109	2600	1700	1.00	400	1.73×10^{-3}
S-140	2600	1700	0.65	400	1.73×10^{-3}
S-151	2600	1700	0.65	1000	6.93×10^{-4}
S-153	2600	1700	0.65	2000	3.47×10^{-4}
S-130	2800	1811	0.65	100	6.93×10^{-3}
S-133	2800	1811	0.65	170	4.08×10^{-3}
S-137	2800	1811	0.65	400	1.73×10^{-3}

Table VIII

Comparison of Predicted and Observed T-111 Stall Strains

Test No.	Stall Strain, Percent	
	Predicted	Observed
S-145	0.23	1.719
S-152	1.00	2.484
S-154	2.25	5.177
S-110	.50	1.195
S-111	1.00	1.464
S-109	2.90	3.012
S-140	0.25	0.209
S-151	1.10	0.643
S-153	2.50	0.987
S-130	0.40	0.271
S-133	0.85	0.610
S-137	2.50	1.327

Table IX

Conventional (Isostatic, Isothermal) Vacuum Creep Test Results for T-111 Heat 650028

Test No.	Temperature		Stress		Rate Ratio*
	°F	°K	ksi	MN/m^2	
S-68	2560	1678	1.0	6.9	0.648
S-69	1625	1158	30	207	0.246
S-99	2700	1755	0.5	3.4	0.531
S-103	1500	1089	40	276	1.670
S-105	1700	1200	35	241	0.189

* Ratio of the experimentally observed minimum creep rate to that predicted in Equation (9).

Table X

Oxygen Analysis Before and After VTVS Creep Testing of T-111 Alloy

Test No.	ppm Oxygen
Pretest	30
S-145	10
S-152	14
S-154	15
S-110	14
S-111	N.A.*
S-109	12
S-140	15
S-151	18
S-153	13
S-130	14
S-133	14
S-137	14

* Not available

Table XI

Grain Growth Data for T-111 VTVS Tests

Test No.	Test Temperature °F	Test Temperature °K	Half Life Hours	Grain Size µm
Pretest	-	-	-	28
S-145	2400	1589	400	24
S-152	2400	1589	1000	26
S-154	2400	1589	2000	28
S-110	2600	1700	100	24
S-111	2600	1700	170	N.A.*
S-109	2600	1700	400	28
S-140	2600	1700	400	26
S-151	2600	1700	1000	29
S-153	2600	1700	2000	39
S-130	2800	1811	100	28
S-133	2800	1811	170	30
S-137	2800	1811	400	37

* Not available

Table XII

Comparison of Experimentally Observed Stall Strains for Long Time Tests with Predictions Made From Short Time Tests Using a Three Term Correlating Parameter for T-111 VTVS Tests

Test No.	Half Life, Hours	Stall Strain, Percent		Percent Difference
		Predicted	Observed	
S-151	1000	0.618	0.643	3.9
S-153	2000	1.553	0.987	57.3
S-152	1000	1.945	2.484	21.7
S-154	2000	4.891	5.177	5.5

Predicting Equation:

$$\text{Parameter} = \log(\text{half life}) - \frac{35,200}{T_{°F}+460} - 0.75 \log(\text{percent stall strain})$$

Table XIII

Influence of Annealing Treatment on the Grain Size and 1% Creep Life of ASTAR 811C Creep Tested at 2400°F (1589°K) and 15 ksi (103 MN/m^2)

Annealing Treatment			Average Grain Size	1% Creep Life
Time, Hours	Temperature °F	°K	μm	Hours
1.0	3000	1922	10	230
0.5	3600	2255	100	825
5.0	3450	2172	120	348
24.0	3270	2072	150	663
100.0	3000	1922	120	790*
100.0	3000	1922	120	710*

* Results of duplicate tests.

Figure 1. Microstructure of T-111 Heat 650050 annealed 1 hour at 3000°F (1922°K) plus 1 hour at 2400°F (1489°K). Magnification 100X

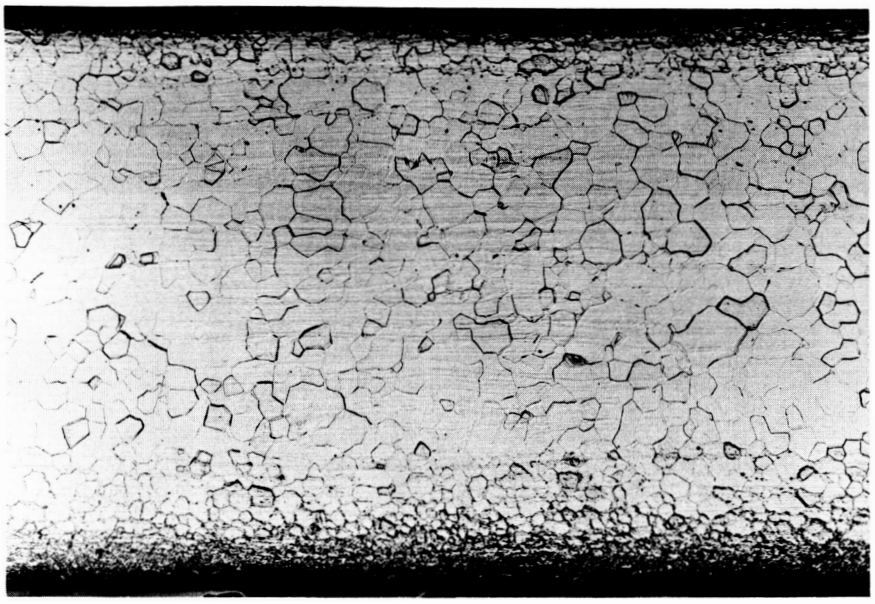

Figure 2. Microstructure of T-111 Heat 650028 annealed 1 hour at 3000°F (1922°K). Magnification 100X

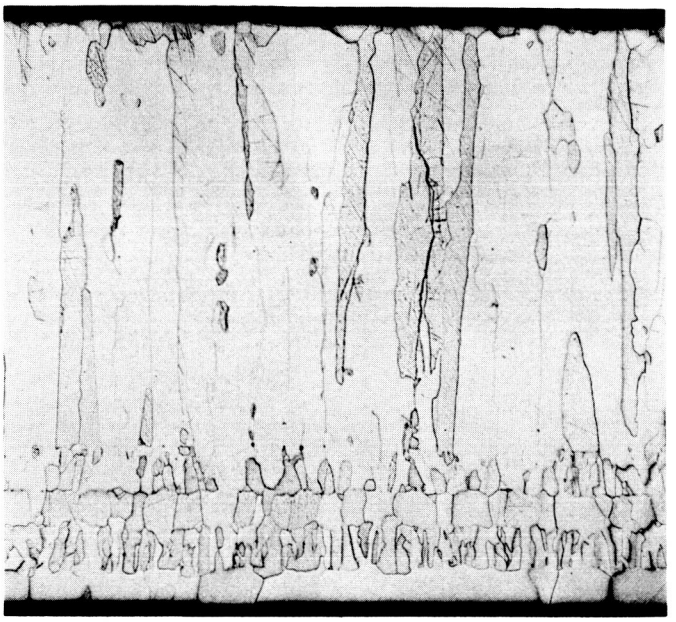

Figure 3. Photomicrograph of CVD tungsten annealed 100 hours at 3272°F (2173°K). Magnification 50X

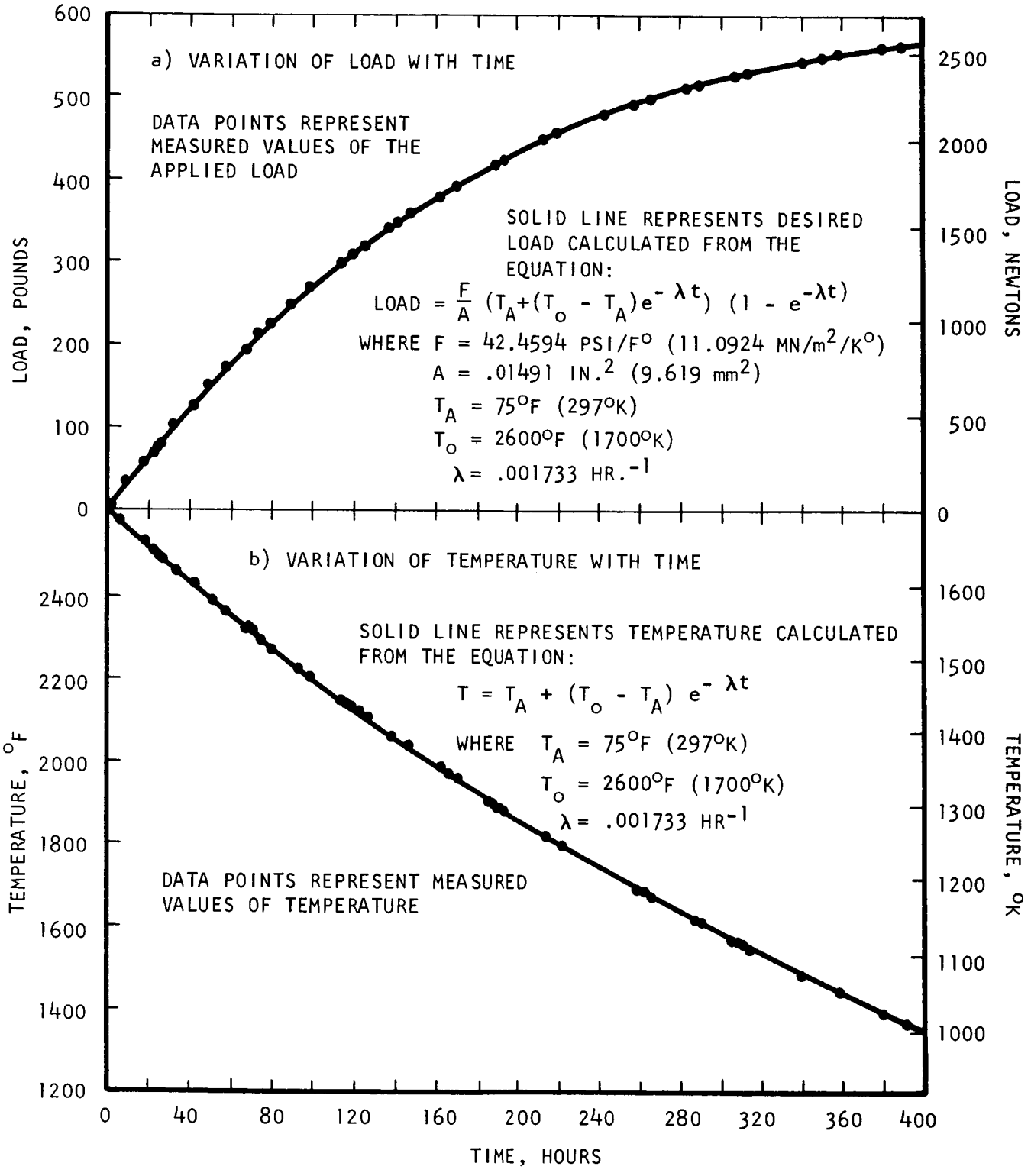

Figure 4. Comparison of desired and experimental load and temperature variation for VTVS Test S-109.

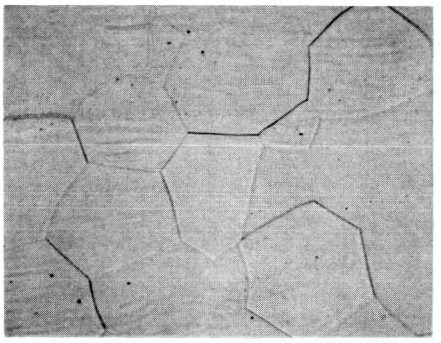

a) Pre-Exposure
GS = 28 O = 104 ppm

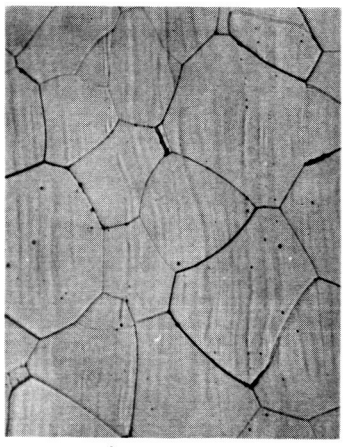

b) 1K-1800* GS=27
Vacuum O=24 ppm

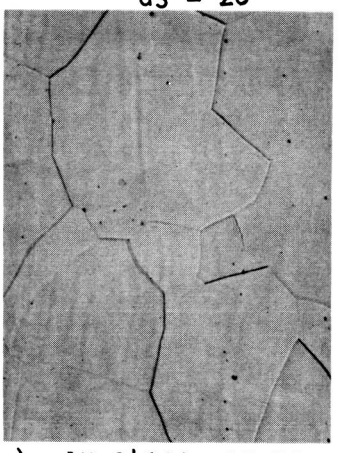

c) 1K-2400* GS=39
Vacuum O=29 ppm

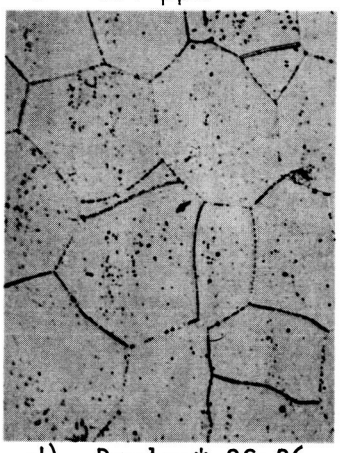

d) Duplex* GS=26
Vacuum O=30 ppm

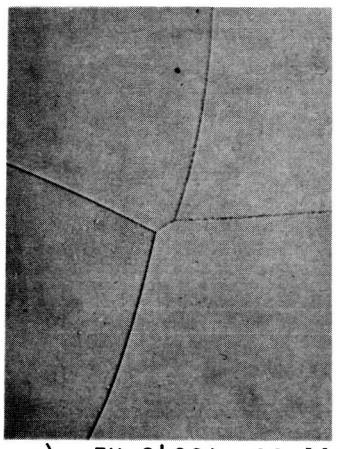

e) 5K-2400* GS=110
Vacuum O=4 ppm

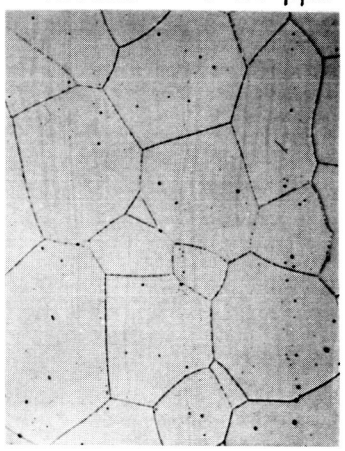

f) 1K-1800* GS=27
Lithium O=12 ppm

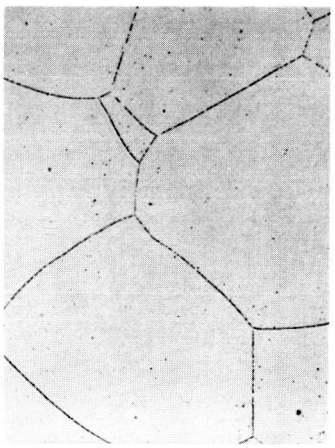

g) 1K-2400* GS=43
Lithium O=3 ppm

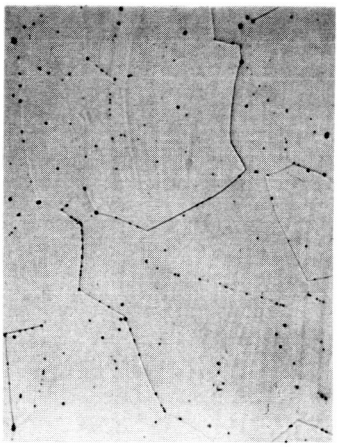

h) Duplex* GS=28
Lithium O=4 ppm

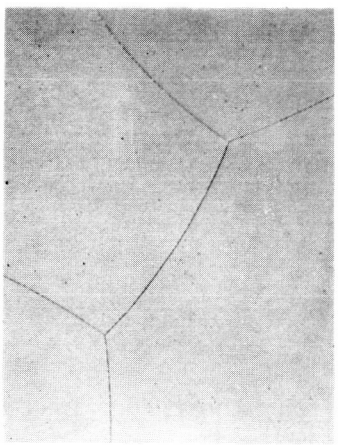

i) 5K-2400* GS=119
Lithium O=6 ppm

Figure 5. Influence of long time elevated temperature exposure to lithium and to 10^{-9} torr vacuum on the microstructure of T-111 alloy annealed 1 hour at 3000°F (1922°K) plus 1 hour at 2400°F (1589°K). Original magnification 1000X, reduced 50% for reproduction. Grain size, "G.S." in μm. "O" refers to oxygen analysis.

* See Table II for explanation of exposure codes.

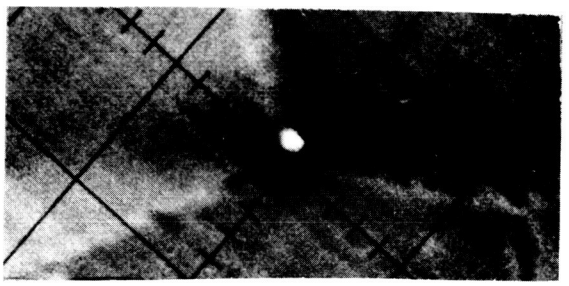

a) Specimen Current Image.
Original magnification 1600X.
Enlarged 250% for reproduction.

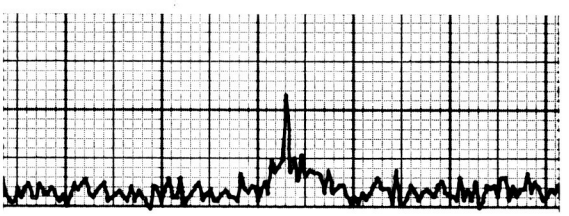

b) Oxygen X-ray intensity.

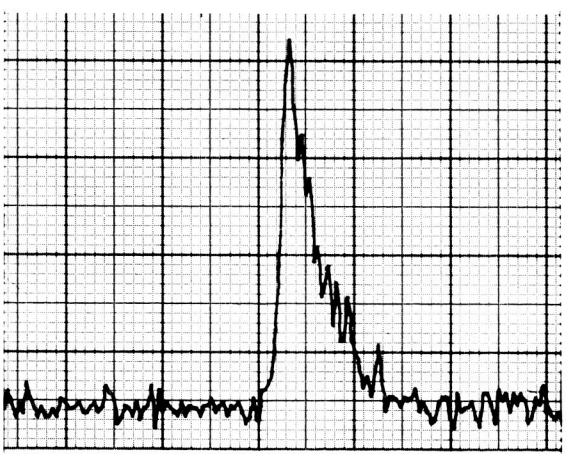

c) Hafnium X-ray intensity.

Figure 6. Electron probe results on the T-111 duplex vacuum specimen showing hafnium and oxygen enrichment in the precipitate.

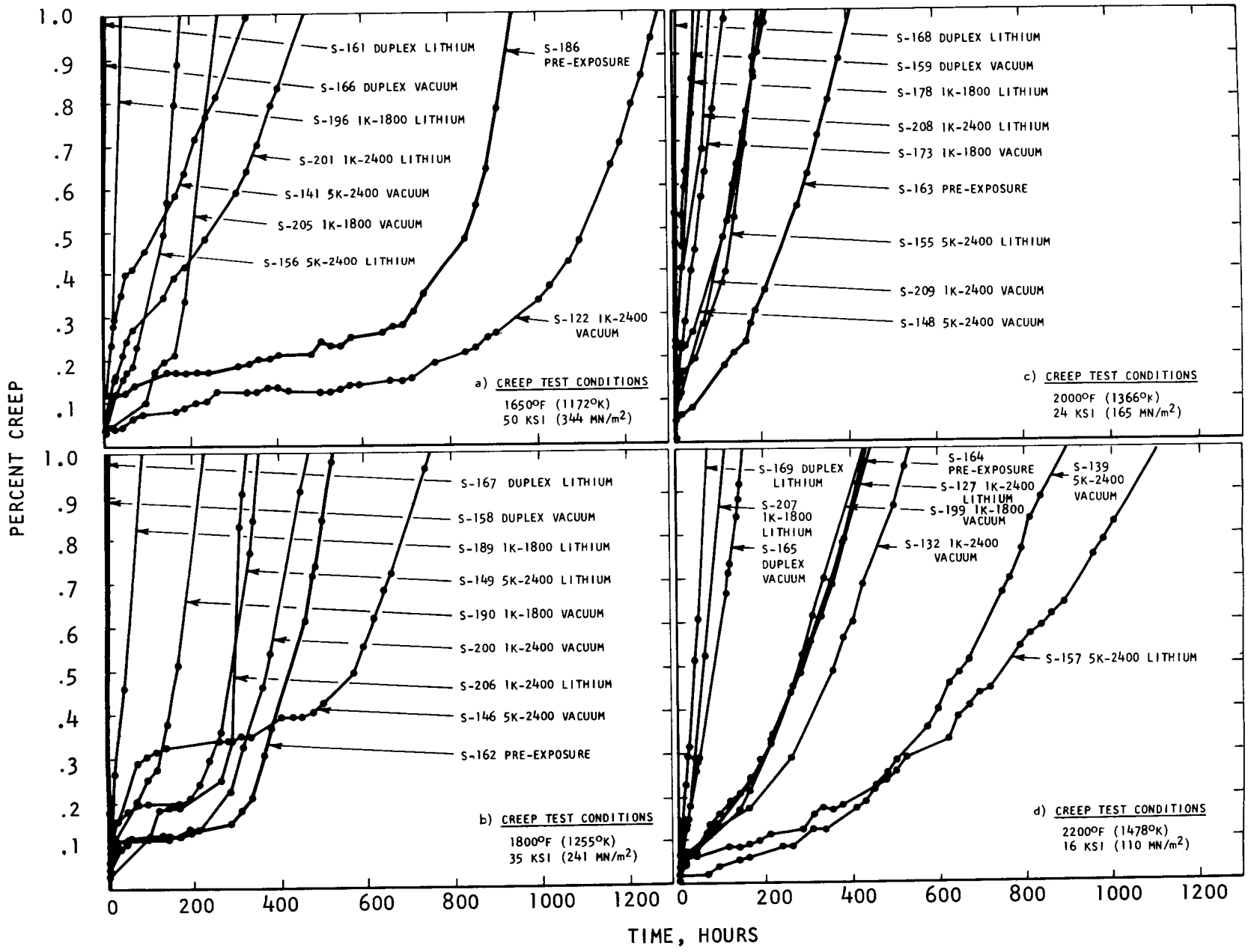

Figure 7a-d. Ultrahigh vacuum creep test data for T-111 Heat 650050 annealed 1 hour at 3000°F (1922°K) plus 1 hour at 2400°F (1589°K) and exposed to lithium or to 10^{-9} torr vacuum for the indicated times and temperatures.

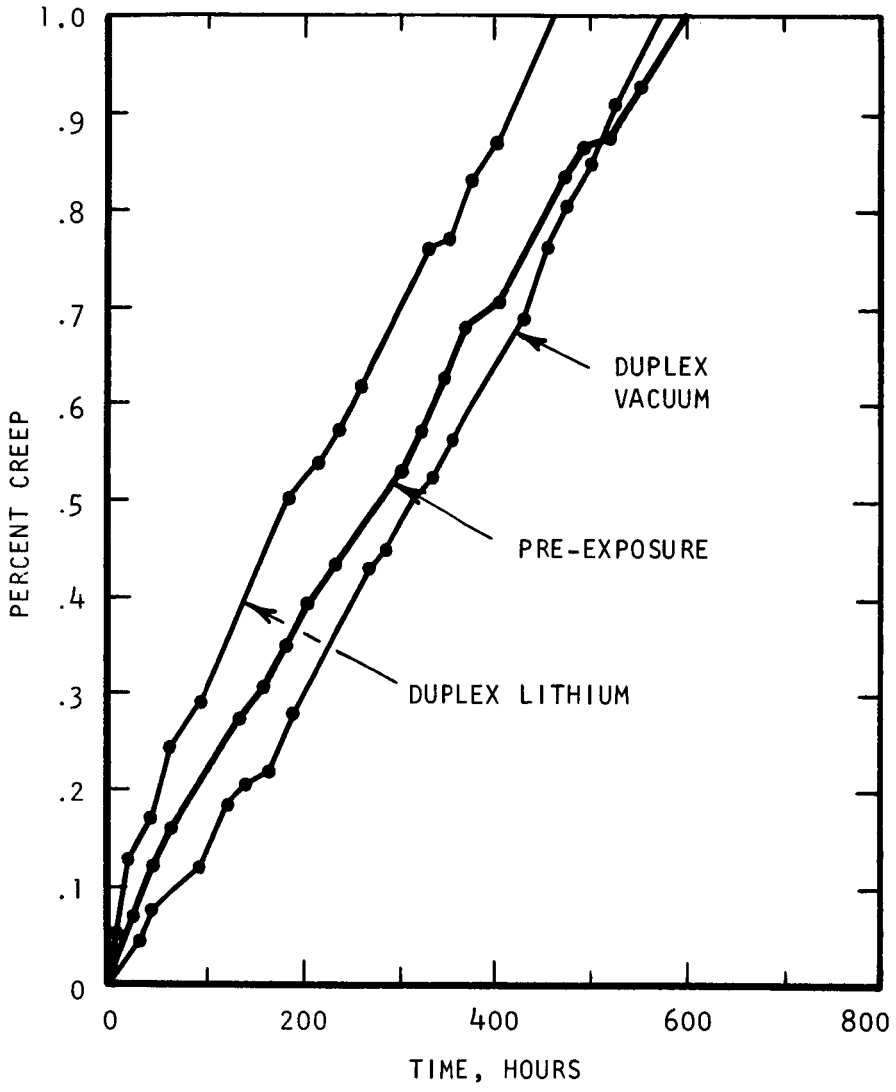

Figure 7e. Creep test conditions 2400°F (1589°K) and 5 ksi (34 MN/m^2).

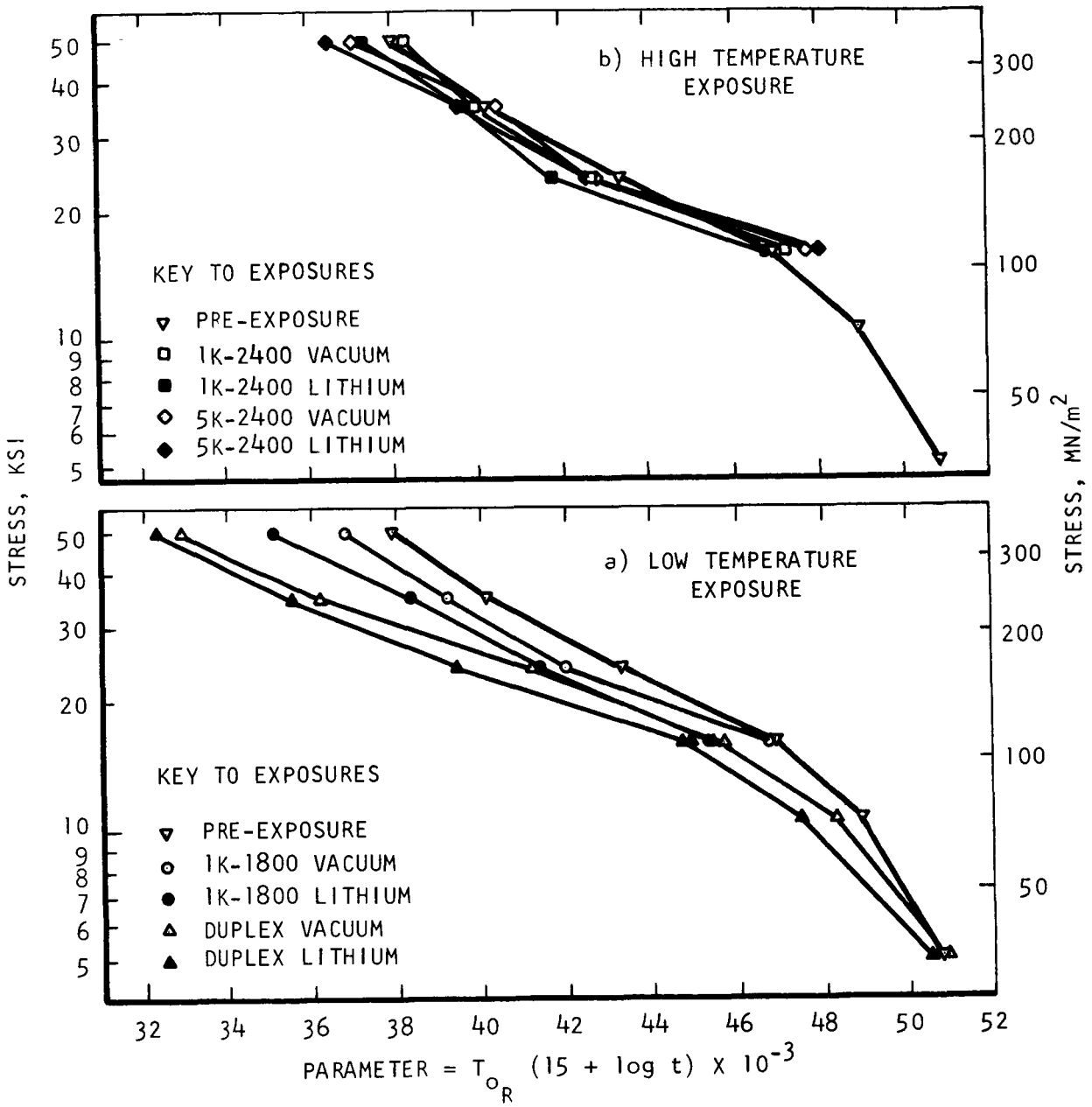

Figure 8. Influence of long time elevated temperature exposure to lithium and to 10^{-9} torr vacuum on the 1% creep life (hours) of T-111 alloy.

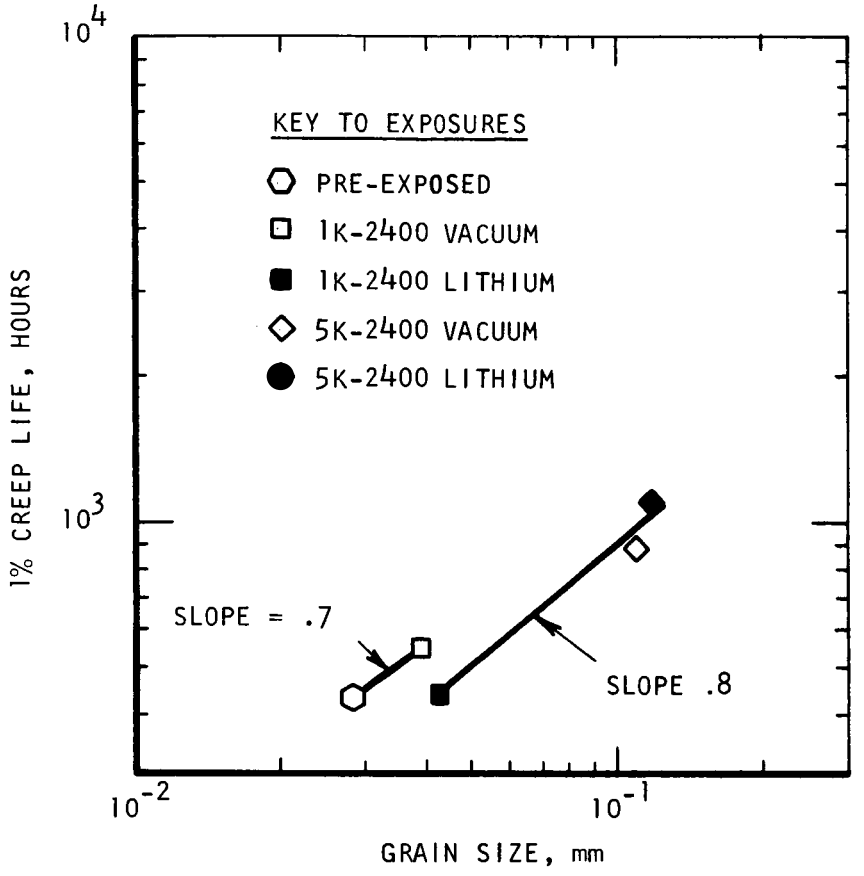

Figure 9. Influence of grain size on the 1% creep life of T-111 alloy exposed to lithium and to vacuum at 2400°F (1589°K) for the indicated periods. Creep test conditions are 2200°F (1478°K) and 16 ksi (110 MN/m^2).

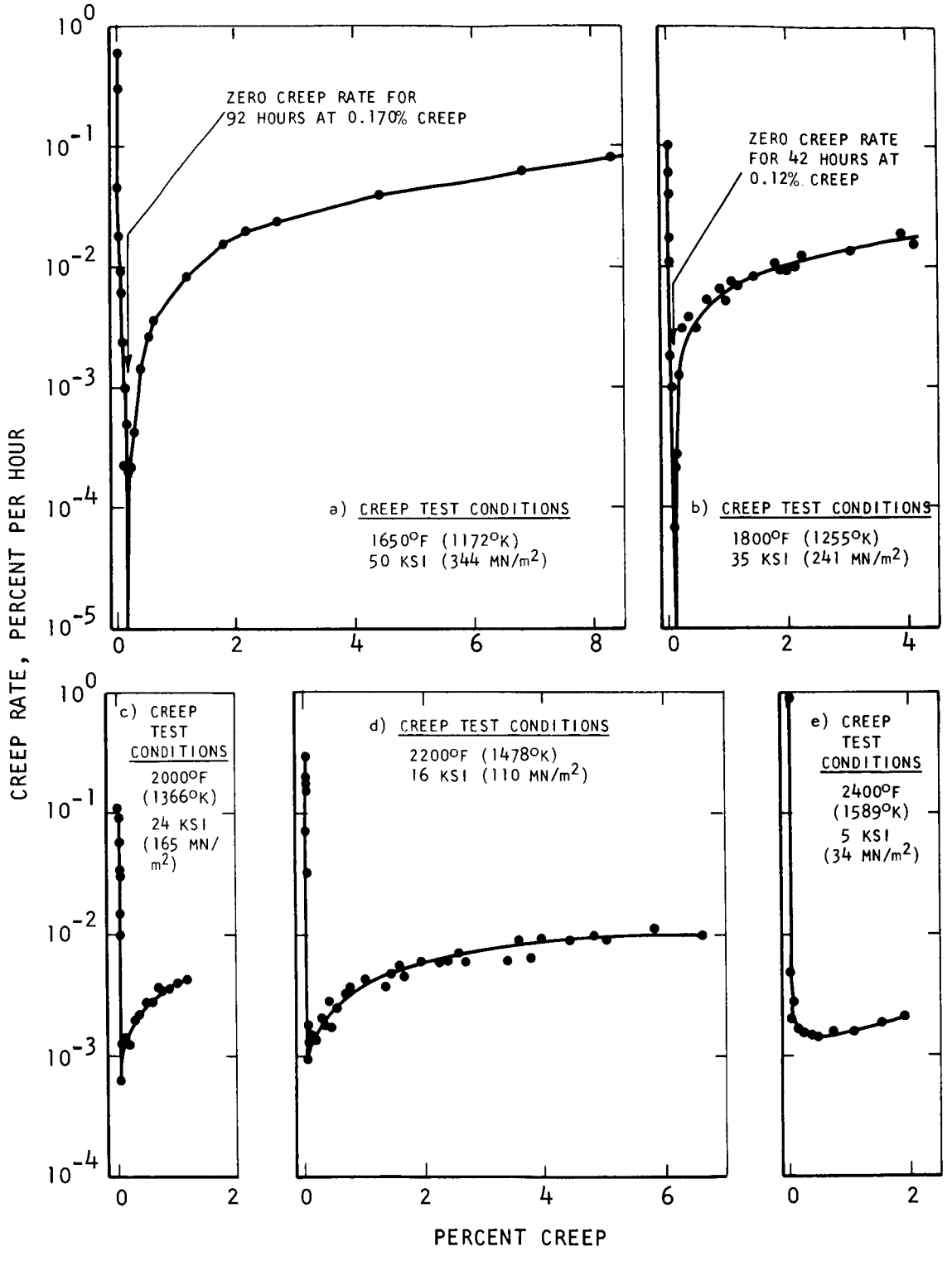

Figure 10. Influence of creep test temperature on the creep curve shape for unexposed T-111 alloy.

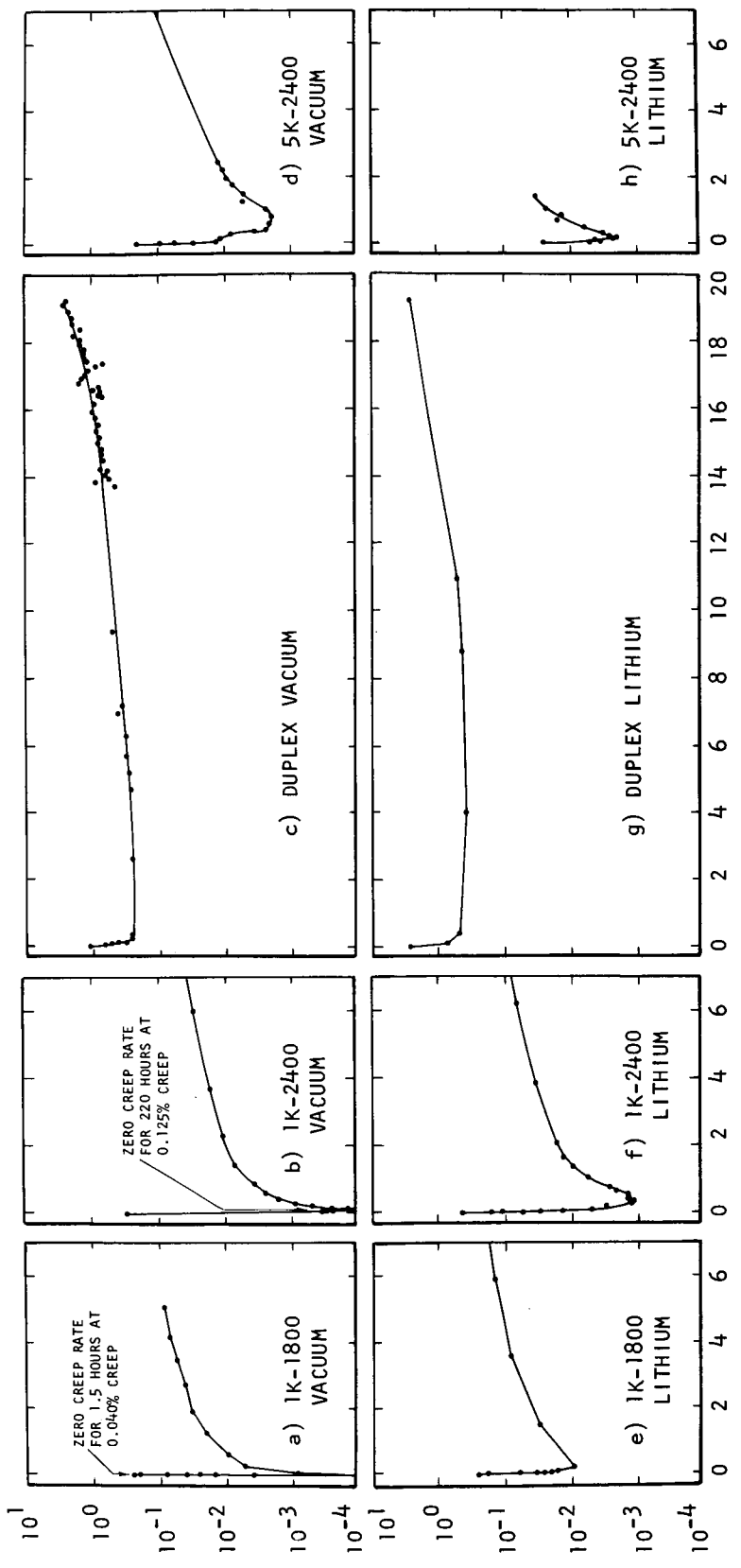

Figure 11. Influence of exposure to lithium and to 10^{-9} torr vacuum on the creep curve shape for T-111 alloy creep tested at 1650°F (1172°K) and 50 ksi (344 MN/m^2).

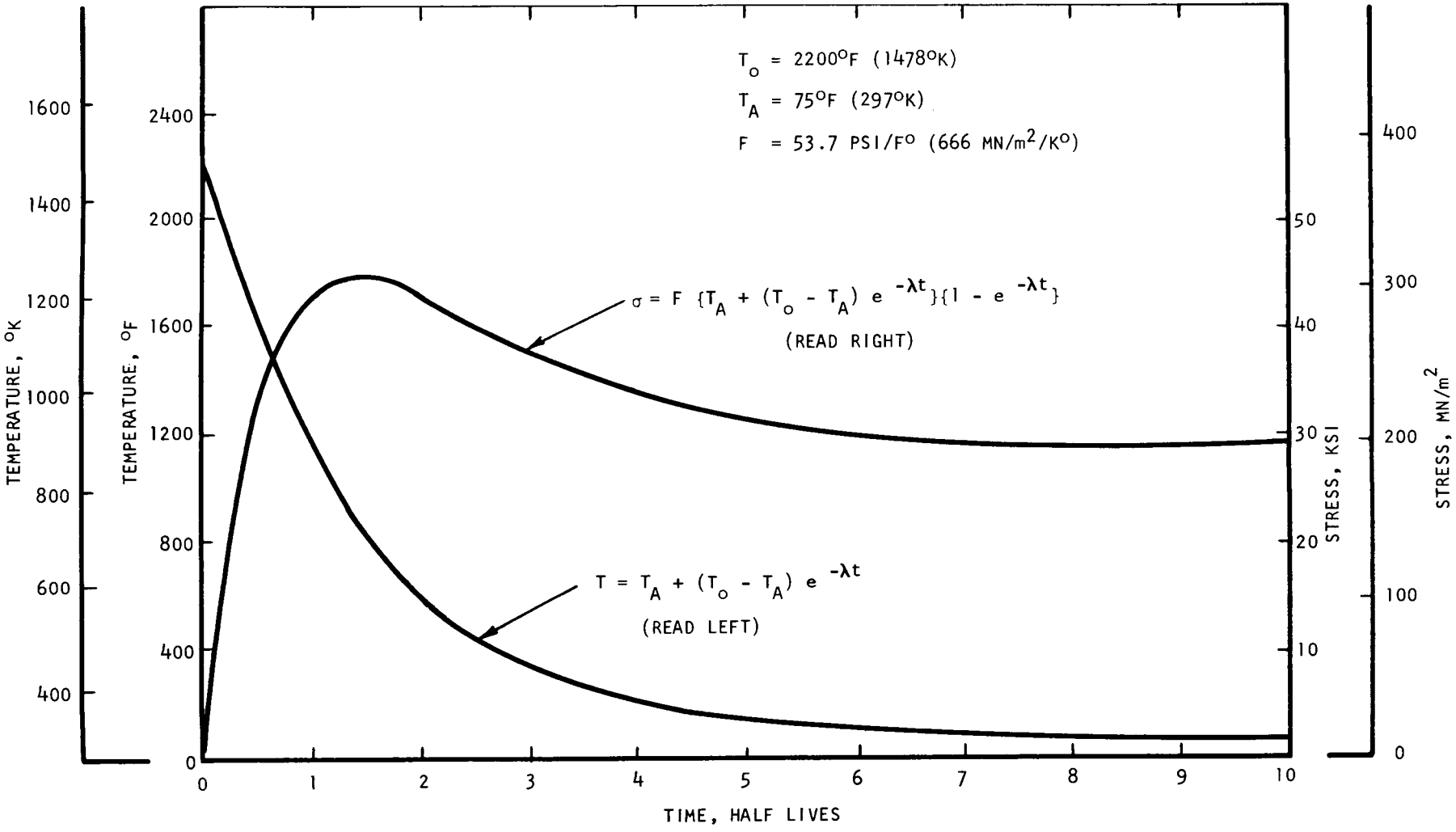

Figure 12. Predicted variation of temperature and stress with time for radioisotope capsule service.

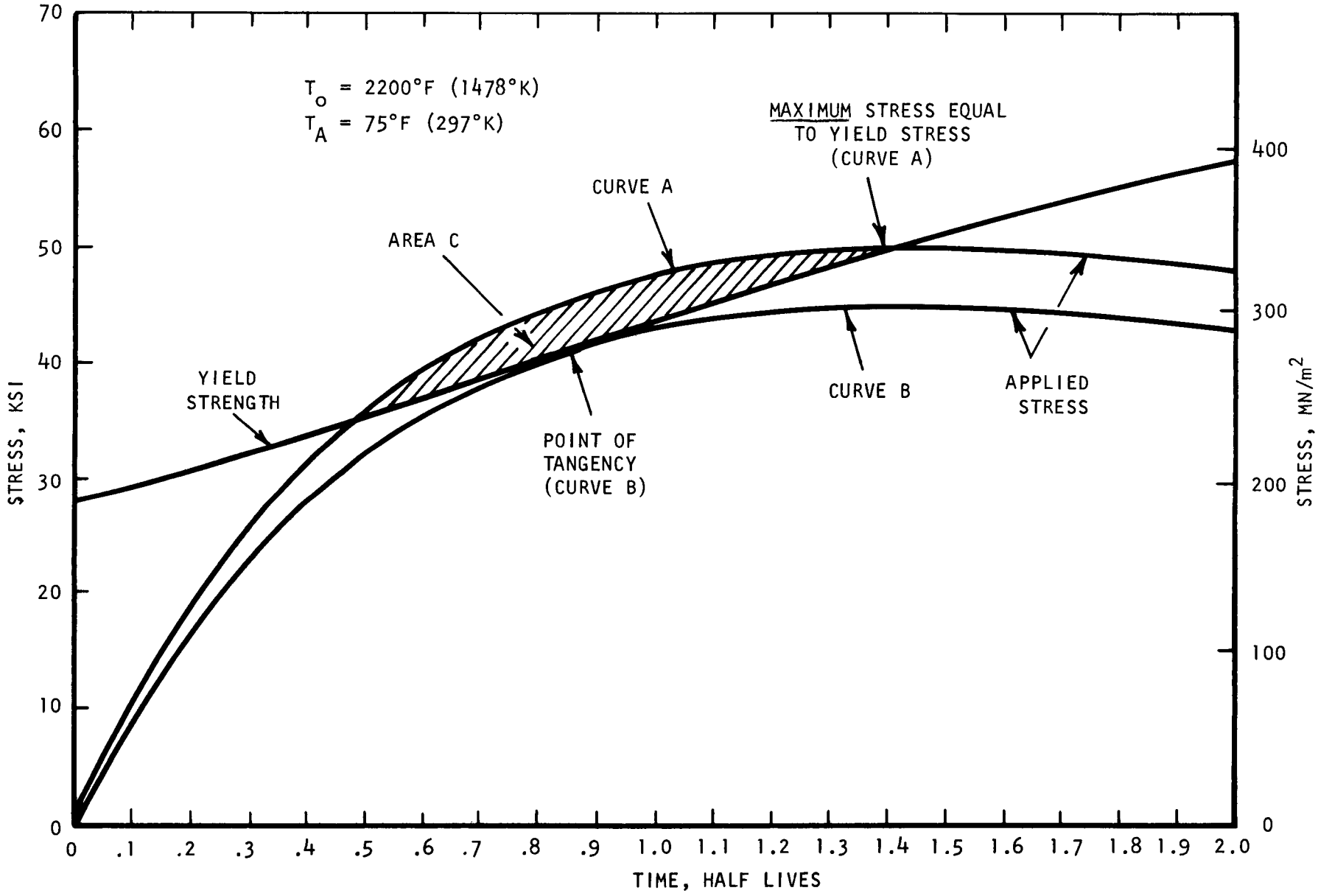

Figure 13. Variation of stress and yield strength of T-111 alloy with time in radioisotope capsule. Upper curve (A) calculated by equating stress to strength at peak stress. Lower curve (B) calculated to be tangent to the yield strength curve.

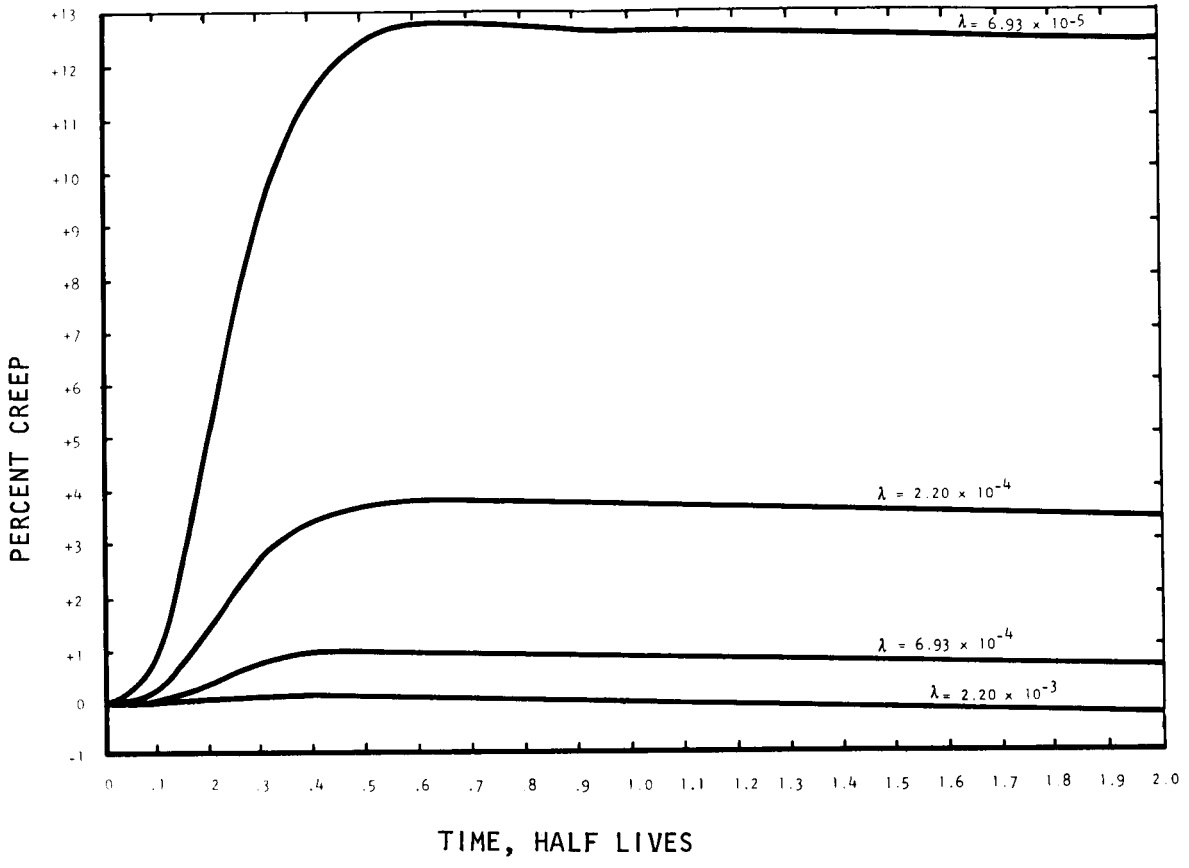

Figure 14. Calculated variable stress and temperature creep curves for T-111 alloy. Starting temperature = 2400°F (1589°K); stress level = 1 (dimensionless see text, Page 13 for explanation of stress level specification).

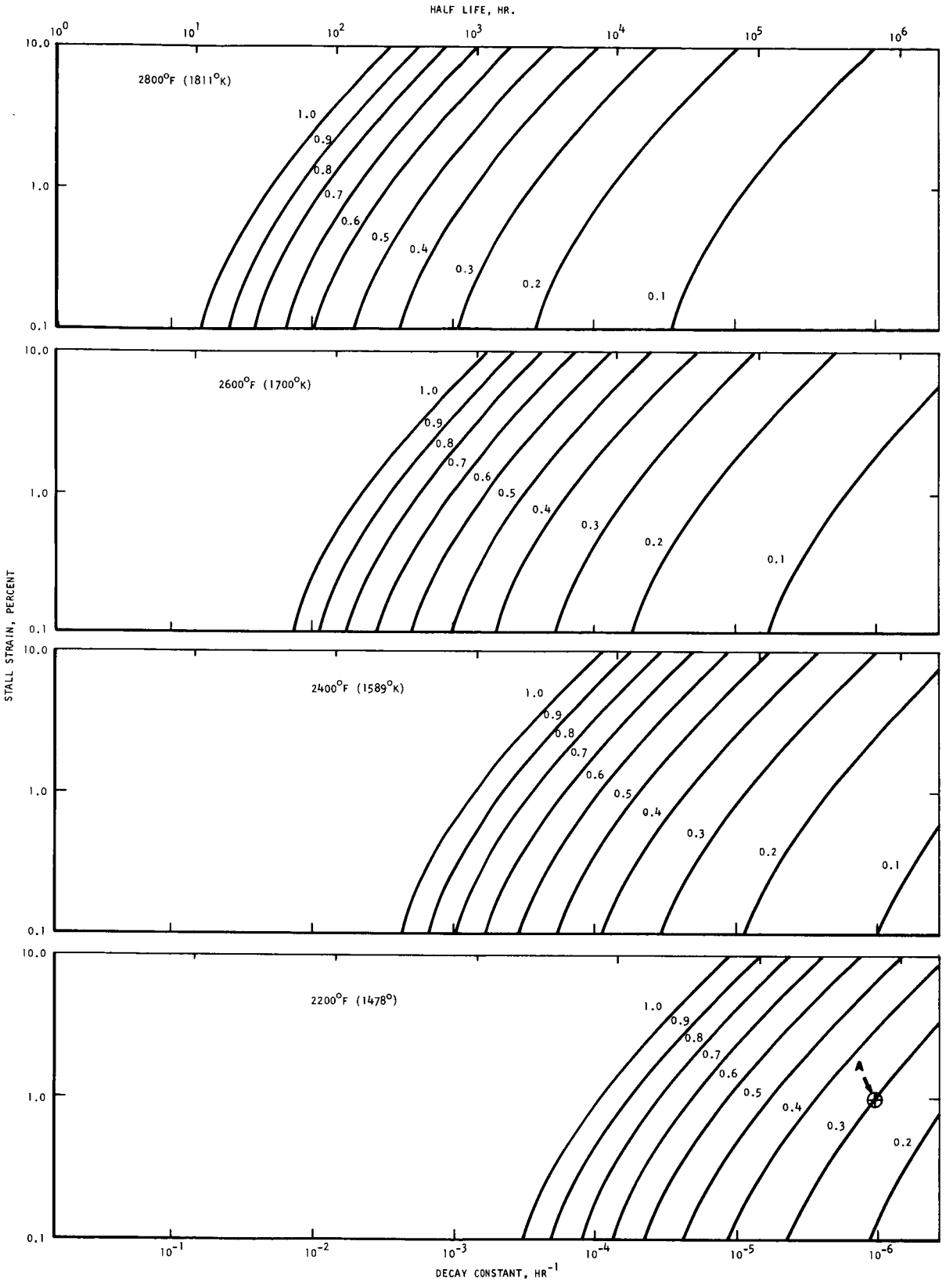

Figure 15. Influence of decay constant on the predicted stall strain of T-111 alloy for various starting temperatures and stress levels (indicated on curves).

4509 C

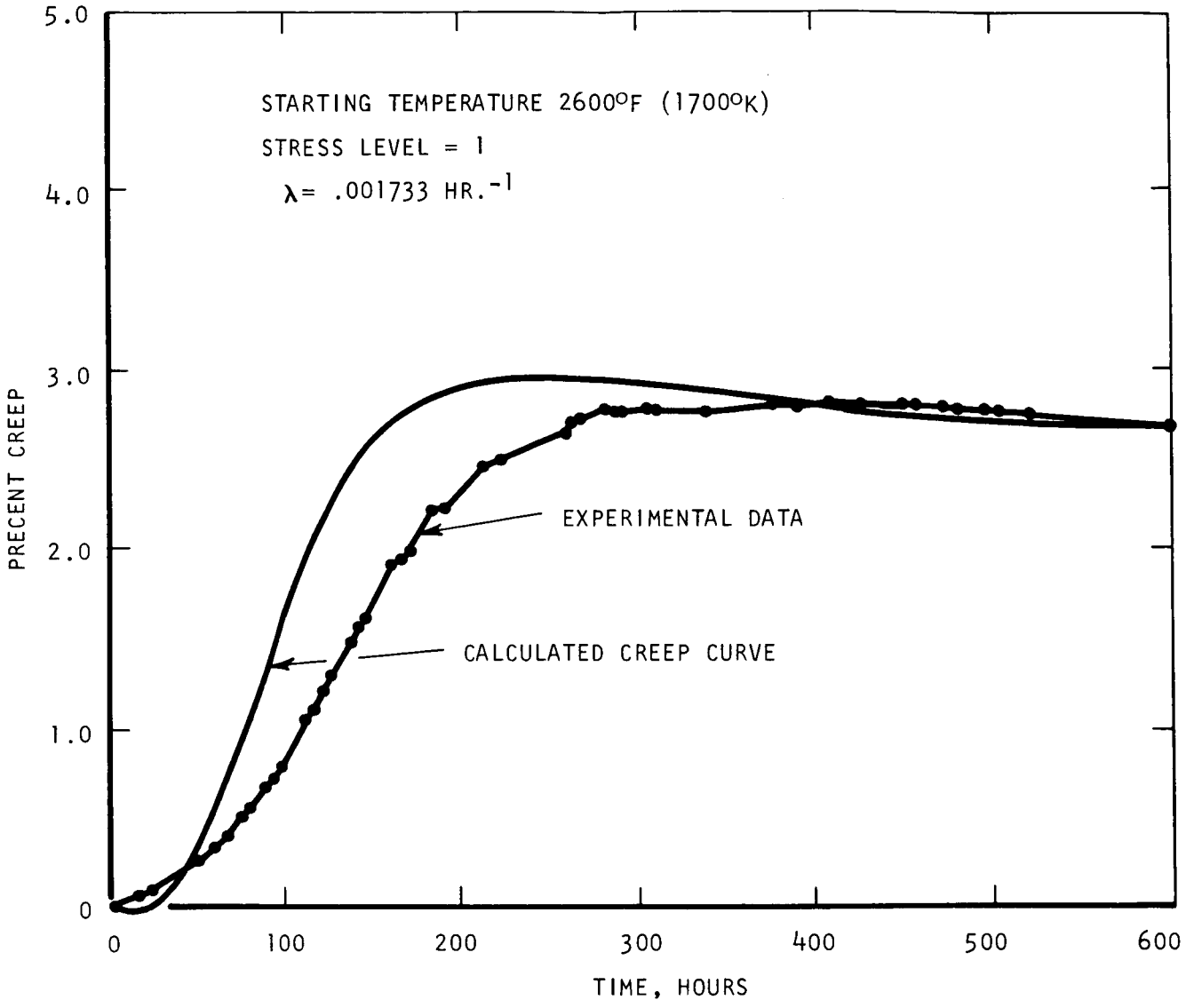

Figure 16. Comparison of calculated and experimental creep curves for T-111 exponentially varying stress and temperature test S-109. Starting temperature = 2600°F (1700°K), stress level = 1, decay constant = .001733 hour^{-1}.

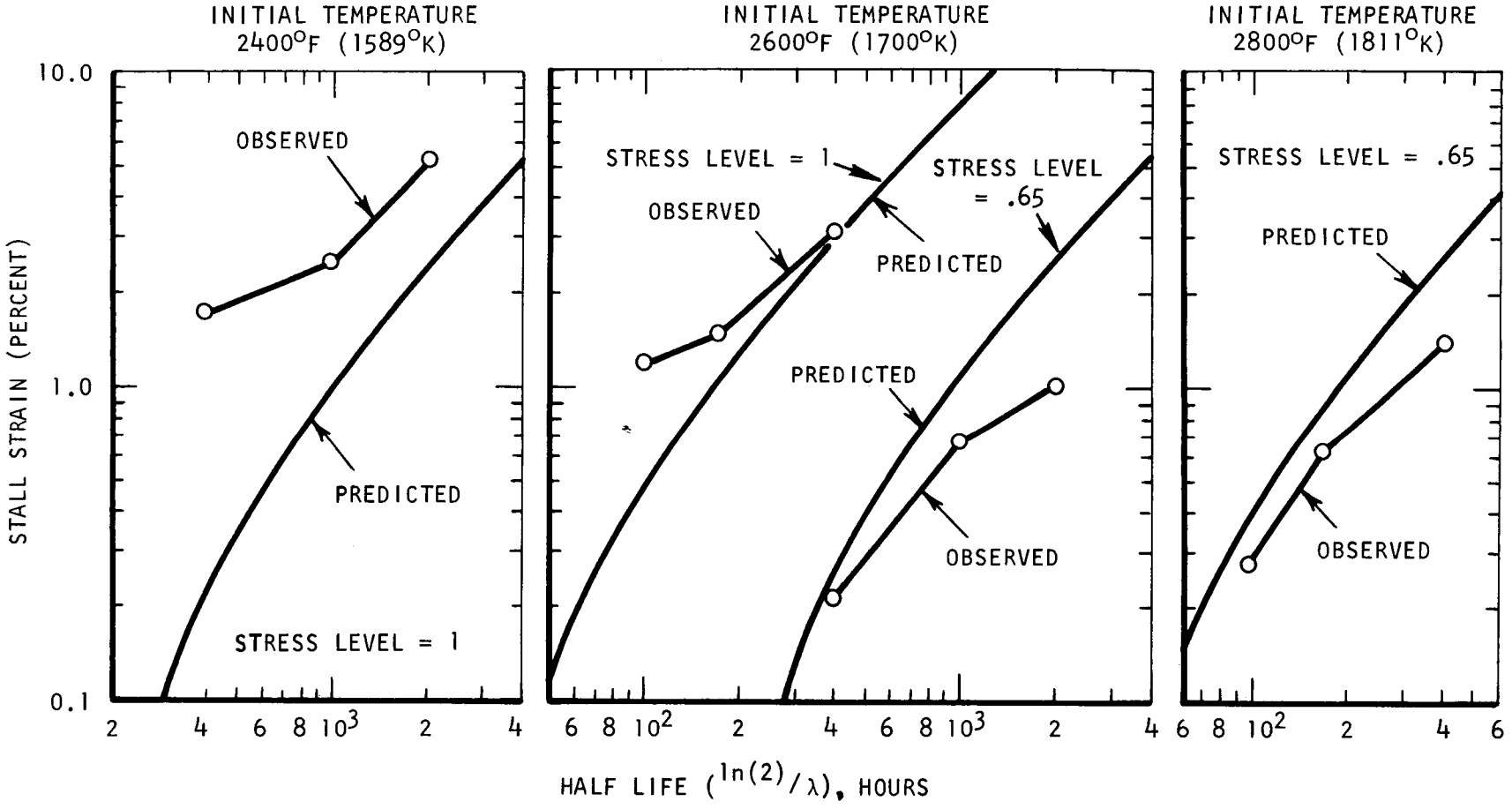

Figure 17. Comparison of predicted and observed stall strains for T-111 alloy tested with exponentially varying stress and temperature.

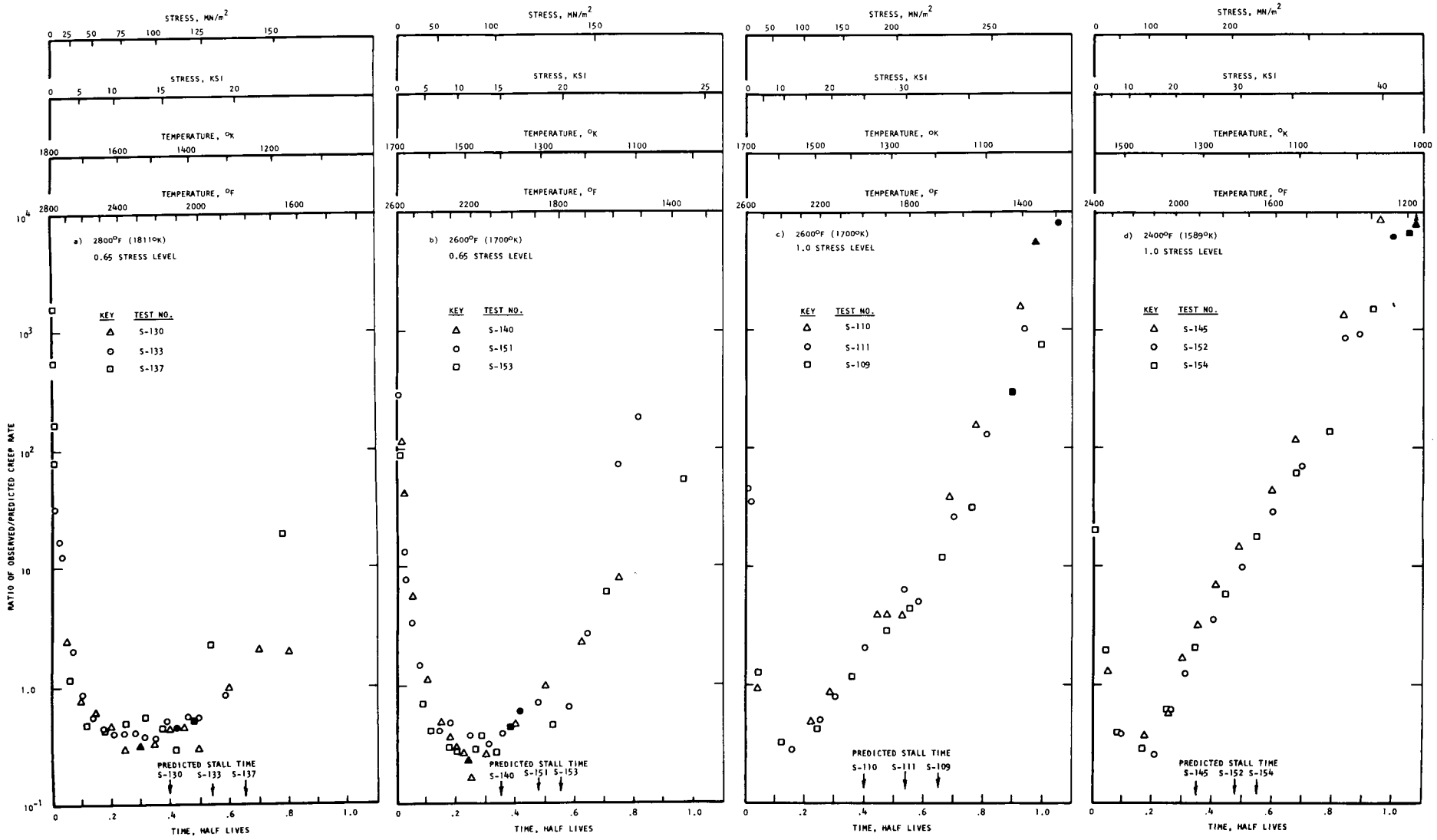

Figure 18. Influence of starting temperature, stress level, and test time (in half lives) on the ratio of the observed to the predicted creep rate for T-111 alloy tested with continuously varying stress and temperature. Note that filled data points represent the time at which stall occurred.

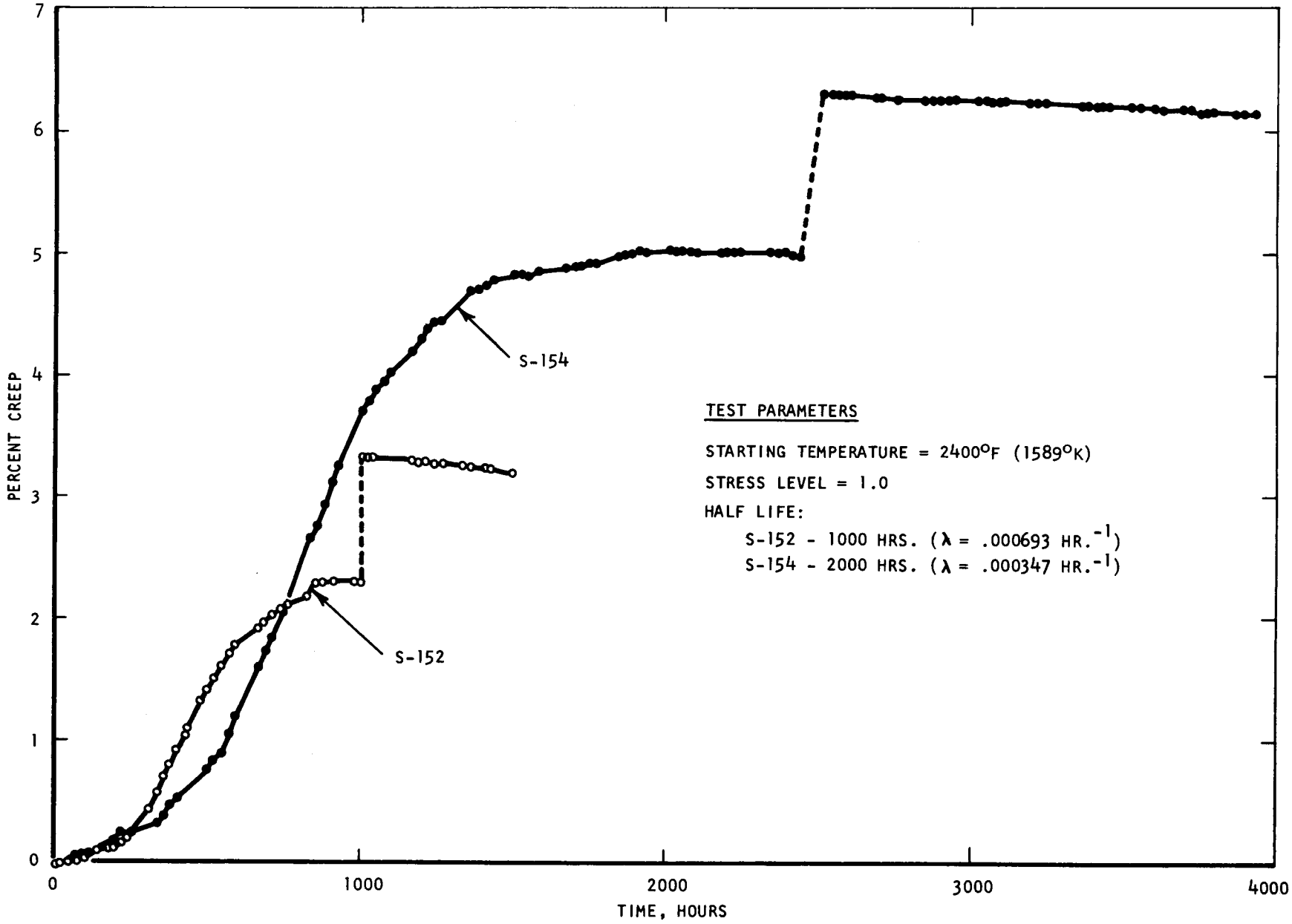

Figure 19. Creep data for T-111 tests S-152 and S-154. Note unexplained discontinuous jumps in both curves.

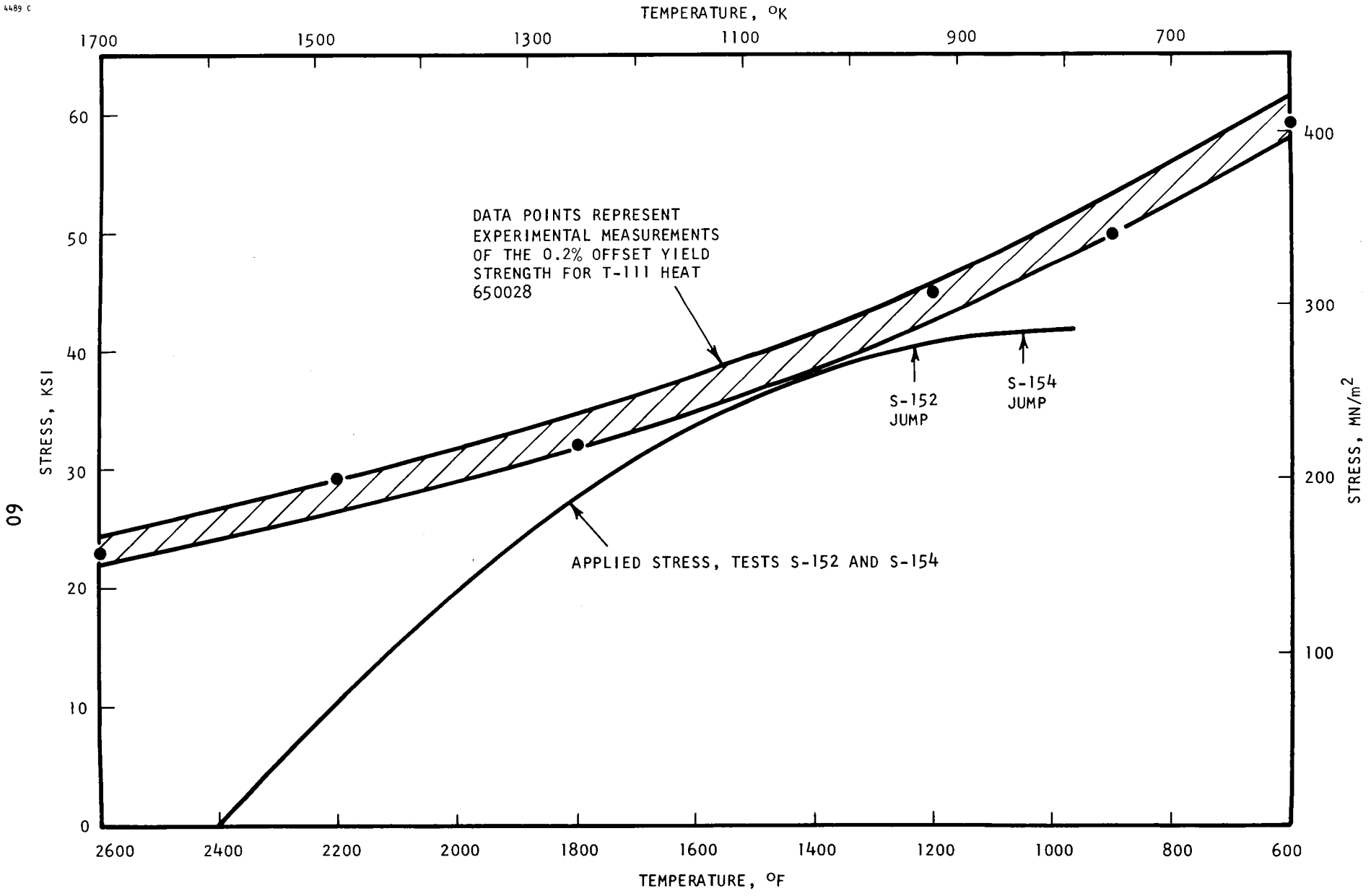

Figure 20. Comparison between applied stress and material yield strength for T-111 tests which exhibited discontinuous creep.

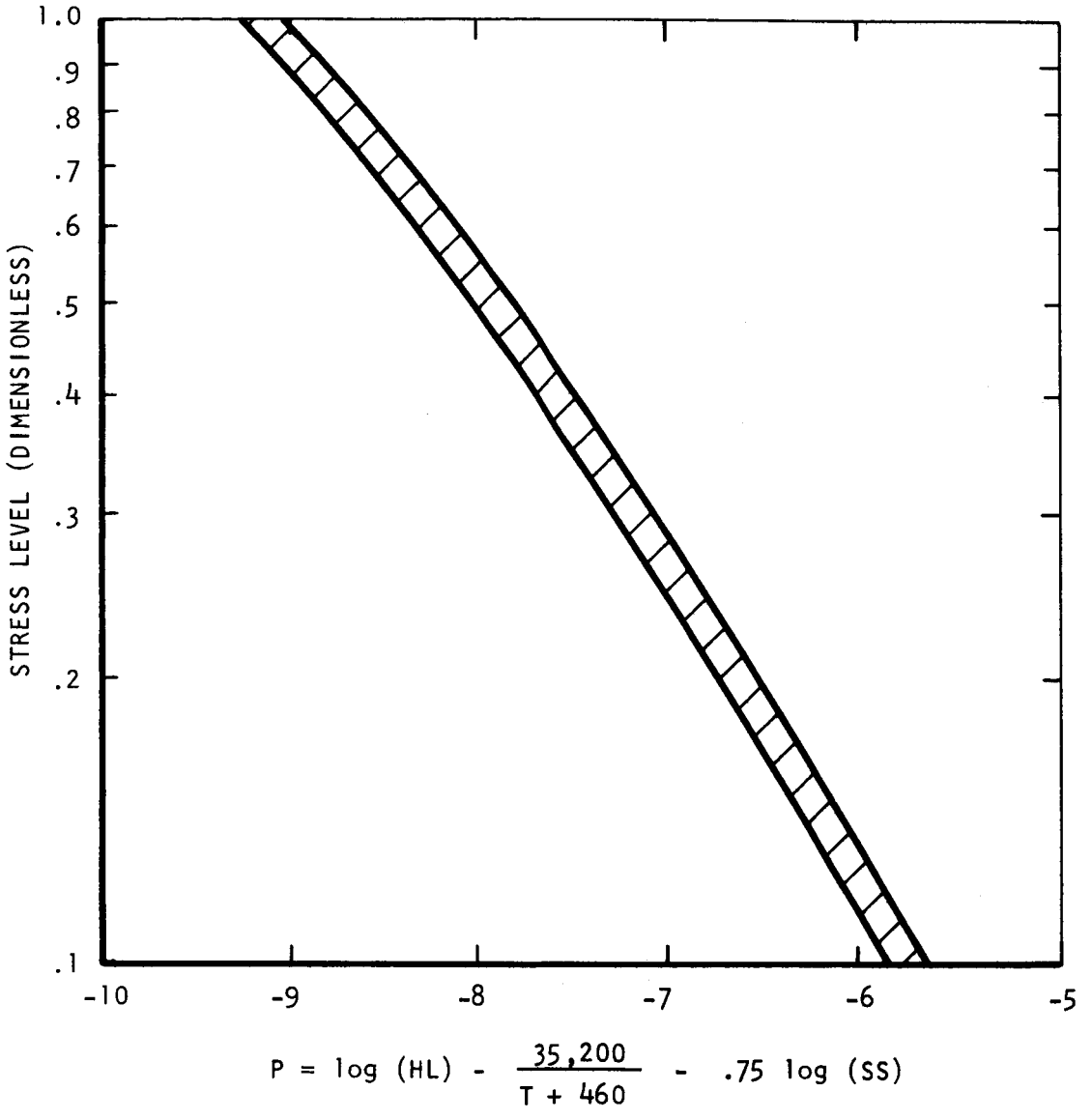

Figure 21. Three-term parametric representation of calculated T-111 stall strain data. HL represents half life in hours, T is starting temperature in °F, and SS is stall strain in percent.

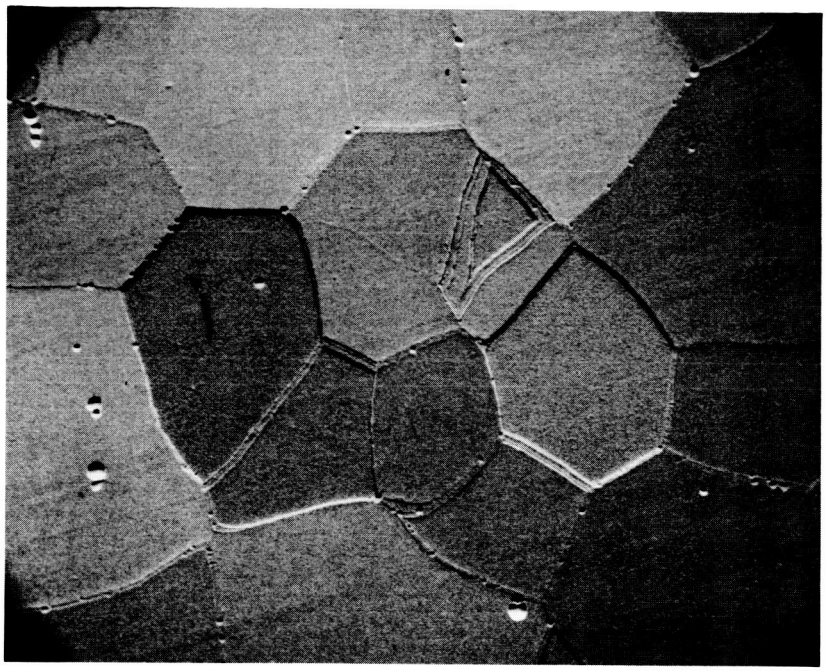

a) Scanning electron micrograph - 540X (note etch pitting)

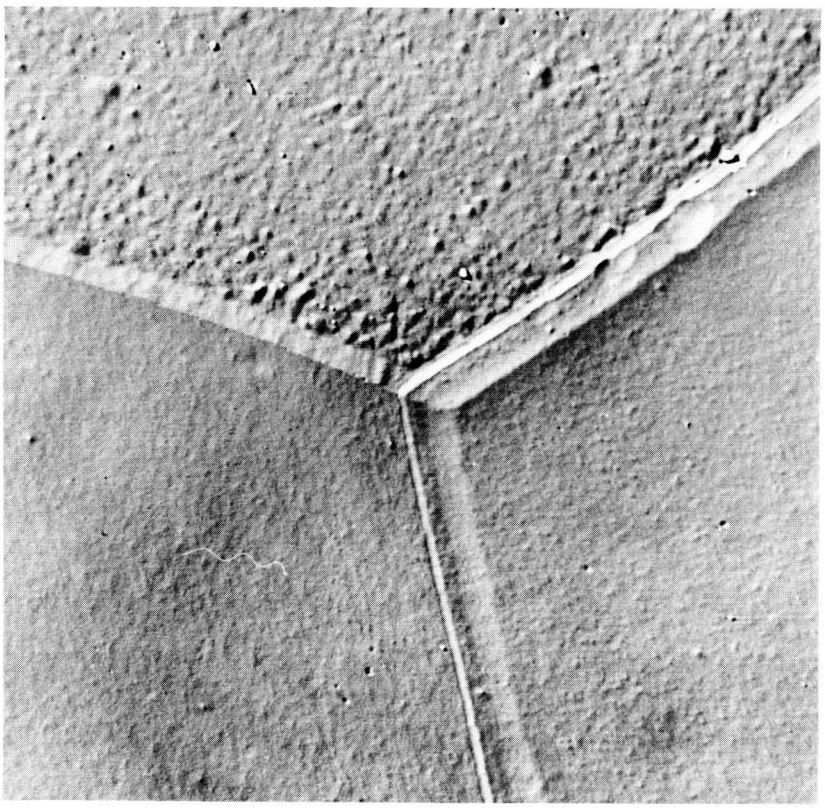

b) Transimission electron micrograph of two stage (cellulose nitrate/carbon) replica. 5000X

Figure 22. Photomicrographs of ASTAR 811C annealed 1/2 hour at 3600°F (2255°K). Average grain size ≃0.1mm.

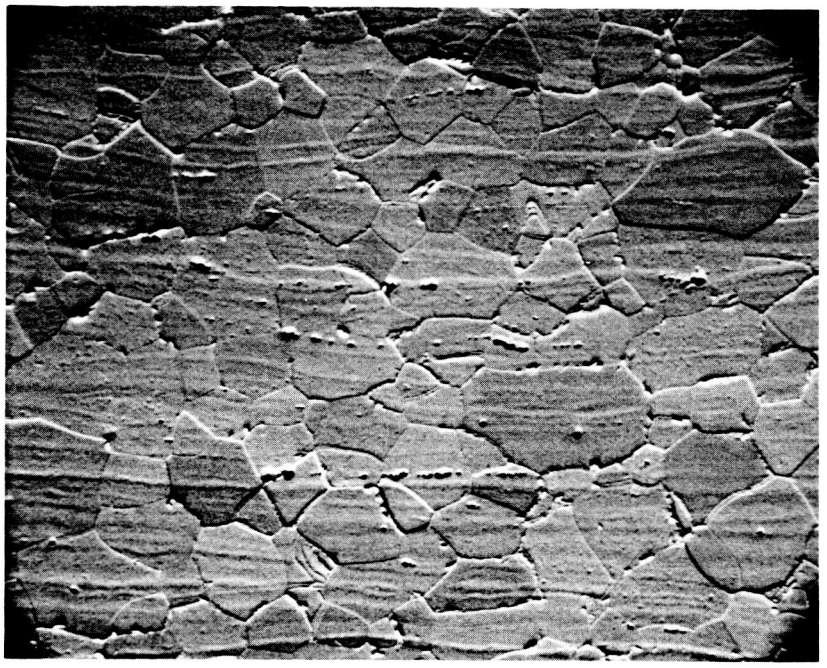

a) Scanning electron micrograph - 540X

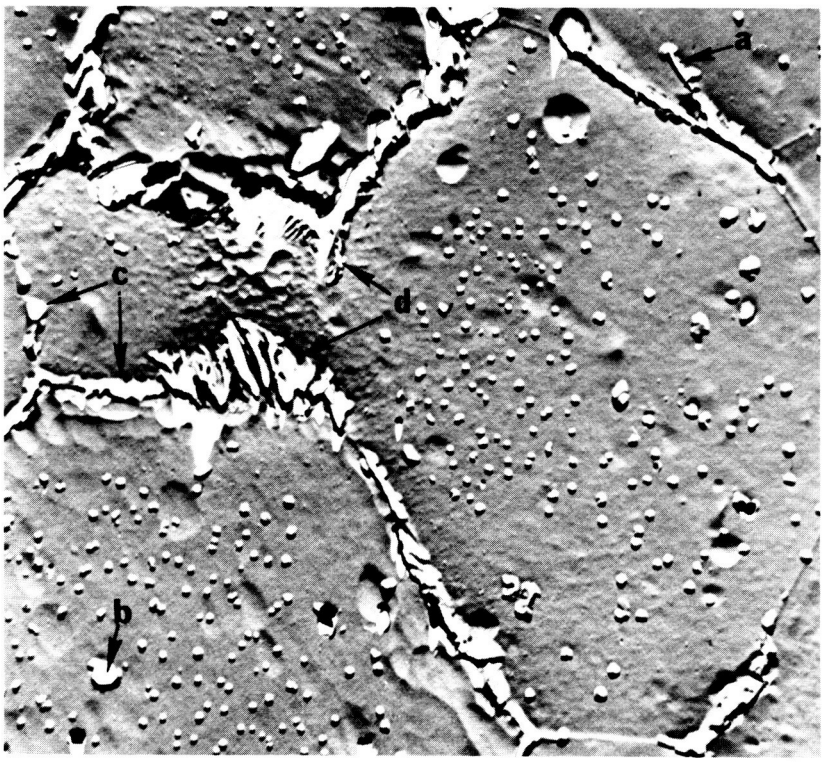

b) Transmission electron micrograph of two-stage (cellulose nitrate/carbon) replica. 5000X

Figure 23. Photomicrographs of ASTAR 811C annealed 1 hour at 3000°F (1922°K). Average grain size ≃0.01mm. Lettered arrows on micrograph refer to explanations given in the text.

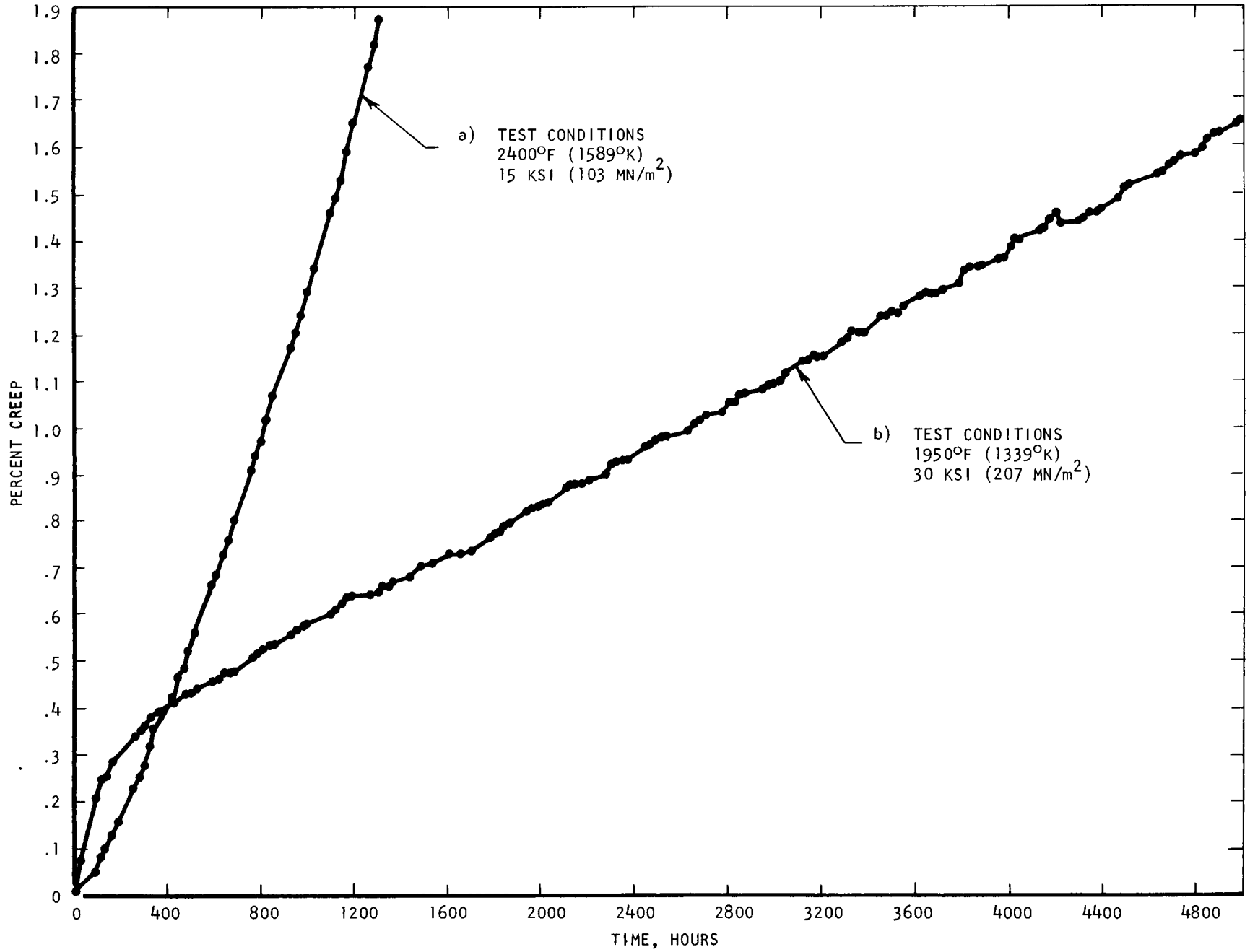

Figure 24. Typical creep curves for ASTAR 811C annealed 1/2 hour at 3600°F (2255°K).

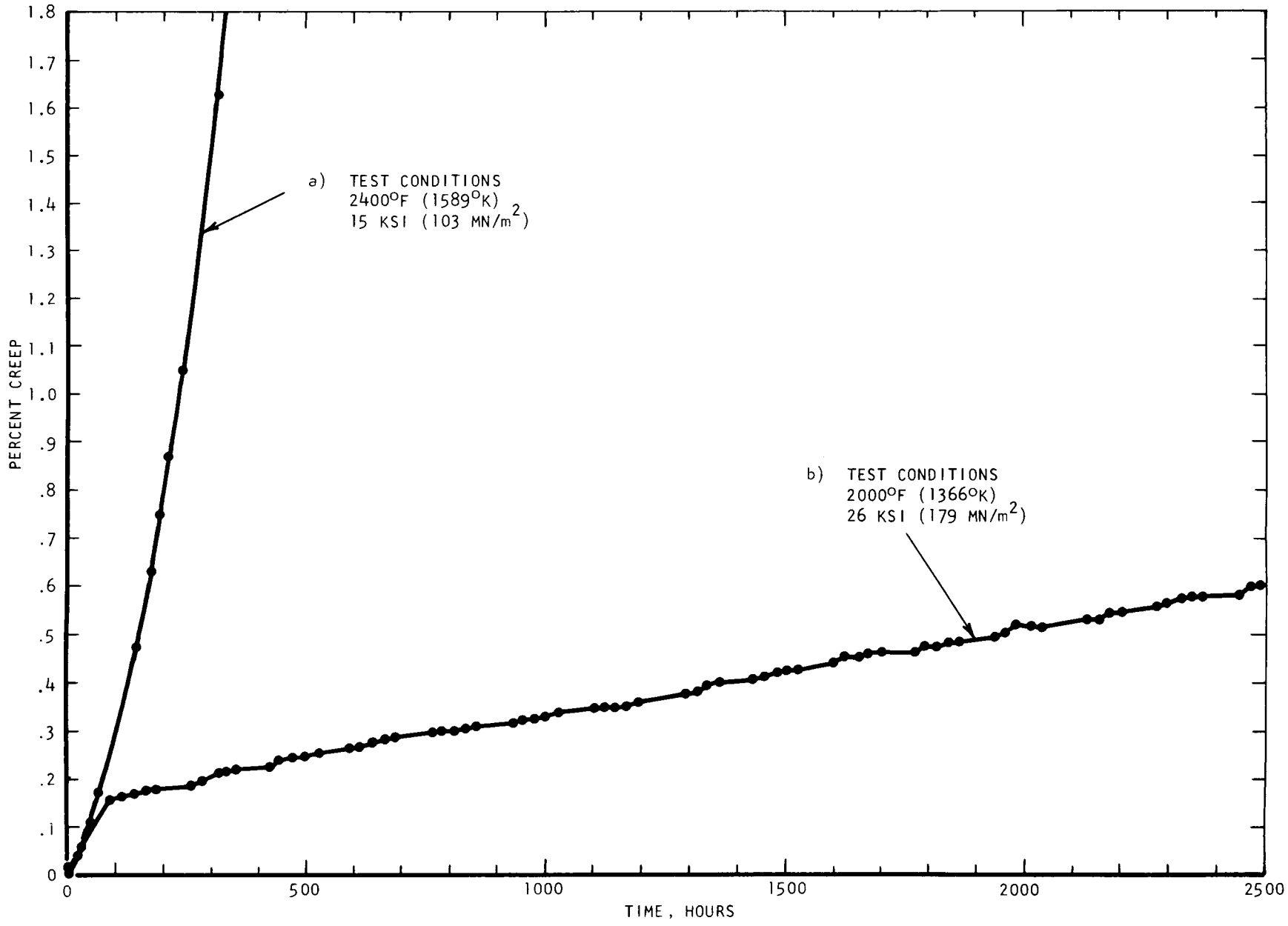

Figure 25. Typical creep curves for ASTAR 811C annealed 1 hour at 3000°F (1922°K).

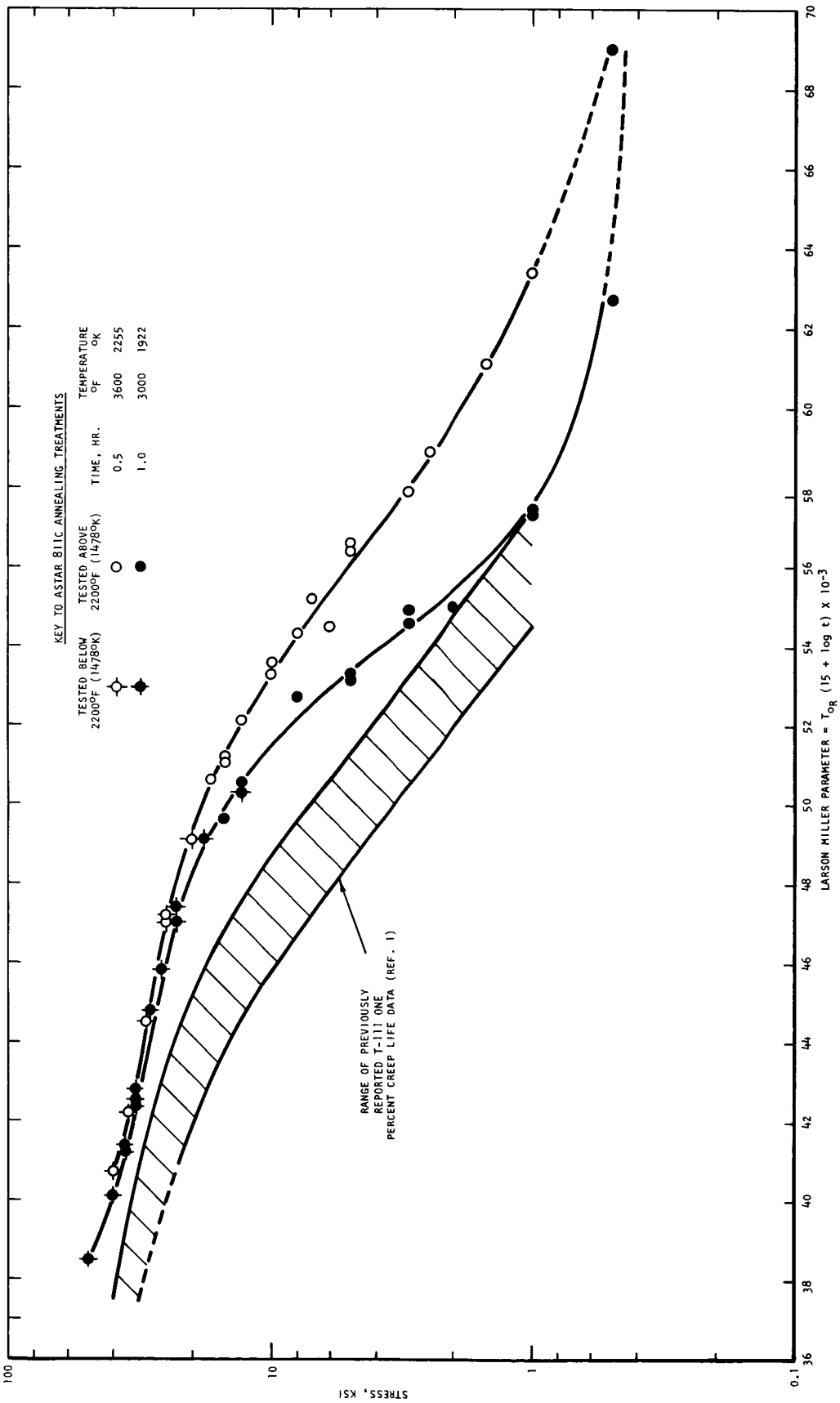

Figure 26. Parametric representation of 1% creep life data for T-111 and ASTAR 811C alloys.

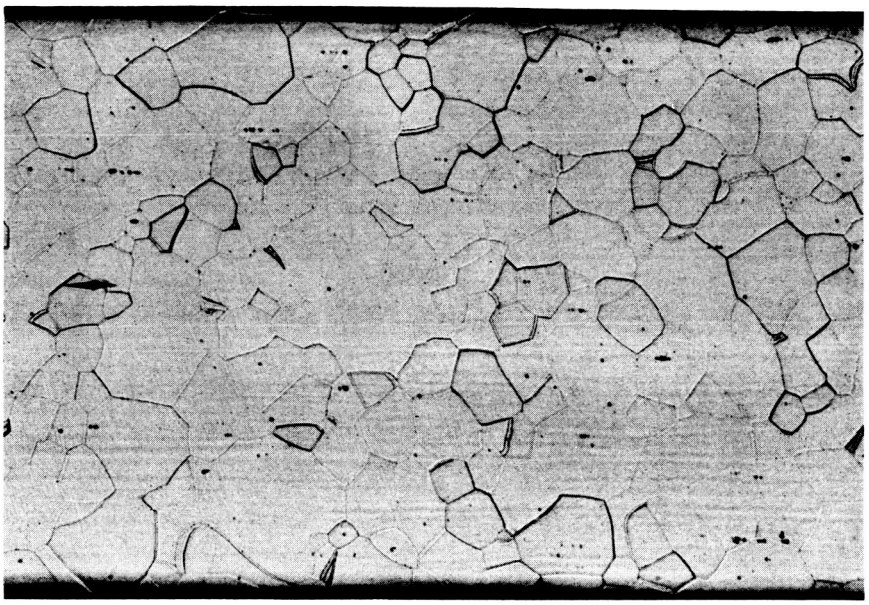

ASTAR 811C Heat 650056 annealed 30 minutes at 3600°F (2255°K)

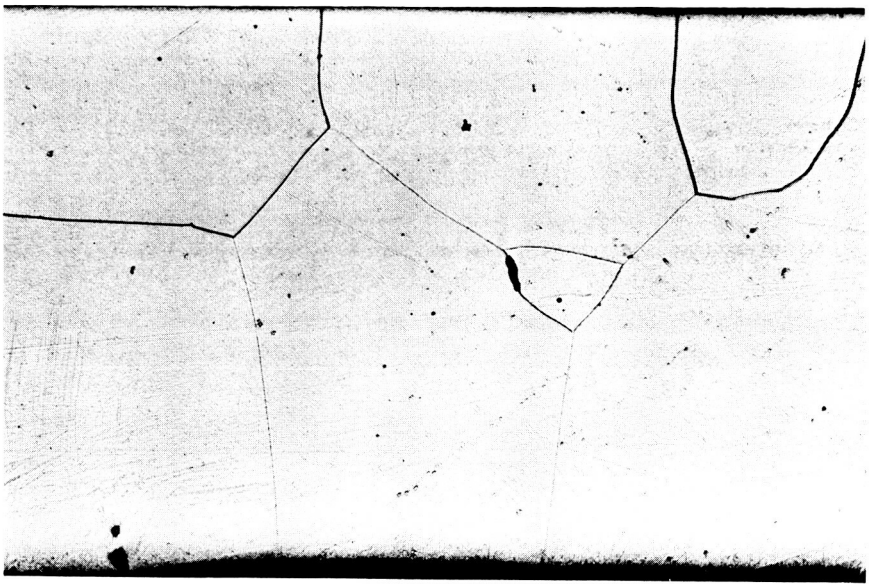

As above, creep tested at 2900°F (1866°K) and 1.5 ksi (10.3 MN/m^2)

Figure 27. Illustrating grain growth which occurred during creep testing of ASTAR 811C alloy at 2900°F (1866°K). 100X

a) Scanning electron micrograph - 540X
(Note severe etch pitting)

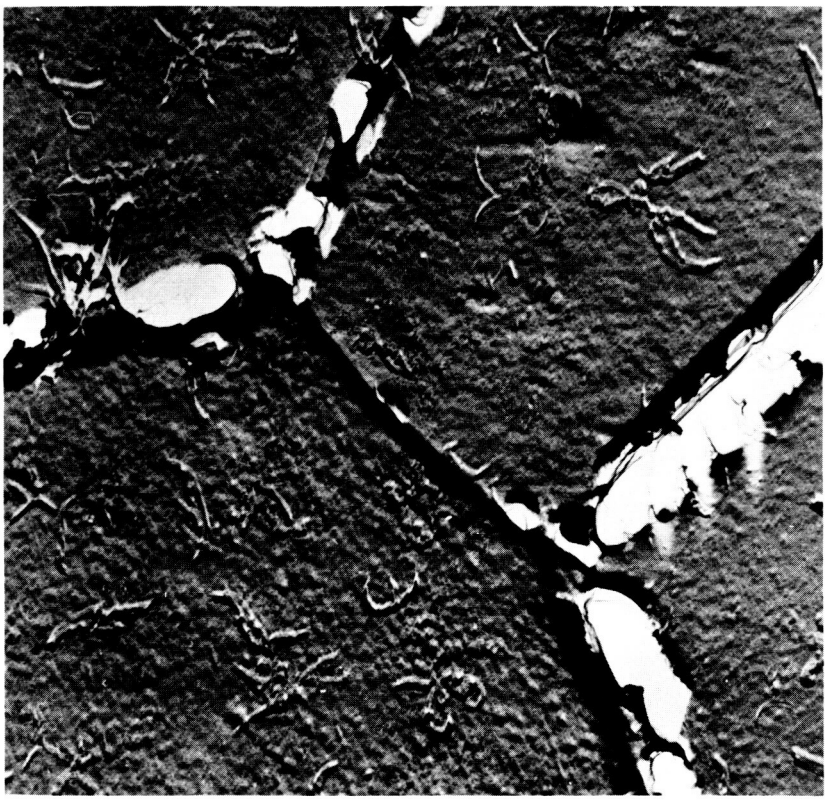

b) Transmission electron micrograph of two stage (cellulose nitrate/Carbon) replica. Note that unusual features within grain are assumed to be artifacts. 5000X

Figure 28. Photomicrographs of ASTAR 811C alloy annealed 1 hour at 3000°F (1922°K) and creep tested at 2400°F (1589°K) and 15 ksi (103 MN/m^2).

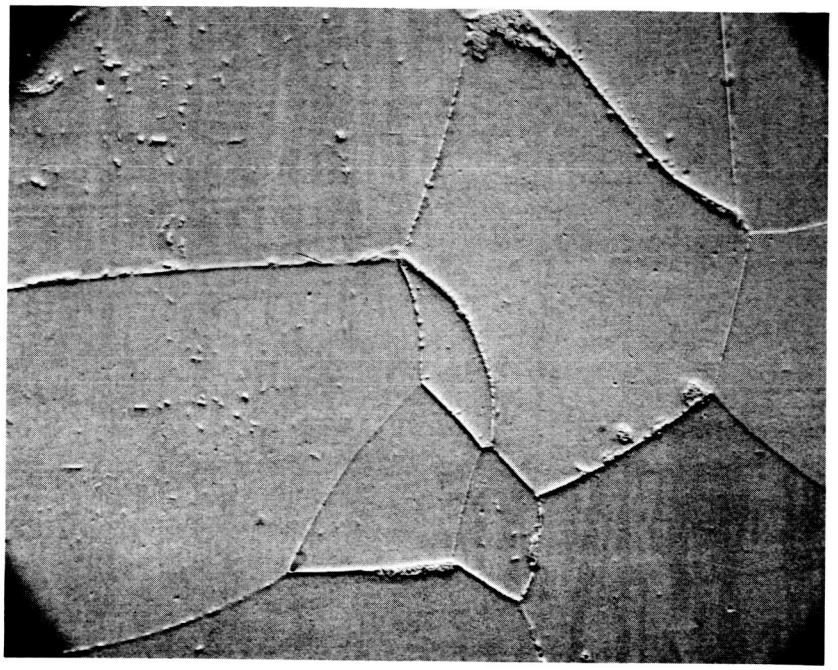

a) Scanning Electron micrograph - 540X

b) Transmission electron micrograph of two-stage (cellulose nitrate/carbon) replica. 5000X

Figure 29. Photomicrographs of ASTAR 811C alloy annealed 1/2 hour at 3600°F (2255°K) and creep tested at 2400°F (1589°K) and 15 ksi (103 MN/m^2).

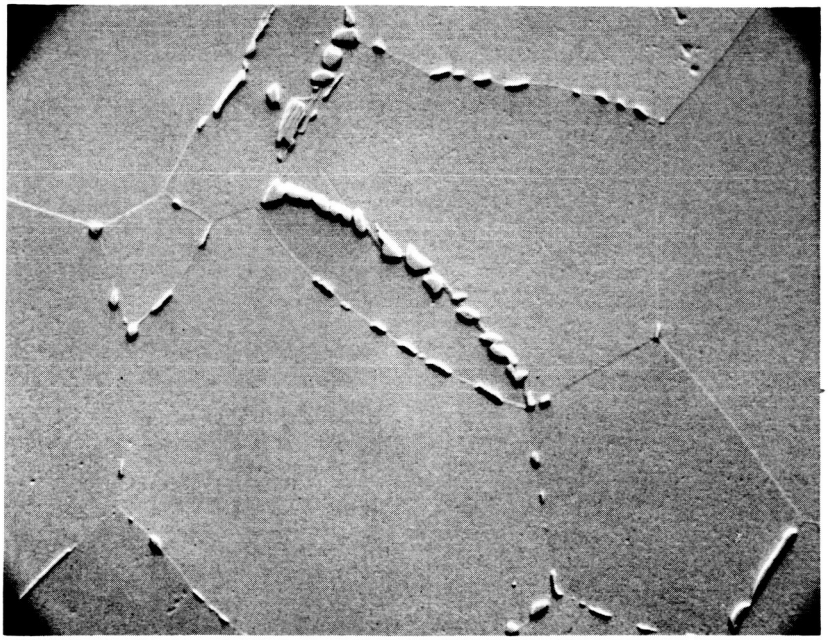

a) Scanning electron micrograph - 540X

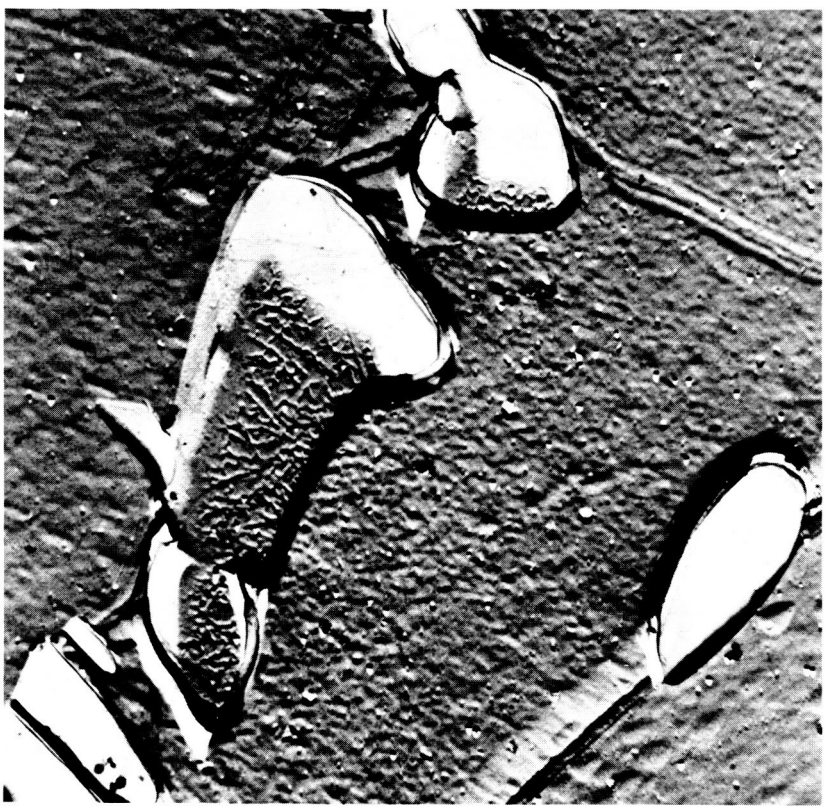

b) Transmission electron micrograph of two stage (cellulose nitrate/carbon) replica. 5000X

Figure 30. Photomicrographs of ASTAR 811C alloy annealed 1/2 hour at 3600°F (2255°K) and creep tested at 2600°F (1700°K) and 2 ksi (13.8 MN/m^2).

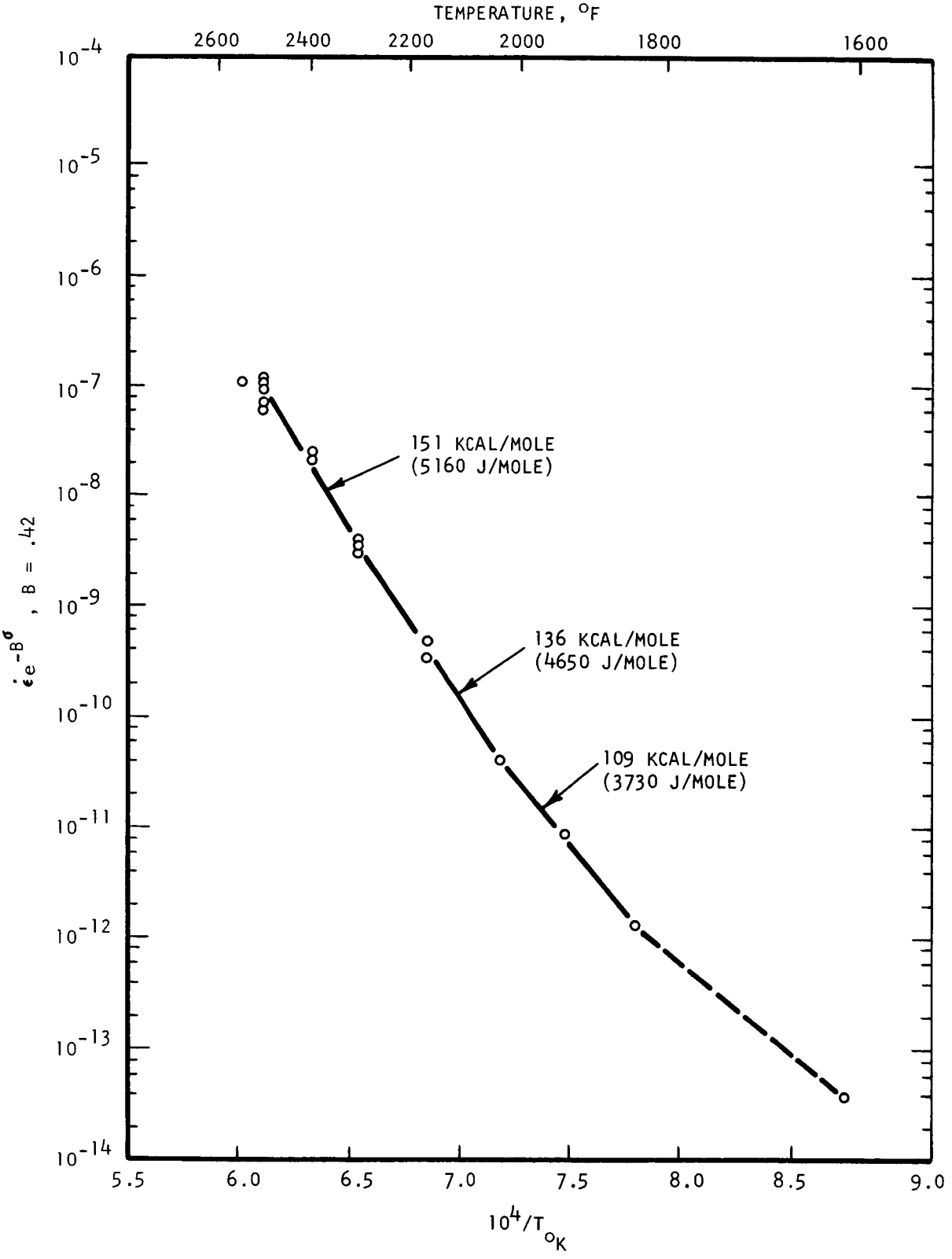

Figure 31. Pseudo-Arrhenius plot of stress-compensated creep rate parameter versus reciprocal temperature for ASTAR 811C alloy annealed 1/2 hour at 3600°F (2255°K).

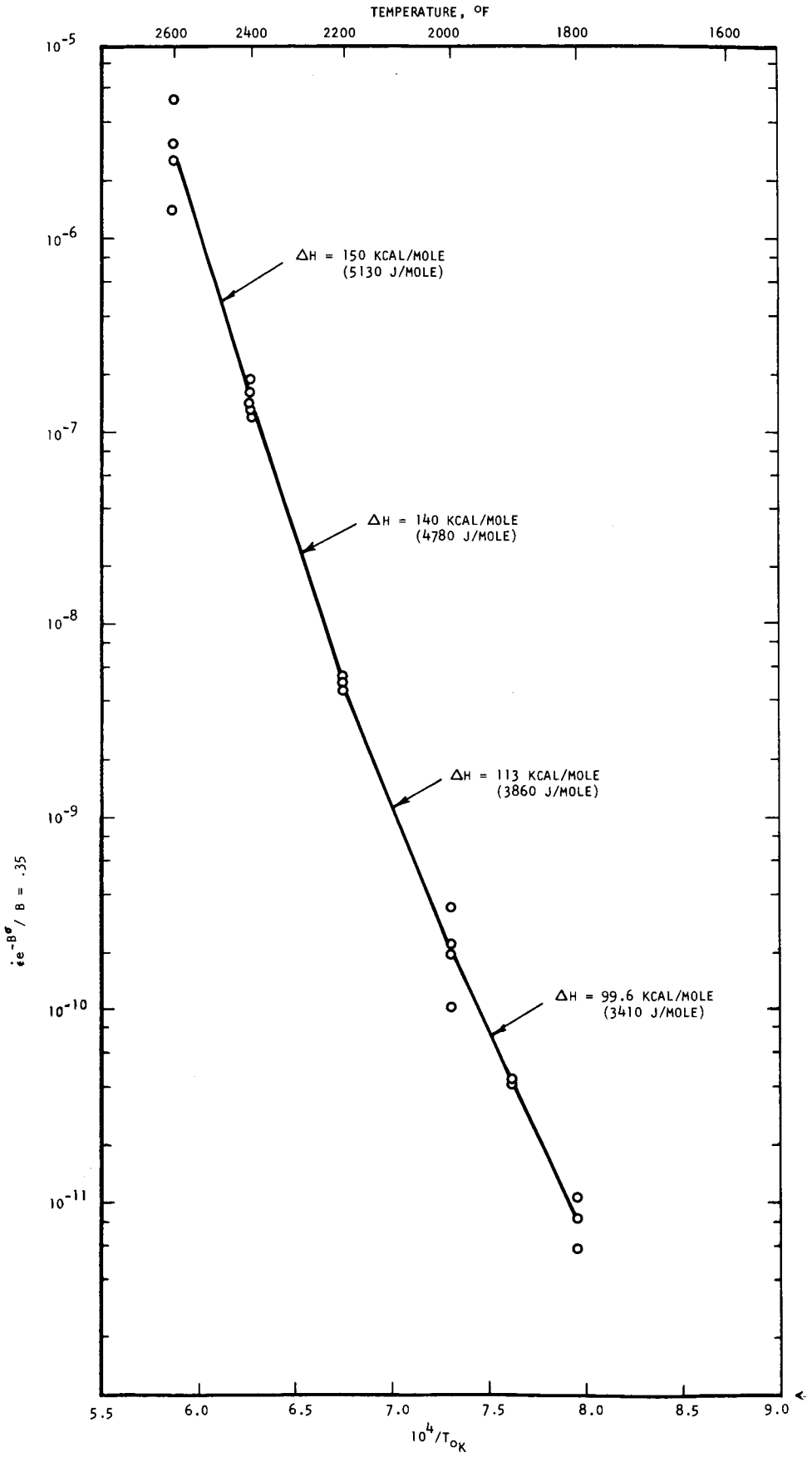

Figure 32. Pseudo-Arrhenius plot of stress-compensated creep rate parameter versus reciprocal temperature for ASTAR 811C alloy annealed 1 hour at 3000°F (1922°K).

4508 c

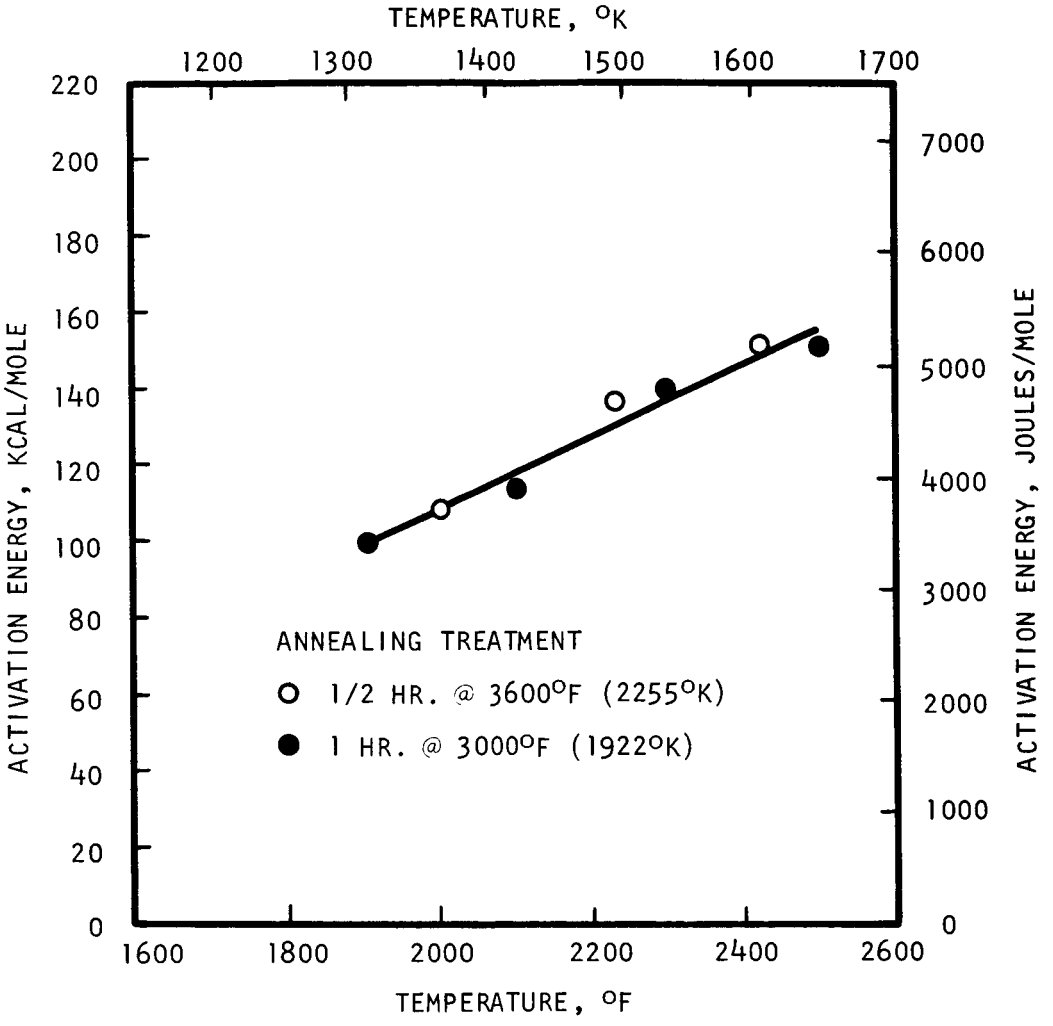

Figure 33. Variation of activation energy for creep with test temperature for ASTAR 811C in two conditions of heat treatment.

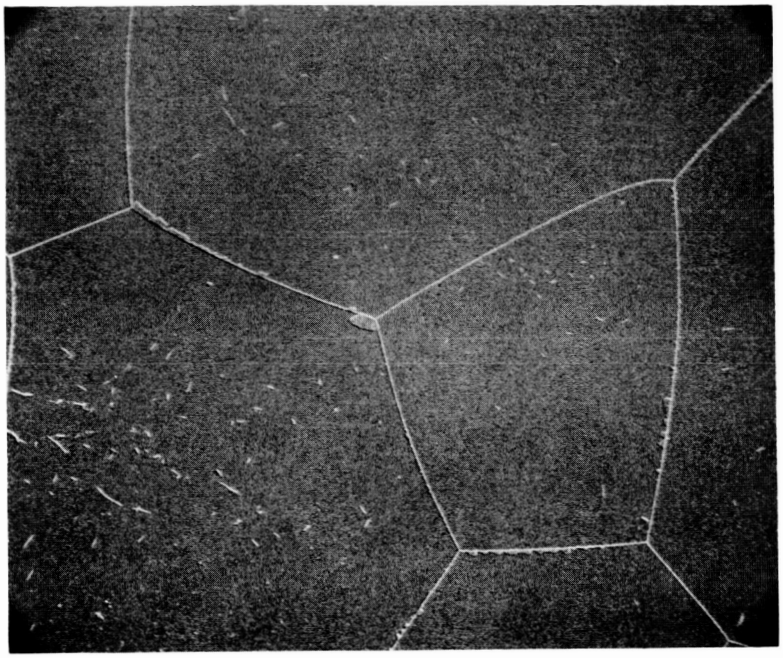

a. 540X

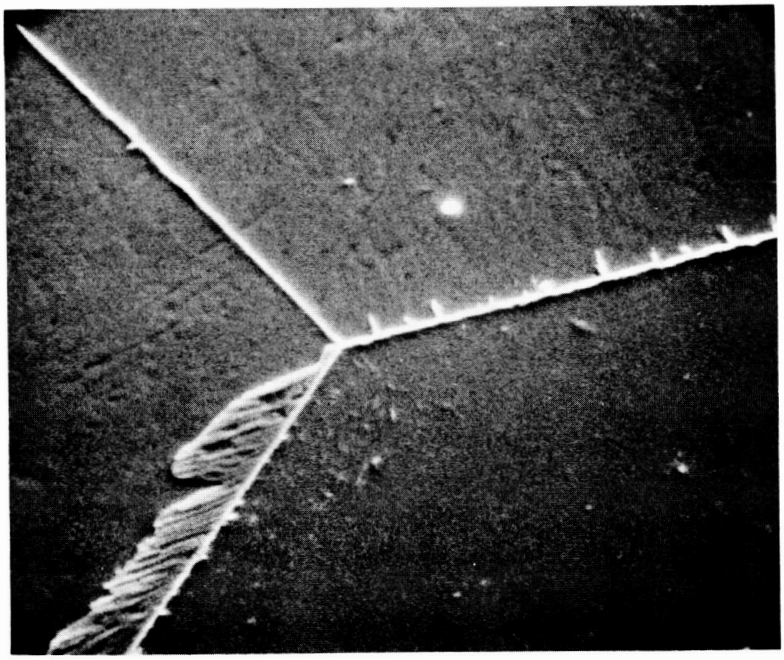

b. 5000X

Figure 34. Microstructure of ASTAR 811C annealed 1/2 hour at 3600°F (2255°K) plus 2 hours at 2400°F (1589°K).

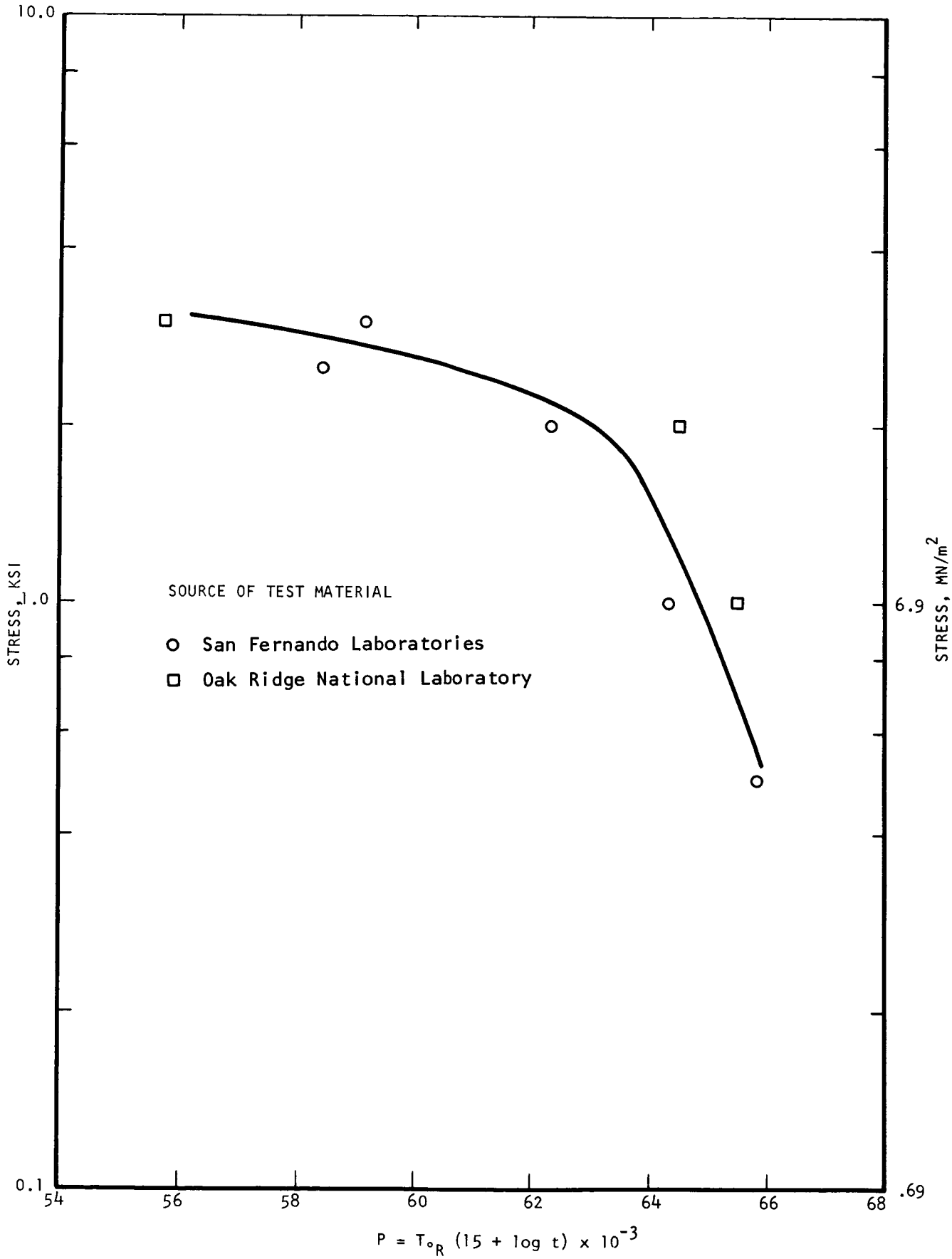

Figure 35. Larson-Miller plot of 1% creep life data for CVD tungsten.

APPENDIX I

PREVIOUSLY PUBLISHED REPORTS ON THE REFRACTORY ALLOY CREEP PROGRAM

J. C. Sawyer and E. B. Evans, "Generation of Valid Long Time Creep Data on Refractory Alloys at Elevated Temperature," First Quarterly Report, Contract NAS 3-2545, October 20, 1963.

J. C. Sawyer and E. B. Evans, "Generation of Valid Long Time Creep Data on Refractory Alloys at Elevated Temperatures," Second Quarterly Report, Contract NAS 3-2545, January 15, 1964.

J. C. Sawyer and E. B. Evans, "Generation of Long Time Creep Data on Refractory Alloys at Elevated Temperatures," Third Quarterly Report, Contract NAS 3-2545, CR-54048, April 20, 1964.

J. C. Sawyer and C. H. Phillеo, "Generation of Long Time Creep Data on Refractory Alloys at Elevated Temperatures," Fourth Quarterly Report, Contract NAS 3-2545, CR-54123, July 1, 1964.

J. C. Sawyer and C. H. Phillеo, "Generation of Long Time Creep Data on Refractory Alloys at Elevated Temperatures," Fifth Quarterly Report, Contract NAS 3-2545, CR-54228, November 9, 1964.

J. C. Sawyer and C. H. Phillеo, "Generation of Long Time Creep Data on Refractory Alloys at Elevated Temperatures," Sixth Quarterly Report, Contract NAS 3-2545, CR-54287, January 15, 1965.

J. C. Sawyer and C. H. Phillеo, "Generation of Long Time Creep Data on Refractory Alloys at Elevated Temperatures," Seventh Quarterly Report, Contract NAS 3-2545, CR-54394, April 28, 1965.

J. C. Sawyer and E. A. Steigerwald, "Generation of Long Time Creep Data on Refractory Alloys at Elevated Temperatures," Eighth Quarterly Report, Contract NAS 3-2545, CR-54457, July 7, 1965.

J. C. Sawyer and E. A. Steigerwald, "Generation of Long Time Creep Data on Refractory Alloys at Elevated Temperatures," Ninth Quarterly Report, Contract NAS 3-2545, CR-54773, October 8, 1965.

J. C. Sawyer and E. A. Steigerwald, "Generation of Long Time Creep Data on Refractory Alloys at Elevated Temperatures," Tenth Quarterly Report, Contract NAS 3-2545, CR-54895, January 8, 1966.

J. C. Sawyer and E. A. Steigerwald, "Generation of Long Time Creep Data on Refractory Alloys at Elevated Temperatures," Eleventh Quarterly Report, Contract NAS 3-2545, CR-54973, April 15, 1966.

J. C. Sawyer and E. A. Steigerwald, "Generation of Long Time Creep Data on Refractory Alloys at Elevated Temperatures," Twelfth Quarterly Report, Contract NAS 3-2545, CR-72044, July 15, 1966.

J. C. Sawyer and E. A. Steigerwald, "Generation of Long Time Creep Data on Refractory Alloys at Elevated Temperatures," Thirteenth Quarterly Report, Contract NAS 3-2545, October 14, 1966.

J. C. Sawyer and E. A. Steigerwald, "Generation of Long Time Creep Data on Refractory Alloys at Elevated Temperatures," Fourteenth Quarterly Report, Contract NAS 3-2545, CR-72185, January 17, 1967.

J. C. Sawyer and E. A. Steigerwald, "Generation of Long Time Creep Data on Refractory Alloys at Elevated Temperatures," Final Report, Contract NAS 3-2545, June 6, 1967.

J. C. Sawyer and E. A. Steigerwald, "Generation of Long Time Creep Data on Refractory Alloys at Elevated Temperatures," Supplement to Final Report, Numerical Creep Data," June 26, 1963 to March 17, 1967, Contract NAS 3-2545, August 15, 1967.

J. C. Sawyer and K. D. Sheffler, "Generation of Long Time Creep Data on Refractory Alloys at Elevated Temperatures," Mid-Contract Report, Contract NAS 3-9439, CR-72319, August 1967.

K. D. Sheffler and E. A. Steigerwald, "Generation of Long Time Creep Data on Refractory Alloys at Elevated Temperatures," Nine Month Summary Report, Contract NAS 3-9439, CR-72391, December 14, 1967.

K. D. Sheffler and E. A. Steigerwald, "Generation of Long Time Creep Data on Refractory Alloys at Elevated Temperatures," Fifteenth Quarterly Report (and Numerical Data Supplement), Contract NAS-3-9439, CR 72431, 14 April 1968.

K. D. Sheffler and E. A. Steigerwald, "Generation of Long Time Creep Data on Refractory Alloys at Elevated Temperatures," Sixteenth Quarterly Report (and Numerical Data Supplement), Contract NAS-3-9439, CR-72433, 15 July 1968.

K. D. Sheffler and J. C. Sawyer, "Generation of Long Time Creep Data on Refractory Alloys at Elevated Temperatures," Seventeenth Quarterly Report (and Numerical Data Supplement), Contract NAS-3-9439, CR-72523, 15 October 1968.

K. D. Sheffler and J. C. Sawyer, "Generation of Long Time Creep Data on Refractory Alloys at Elevated Temperatures," Eighteenth Quarterly Report (and Numerical Data Supplement), Contract NAS-3-9439, CR-72524, 15 January 1969.

K. D. Sheffler, "Generation of Long Time Creep Data on Refractory Alloys at Elevated Temperatures, Nineteenth Quarterly Report (and Numerical Data Supplement), Contract NAS-3-9439, CR 72547, 31 March 1969.

K. D. Sheffler, "Generation of Long Time Creep Data on Refractory Alloys at Elevated Temperatures", Twentieth Quarterly Report (and Numerical Data Supplement), Contract NAS 3-9439, CR 72632, 7 July 1969.

K. D. Sheffler, "Generation of Long Time Creep Data on Refractory Alloys at Elevated Temperatures," Twenty First Quarterly Report (and Numerical Data Supplement) Contract NAS-3-9439, CR-72619, 10 October 1969.

K. D. Sheffler, "Generation of Long Time Creep Data on Refractory Alloys at Elevated Temperatures," Final Report (and Numerical Data Supplement), Contract NAS-3-9439.

K. D. Sheffler, J. C. Sawyer and E. A. Steigerwald, "Mechanical Behavior of Tantalum Base T-111 Alloy at Elevated Temperature," Topical Report No. 1, Contract NAS-3-9439, TRW ER-7365, NASA CR-1436, September 1969.

K. D. Sheffler and J. C. Sawyer, "Creep Behavior of T-111 Alloy Under the Influence of Continuously Varying Stresses," Topical Report No. 2, NAS-3-9439, TRW ER-7373.

K. D. Sheffler, "Analytical Studies of the Variable-Stress, Variable Temperature Creep Behavior of T-111 Alloy," Topical Report, Contract NAS-3-13469, NASA-CR-72771, TRW ER-7590, July 1970.

K. D. Sheffler, "Generation of Long Time Creep Data on Refractory Alloys at Elevated Temperatures," Semi-Annual Report, Contract NAS-3-13469, TRW ER-7506, NAS-CR-72871, 16 November 1970.

K. D. Sheffler, "Generation of Long Time Creep Data on Refractory Alloys at Elevated Temperatures," Final Report, Contract NAS-3-13469, TRW ER-7541, NASA-CR-72997, 20 May 1971.

K. D. Sheffler and R. R. Ebert, "Generation of Long Time Creep Data on Refractory Alloys at Elevated Temperatures," Semi-Annual Report, Contract NAS-3-15554, TRW ER-7567, NASA-CR-12087, 8 May 1972.

APPENDIX II

SUMMARY OF ULTRAHIGH VACUUM CREEP TEST RESULTS GENERATED ON THE REFRACTORY ALLOY CREEP PROGRAM

TABLE II-1. Summary of Arc-Melted Tungsten Ultra-High Vacuum Creep Test Results

Test No.	Heat No.	Heat Treatment Time Hours	Heat Treatment Temperature °F	Heat Treatment Temperature °K	Stress KSI	Stress MN/M²	Test Temperature °F	Test Temperature °K	1% Creep Life Hours	Termination of Test Time, Hours	Termination of Test Percent Creep	1% Creep Larson-Miller Parameter $T_{\bullet R}$ (15+logt) x10⁻³
S-5	KC-1357	24	3200	2033	3.0	20.7	3200	2033	6	32	5.38	57.8
S-7	KC-1357	2	3200	2033	0.4	2.8	3200	2033	***	714	118	***
S-9	KC-1357	2	3200	2033	1.0	6.9	3200	2033	675	3886	2.760	65.4
S-17	KC-1357	2	2800	1811	4.0	28.0	2800	1811	20	908	5.452	53.1
S-18	KC-1357	2	2800	1811	3.0	20.7	2800	1811	125	908	5.535	55.8

*** Insufficient creep to extrapolate

TABLE II-2. Summary of Vapor-Deposited Tungsten Ultra-High Vacuum Test Results

Test No.	Heat No.	Heat Treatment Time Hours	Heat Treatment Temperature °F	Heat Treatment Temperature °K	Stress KSI	Stress MN/M²	Test Temperature °F	Test Temperature °K	1% Creep Life Hours	Termination of Test Time, Hours	Termination of Test Percent Creep	1% Creep Larson-Miller Parameter T_{e_R} (15+logt) x10⁻³
B-17	--	1	3200	2033	1.0	6.9	3200	2033	1140	2671	1.570	66.0
B-24	--	1	2800	1811	2.0	13.8	2800	1811	1500	6812	3.708	59.2
S-102	--	100	3272	2273	0.5	3.5	2912	1873	30,000*	2811.5	0.037	65.8
S-117	--	100	3272	2273	1.0	6.9	2912	1873	13,000*	5400	0.446	64.3
S-150	--	100	3272	2273	2.0	13.8	2912	1873	2970	3337.5	1.144	62.3
S-185	--	100	3272	2273	3.0	20.7	2912	1873	348	456.1	1.420	59.1
S-191	--	100	3272	2273	2.5	17.3	2912	1873	203	481.6	2.190	58.4
S-192	ORNL	AS RECEIVED			1.0	6.9	3000	1922	9000*	4995.1	0.570	65.5
S-202	ORNL	AS RECEIVED			3.0	20.7	2732	1773	257	1196.3	3.055	55.7
S-211	ORNL	AS RECEIVED			2.0	13.8	3002	1923	4000*	1725.4	0.525	64.5

*Extrapolated

TABLE II-3. Summary of Tungsten-25% Re Ultra-High Vacuum Creep Test Results

Test No.	Heat No.	Heat Treatment Time Hours	Heat Treatment Temperature °F	Heat Treatment Temperature °K	Stress KSI	Stress MN/M²	Test Temperature °F	Test Temperature °K	1% Creep Life Hours	Termination of Test Time, Hours	Termination of Test Percent Creep	1% Creep Larson-Miller Parameter T_R (15+logt) x10⁻³
S-3	3.5-75002	48	3200	2033	5.0	34.4	3200	2033	12	45	6.03	58.9
S-4	3.5-75002	45	3200	2033	3.0	20.7	3200	2033	25	97	5.22	60.0
S-6	3.5-75002	1	3200	2033	0.5	3.4	3200	2033	***	253	0.090	***
S-8	3.5-75002	1	3200	2033	1.5	10.3	3200	2033	315	1306	5.113	64.0
S-55A	3.5-75002	1	2550	1673	10	68.9	1600	1144	--	200	0.005	--
S-55B	3.5-75002		--		10	68.9	1650	1172	--	203	0.005	--
S-55C	3.5-75002		--		10	68.9	1700	1200	--	196	0.008	--
S-55D	3.5-75002		--		10	68.9	1750	1228	--	241	0.018	--
S-55E	3.5-75002		--		10	68.9	1800	1255	--	257	0.035	--
S-61A	3.5-75002		--		15	100.4	1600	1144	--	235	0.008	--
S-61B	3.5-75002		--		15	100.4	1650	1172	--	169	0.022	--
S-61C	3.5-75002		--		15	100.4	1700	1200	--	196	0.038	--
S-61D	3.5-75002		--		15	100.4	1750	1228	--	200	0.058	--
S-61E	3.5-75002		--		15	100.4	1800	1255	--	194	0.078	--

*** Insufficient creep to extrapolate

TABLE II-4. Summary of Sylvania A Ultra-High Vacuum Creep Test Results

Test No.	Heat No.	Heat Treatment Time Hours	Heat Treatment Temperature °F	Heat Treatment Temperature °K	Stress KSI	Stress MN/M²	Test Temperature °F	Test Temperature °K	1% Creep Life Hours	Termination of Test Time, Hours	Termination of Test Percent Creep	1% Creep Larson-Miller Parameter $T_{\bullet R}$ (15+logt) x10⁻³
S-12	--	2	3200	2033	5.0	34.4	3200	2033	35	170	5.25	60.6
S-15	--	2	3200	2033	3.0	20.7	3200	2033	250	907	5.862	63.7

TABLE II-5. Summary of AS-30 Ultra-High Vacuum Creep Test Results

Test No.	Heat No.	Heat Treatment Time Hours	Heat Treatment Temperature °F	Heat Treatment Temperature °K	Stress KSI	Stress MN/M²	Test Temperature °F	Test Temperature °K	1% Creep Life Hours	Termination of Test Time, Hours	Termination of Test Percent Creep	1% Creep Larson-Miller Parameter $T_{\bullet R}$ (15+logt) x10⁻³
B-2	C5	AS-ROLLED			12.0	82.7	2000	1366	390	806	1.020	43.3
B-6	C5	AS-ROLLED			11.0	75.8	2000	1366	450	1192	1.016	43.5
B-7	C5	AS-ROLLED			8.0	55.1	2200	1478	115	230	1.025	45.4

TABLE II-6. Summary of Cb-132M Ultra-High Vacuum Creep Test Results

Test No.	Heat No.	Heat Treatment Time Hours	Heat Treatment Temperature °F	Heat Treatment Temperature °K	Stress KSI	Stress MN/M²	Test Temperature °F	Test Temperature °K	1/2% Creep Life Hours	Termination of Test Time, Hours	Termination of Test Percent Creep	1/2% Creep Larson-Miller Parameter $T_{\circ R}$ (15+logt) x10⁻³
B-13	KC-1454	1	3092	1973	20.0	138.0	2056	1398	275	568	1.170	43.8
B-14	KC-1454	1	3092	1973	16.3	82.3	2056	1398	340	691	1.026	44.0
B-15	KC-1454	1	3092	1973	7.4	51.0	2256	1508	250	596	1.100	47.2

TABLE II-7. Summary of TZM Ultra-High Vacuum Creep Test Results

Test No.	Heat No.	Heat Treatment Time Hours	Heat Treatment Temperature °F	Heat Treatment Temperature °K	Stress KSI	Stress MN/M²	Test Temperature °F	Test Temperature °K	1/2% Creep Life Hours	Termination of Test Time, Hours	Termination of Test Percent Creep	1/2% Creep Larson-Miller Parameter $T_{\bullet_R}$ (15+logt) x10⁻³
B-1	7502	1	2200	1478	12.6	86.5	2130	1439	605	646	1.105	46.1
B-3	7502	1	2200	1478	10.0	68.9	2000	1366	14,200*	10,048	0.375	47.1
B-29	7502	1	2200	1478	41.0	282.0	2000	1366	100	664	6.215	41.8
B-35	7502	1	2200	1478	44.0	303.0	1800	1255	7000	7659	0.535	42.6
B-4	7502	1	2200	1478	10.0	68.9	2000	1366	25,000*	10,012	0.368	47.7
	PLUS											
		1	2850	1839								
B-16	KDTZM-1175	1	2300	1533	23.4	161.0	1855	1286	62,500*	4376	0.035	45.8
B-18	KDTZM-1175	1	2300	1533	55.0	379.0	1600	1144	60,000*	2159	0.018	40.7
B-21	KDTZM-1175	1	2300	1533	65.0	448.0	1600	1144	15,000*	1630	0.085	39.5
B-25	KDTZM-1175	1	2300	1533	44.0	303.0	1800	1255	50,000*	10,152	0.182	44.5
B-38	KDTZM-1175	1	2300	1533	22.0	151.0	2000	1366	16,293	45,354.5	1.080	47.1
B-34	7463	1/2	2250	1505	41.0	282.0	2000	1366	790	1440	1.658	44.0

*Extrapolated data

TABLE II-8. Summary of Cb Modified TZM Ultra-High Vacuum Creep Test Results

Test No.	Heat No.	Heat Treatment Time Hours	Heat Treatment Temperature °F	Heat Treatment Temperature °K	Stress KSI	Stress MN/M²	Test Temperature °F	Test Temperature °K	1/2% Creep Life Hours	Termination of Test Time, Hours	Termination of Test Percent Creep	1/2% Creep Larson-Miller Parameter $T_{\bullet_R}$ (15+logt) x10⁻³
B-23A	4305-4	1	2500	1644	20.0	138.0	2000	1366	20,000*	686	0.032	47.5
B-23B	4305-4	-	--	--	28.0	193.0	2000	1366	10,000*	307	0.028	46.7
B-23C	4305-4	-	--	--	40.0	276.0	2000	1366	630*	185	0.188	43.8
B-23D	4305-4	-	--	--	46.0	317.0	1800	1255	4000*	403	0.078	42.0
B-23E	4305-4	-	--	--	34.0	234.0	2100	1422	1000*	329	0.170	46.1
B-27	4305-4	1	2500	1644	41.0	282.0	2000	1366	1090	1584	1.040	44.5

* Extrapolated

TABLE II-9. Summary of TZC Ultra-High Vacuum Creep Test Results

Test No.	Heat No.	Heat Treatment Time Hours	Heat Treatment Temperature °F	Heat Treatment Temperature °K	Stress KSI	Stress MN/M²	Test Temperature °F	Test Temperature °K	1/2% Creep Life Hours	Termination of Test Time, Hours	Termination of Test Percent Creep	1/2% Creep Larson-Miller Parameter $T_{\bullet R}$ (15+logt) x10⁻³
B-8A	M-80	1	3092	1973	18.0	124.0	2200	1478	1100	2128	1.060	48.3
B-10	M-80	1	3092	1973	17.0	117.0	2200	1478	2500	2749	0.545	48.9
B-9	M-80	1	3092	1973	20.0	138.0	2000	1366	10,408	16,002	0.670	46.8
B-11	M-80	1	3092	1973	25.0	172.0	1856	1287	75,000*	14,406	0.182	46.0
B-12	M-80	1	3092	1973	19.0	131.0	2056	1398	75,000*	14,239	0.280	49.2
B-20	M-91	1	3092	1973	20.0	138.0	2000	1366	3650	12,795	1.008	45.7
B-31	M-91	1	3092	1973	14.0	96.5	2200	1478	329	912	1.092	46.6
B-19	M-91	1	2300	1533	44.0	303.0	1800	1255	1075	4604	1.015	41.1
B-28	M-91	1	2300	1533	28.0	193.0	2000	1366	1100	4214	1.138	44.4
B-30	M-91	1	2500	1644	22.0	152.0	2200	1478	70	259	1.280	44.8
B-32	M-91	1	2500	1644	20.0	138.0	1935	1330	14,400	16,130	0.535	45.9
B-33	M-91	1	2500	1644	22.0	152.0	1900	1311	7720	9697	0.585	44.6
B-36	4345	1	2500	1644	22.0	152.0	2000	1366	5940	8563	0.640	46.2
B-37	4345	1	2400	1589	22.0	152.0	2000	1366	8853	9020	0.500	46.3

* Extrapolated

TABLE II-10. Summary of T-222 Ultra-High Vacuum Creep Test Results

Test No.	Heat No.	Heat Treatment Time Hours	Heat Treatment Temperature °F	Heat Treatment Temperature °K	Stress KSI	Stress MN/M²	Test Temperature °F	Test Temperature °K	1% Creep Life Hours	Termination of Test Time, Hours	Termination of Test Percent Creep	1% Creep Larson-Miller Parameter $T_{\bullet_R}$ (15+logt) x10⁻³
S-13	AL-TA-43	1	3000	1922	12.0	82.7	2200	1478	560	1890	5.720	47.2
S-14	AL-TA-43	1	3000	1922	19.2	132.0	2056	1398	890	1314	1.685	45.1
S-20	AL-TA-43	1	2800	1811	12.0	82.7	2200	1478	405	1389	5.060	46.9

TABLE II-11. Summary of ASTAR 811C Ultra-High Vacuum Creep Test Results

Test No.	Heat No.	Heat Treatment Time Hours	Heat Treatment Temperature °F	Heat Treatment Temperature °K	Stress KSI	Stress MN/M²	Test Temperature °F	Test Temperature °K	1% Creep Life Hours	Termination of Test Time, Hours	Termination of Test Percent Creep	1% Creep Larson-Miller Parameter $T_{\bullet R}$ (15+logt) x10⁻³
S-29	NASV-20-WS	.5	3600	2255	2.0	13.8	2600	1700	21,190	21,560	1.028	59.3
S-70	VAM-95	.25	3520	2211	20	138.0	2100	1422	3600*	983.4	0.342	47.5
S-71	VAM-95	.15	3600	2255	20	138.0	2100	1422	3600*	767.5	0.320	47.5
S-70A	VAM-95	-	--	--	15	103.0	2200	1478	6000*	655.8	0.108	50.0
S-71A	VAM-95	-	--	--	15	103.0	2200	1478	6000*	678.9	0.112	50.0
S-70B	VAM-95	-	--	--	10	69.0	2300	1533	6000*	1106.4	0.153	51.9
S-71B	VAM-95	-	--	--	10	69.0	2300	1533	6000*	1082.2	0.178	51.9
S-73	VAM-95	.33	3600	2255	15	103.0	2400	1589	435	720.5	1.860	50.5
S-74	650056	.33	3600	2255	15	103.0	2400	1589	825	1466.0	2.185	51.2
S-75	VAM-95	1.0	3000	1922	15	103.0	2400	1589	144	162.3	1.195	49.1
S-76	650056	.5	3600	2255	25	162.0	2175	1464	695	4962.5	15.088	47.0
S-77	650056	.5	3600	2255	10	69.0	2400	1589	5287	5907.9	1.150	53.6
S-78	650056	.5	3600	2255	5	35.0	2550	1672	5611	6210.4	1.210	56.6
S-79	VAM-95	5	3450	2172	15	103.0	2400	1589	542	714.4	1.378	50.8
S-81	VAM-95	24	3270	2072	15	103.0	2400	1589	560	666.5	1.330	50.8
S-85	650056	.5	3600	2255	20	138.0	2175	1464	4410	5346.7	1.240	49.1
S-86	650056	.5	3600	2255	15	103.0	2300	1533	4390	5206.1	1.240	51.1

* Extrapolated

TABLE II-11. Summary of ASTAR 811C Ultra-High Vacuum Creep Test Results

Test No.	Heat No.	Heat Treatment Time Hours	Heat Treatment Temperature °F	Heat Treatment Temperature °K	Stress KSI	Stress MN/M²	Test Temperature °F	Test Temperature °K	1% Creep Life Hours	Termination of Test Time, Hours	Termination of Test Percent Creep	1% Creep Larson-Miller Parameter $T_{\bullet_R}$ (15+logt) x10⁻³
S-87+	NASV-20	1	3000	1922	15	103.0	2400	1589	68	329	11.470	48.1
S-100++	NASV-20	1	3000	1922	15	103.0	2400	1589	152	330.9	10.750	49.1
S-104+	NASV-20	1	3000	1922	8	55.1	2400	1589	1575	1777.0	1.206	52.1
S-108++	NASV-20	1	3000	1922	8	55.1	2400	1589	1894	2851.9	1.506	52.3
S-90	650056	0.5	3600	2255	35	241.0	1850	1283	1858	4323.6	2.402	42.2
S-91	650056	0.5	3600	2255	30	207.0	1950	1339	2656	6385.0	2.018	44.5
S-92	650056	0.5	3600	2255	25	162.0	2050	1394	6095	6763.6	1.095	47.2
S-93	650056	0.5	3600	2255	3	20.7	2700	1755	2064	4364.0	3.798	57.9
S-94	650056	0.5	3600	2255	40	276.0	1600	1144	60,000*	23,691.7	0.635	40.7
S-95	650056	0.5	3600	2255	8	55.1	2500	1644	2266	3963.8	2.392	54.3
S-96	650056	0.5	3600	2255	2.5	16.2	2750	1783	2270	5303.4	3.552	58.9
S-97	650056	0.5	3600	2255	1.5	10.3	2900	1866	1580	4504.7	4.918	61.1
S-101	650056	1	3000	1922	15	103.0	2400	1589	230	673.9	12.182	49.6
S-106	650056	0.5	3600	2255	6	41.4	2500	1644	2778	2971.2	1.160	54.5
S-112	650056	0.5	3600	2255	7	48.2	2500	1644	4420	4512.8	1.022	55.2

* Extrapolated

\+ Post Exposure Samples From G. E. Alkali Metal Exposure Program

++ Pre-Exposure Samples From G. E. Alkali Metal Exposure Program

TABLE II-11. Summary of ASTAR 811C Ultra-High Vacuum Creep Test Results

Test No.	Heat No.	Heat Treatment Time Hours	Heat Treatment Temperature °F	Heat Treatment Temperature °K	Stress KSI	Stress MN/M²	Test Temperature °F	Test Temperature °K	1% Creep Life Hours	Termination of Test Time, Hours	Termination of Test Percent Creep	1% Creep Larson-Miller Parameter T_R (15+logt) x10⁻³
S-113	650056	0.5	3600	2255	5	34.4	2500	1644	11,178	13,031.5	1.278	56.4
S-114	650056	0.5	3600	2255	1	6.9	2900	1866	7380	7728	1.052	63.4
S-118	650056	1	3000	1922	29	199.8	2000	1366	1620	1655.3	1.010	44.8
S-119	650056	0.5	3600	2255	10	68.9	2500	1644	1035	1145.3	1.178	53.3
S-120	650056	0.5	3600	2255	13	89.5	2300	1533	7250	8306.7	1.188	52.1
S-123	650056	0.5	3600	2255	17	117.0	2300	1533	2225	2257.3	1.015	50.6
S-125	650056	1	3000	1922	23	158.3	2000	1366	18,000*	13,412.7	0.735	47.4
S-126	650056	1	3000	1922	26	179.0	2000	1366	4360	4633	1.052	45.8
S-128	650056	1	3000	1922	36	248.0	1900	1311	290	649	1.390	41.2
S-129	650056	1	3000	1922	5	34.4	2600	1700	300	435.4	1.762	53.5
S-131	650056	1	3000	1922	40	276.0	1800	1255	580	866.5	1.145	40.1
S-134	650056	1	3000	1922	33	234.0	2000	1366	180	353.5	1.552	42.4
S-135	650056	1	3000	1922	13	89.7	2400	1589	510	531.3	1.040	50.6
S-136	650056	1	3000	1922	23	159.0	2200	1478	500	500.9	1.008	47.0
S-138	650056	100	3000	1922	15	103.0	2400	1589	790	934.2	1.245	51.1

* Extrapolated

4550 C

TABLE II-11. Summary of ASTAR 811C Ultra-High Vacuum Creep Test Results

Test No.	Heat No.	Heat Treatment Time Hours	Heat Treatment Temperature °F	Heat Treatment Temperature °K	Stress KSI	Stress MN/M²	Test Temperature °F	Test Temperature °K	1% Creep Life Hours	Termination of Test Time, Hours	Termination of Test Percent Creep	1% Creep Larson-Miller Parameter T_R (15+logt) x10⁻³
S-142	650056	1	3000	1922	50	344.0	1600	1144	4751	4998.3	1.008	38.5
S-143	650056	1	3000	1922	18	124.0	2200	1478	2800	3650.0	1.560	49.1
S-144	650056	1	3000	1922	8	55.2	2400	1589	2575	5540.7	7.028	52.7
S-147	650056	1	3000	1922	3	20.6	2600	1700	740	1033.9	1.760	54.6
S-160	650056	1	3000	1922	33	228.0	1900	1311	1340	2019.4	1.292	42.8
S-174	650056	1	3000	1922	36	248.0	1800	1255	2144	4867.6	1.918	41.4
S-175	650068	1	3000	1922	15	103.0	2400	1589	225	290.5	1.250	49.6
S-176	650056	100	3000	1922	15	103.0	2400	1589	710	1104.1	1.775	51.1
S-177	650056	1	3000	1922	13	89.5	2200	1478	8370	8876.9	1.090	50.3
S-180	650056	1	3000	1922	1	6.9	2800	1811	373	1455.4	1.550	57.3
S-183	650056	5	3450	2172	15	103.0	2400	1589	848	1945.2	3.345	51.3
S-188	650056	1	3000	1922	2	13.8	2600	1700	926	1075.9	1.280	55.0
S-193	650056	1	3000	1922	1	6.9	2600	1700	5800*	4991.1	0.932	57.4
S-194	650056	24	3270	2072	15	103.0	2400	1589	663	2057.2	4.132	51.0
S-195	650056	1	3000	1922	5	34.4	2400	1589	3875	4492.6	1.348	53.2
S-197	650056	1	3000	1922	0.5	3.5	2800	1811	17,000*	4025.0	0.615	62.7

* Extrapolated

TABLE II-11. Summary of ASTAR 811C Ultra-High Vacuum Creep Test Results

Test No.	Heat No.	Heat Treatment Time Hours	Heat Treatment Temperature °F	Heat Treatment Temperature °K	Stress KSI	Stress MN/M²	Test Temperature °F	Test Temperature °K	1% Creep Life Hours	Termination of Test Time, Hours	Termination of Test Percent Creep	1% Creep Larson-Miller Parameter $T_{\bullet R}$ (15+logt) x10⁻³
S-203	650056	1	3000	1922	0.5	3.5	3000	1922	90,000*	2492.0	0.128	69.0
S-204	650056	1	3000	1922	3	20.6	2400	1589	15,000*	2878.3	0.170	54.9
S-210	650056	1	3000	1922	33	228.0	1800	1255	6500*	2205.6	0.598	42.5
S-212	650068	1	2800	1811	15	103.0	2400	1589	71	98	1.644	48.2
S-213	650068	1	3200	2033	15	103.0	2400	1589	527	627.5	1.278	50.7
S-214	650068	1	3400	2144	15	103.0	2400	1589	840	939.1	1.118	51.2
S-215	650068	1	3600	2255	15	103.0	2400	1589	1033	1197.4	1.185	51.5

* Extrapolated

TABLE II-12. Summary of T-111 Ultra-High Vacuum Creep Test Results

Test No.	Heat No.	Heat Treatment Time Hours	Heat Treatment Temperature °F	Heat Treatment Temperature °K	Stress KSI	Stress MN/M²	Test Temperature °F	Test Temperature °K	1% Creep Life Hours	Termination of Test Time, Hours	Termination of Test Percent Creep	1% Creep Larson-Miller Parameter T_R (15+logt) x10⁻³
S-16	70616	1	2600	1700	8.0	55.1	2200	1477	725	1675	2.570	47.5
S-19	70616	1	3000	1922	8.0	55.1	2200	1477	2000	4870	3.368	48.7
S-21	70616	1	3000	1922	12.0	82.6	2200	1477	1140	3840	6.548	48.0
S-23	70616	1	3000	1922	12.0	82.6	2120	1433	3150	3698	1.225	47.7
S-22	70616	1	3000	1922	20.0	138.0	2000	1366	670	1099	2.010	43.8
S-24	70616	1	3000	1922	20.0	138.0	1860	1289	4730	4946	1.090	43.3
S-25	D-1670	1	3000	1922	15.0	103.0	2000	1366	1340	1584	1.210	44.6
S-26	D-1670	1	3000	1922	17.0	117.0	1800	1255	9540	9624	1.030	42.9
S-25A	D-1670	1	3000	1922	1.5	10.3	2600	1700	1100*	482	0.632	55.2
S-28	D-1670	1	3000	1922	0.5	3.4	2600	1700	640,000*	38,129.3	0.568	63.7
S-27	D-1102	1	3000	1922	13.0	89.5	2000	1366	1880	3459	2.082	45.0
S-32	D-1102	1	3000	1922	5.0	34.4	2200	1477	4050	4322	1.042	49.5
S-40	D-1102	1	3000	1922	17.0	117.0	1800	1255	8558	8717	1.028	42.8
S-33	65076	1	3000	1922	8.0	55.1	2200	1477	2850	2976	1.048	49.1
S-34	65076	1	3000	1922	11.0	75.8	2000	1366	10,800	10,875	1.010	46.9
S-37	65080	1	3000	1922	8.0	55.1	2200	1477	260	274	1.230	46.3
S-39	65080	1	3000	1922	13.0	89.5	1800	1255	8202	8728	1.070	42.7

* Extrapolated

TABLE II-12. Summary of T-111 Ultra-High Vacuum Creep Test Results

Test No.	Heat No.	Heat Treatment Time Hours	Heat Treatment Temperature °F	Heat Treatment Temperature °K	Stress KSI	Stress MN/M²	Test Temperature °F	Test Temperature °K	1% Creep Life Hours	Termination of Test Time, Hours	Termination of Test Percent Creep	1% Creep Larson-Miller Parameter $T_{\bullet R}$ (15+logt) x10⁻³
S-45	65080	1	3000	1922	3.0	20.0	2200	1477	554	697	1.165	47.1
S-30	65079	1	3000	1922	3.5	24.1	2400	1589	860	2137	2.372	51.3
S-31	65079	1	3000	1922	5.0	34.4	2200	1478	6160	6594	1.092	50.0
S-35	65079	1	3000	1922	5.0	34.4	2200	1478	5400	5522	1.048	49.9
S-42	65079	1	3000	1922	3.5	24.1	2300	1533	3810	4247	1.122	51.3
S-47	65079	1	3000	1922	24.0	165.0	1750	1228	19,896	22,476.2	1.298	43.3
S-48	65079	1	3000	1922	2.4	165.0	2330	1550	5500	6284	1.200	52.3
S-50	65079	1	3000	1922	8.5	72.2	2000	1366	24,000*	5735	0.272	47.7
S-43	65079	1/4	3000	1922	18.0	124.0	2000	1366	1500*	361	0.108	44.7
S-44A	65079	1	3000	1922	9.5	65.5	2172	1462	3250*	467	0.152	48.7
S-44B	65079	1/4	3000	1922	3.3	22.7	2371	1573	2030*	335	0.168	51.9
S-44C	65079	1/4	3000	1922	18.0	124.0	2000	1366	1670*	1146	0.688	44.8
S-44D	65079	1/4	3000	1922	23.0	158.0	1800	1255	14,650*	1391	0.112	43.3
S-59	D-1183	1	3000	1922	13.0	89.5	2000	1366	13,350	15,219.0	1.192	47.1
S-60	D-1183	1	3000	1922	35.0	241.0	1600	1144	8550	17,794.5	11.218	39.0
S-68	650028	1	3000	1922	1.0	6.9	2560	1678	2300	14,783.9	1.660	55.5

* Extrapolated

TABLE II-12. Summary of T-111 Ultra-High Vacuum Creep Test Results

Test No.	Heat No.	Heat Treatment Time Hours	Heat Treatment Temperature °F	Heat Treatment Temperature °K	Stress KSI	Stress MN/M²	Test Temperature °F	Test Temperature °K	1% Creep Life Hours	Termination of Test Time, Hours	Termination of Test Percent Creep	1% Creep Larson-Miller Parameter $T_{\bullet_R}$ (15+logt) x10⁻³
S-69	650028	1	3000	1922	30.0	207.0	1625	1158	16,625	18,120.7	1.312	40.1
B-43	650028	1	3000	1922	20.0	138.0	2000	1366	1823	1840.8	1.012	44.8
B-44	650038	1	3000	1922	35.0	241.0	2000	1366	1093	55.1	7.582	39.8
P-1	8049	1	3000	1922	19.0	131.0	2000	1366	2070	3649	2.142	45.1
S-80	650028	1	3000	1922	37.0	255.0	1300	978	***	3192.8	0.775	***
S-82A	650028	-	--	--	50.0	344.0	900	755	***	5610.8	0.075	***
S-83	650028	1	3000	1922	45.0	310.0	1100	866	7	1177.1	2.945	24.8
S-84	650028	1	3000	1922	1.5	10.4	2400	1589	3250	5273.6	1.502	52.9
S-41	65080	15	3000	1922	8.0	55.1	2200	1478	234	259	1.080	46.2
S-98	848001	1	3000	1922	1	6.9	2560	1678	12,000*	8438.7	0.602	57.4
S-99	650028	1	3000	1922	0.5	3.5	2700	1455	250,000*	9045	0.350	64.5
S-103	650028	1	3000	1922	40	276.0	1500	1089	90,000*	21,020.3	0.285	39.1
S-105	650028	1	3000	1922	35	241.0	1700	1200	1060	3211.6	8.990	39.0
S-107	848001	1	3000	1922	20	138.0	1900	1311	380	1197.6	3.042	41.5
S-115	848001	1	3000	1922	17	117.0	1900	1311	2100	2106.7	1.002	43.2
S-116	848001	1	3000	1922	15	103.3	1900	1311	5400	5472.0	1.018	44.2

* Extrapolated

*** Insufficient to Extrapolate

Table II-13. Summary of T-111 Linearly Increasing Stress Ultra-High Vacuum Creep Test Results

Test No.	Heat No.	Heat Treatment Time Hours	Heat Treatment Temperature °F	Heat Treatment Temperature °K	Stress Rate PSI/Hr	Test Temperature °F	Test Temperature °K	1% Creep Life Hours	Termination of Test Time, Hours	Termination of Test Percent Creep
S-36	65080	1	3000	1922	16	2200	1478	600	624	1.120
S-38	65080	1	3000	1922	1	2200	1478	3830	4686	1.562
S-46	65079	1	3000	1922	16	2200	1478	1000*	761	0.225
S-49	65079	1	3000	1922	20	1800	1255	1660	1964	5.125
S-51	D-1183	1	3000	1922	16	2200	1478	1080	1274	5.823
S-52	65079	1	3000	1922	13	2000	1366	1596	1657	1.150
S-53	65079	1	3000	1922	5	2200	1478	2240	2970	5.292
S-54	65079	1	3000	1922	5	2000	1366	3850	6506	6.478
S-56	65079	1	3000	1922	5	1800	1255	5500	6375	5.280
S-57	65079	1	3000	1922	1	2200	1478	7748	8833	1.510
S-62	65079	1	3000	1922	2	2000	1366	8300	8599	1.150

* Extrapolated

TABLE II-14. Summary of Pure Ta Ultra-High Vacuum Creep Test Results

Test No.	Heat No.	Heat Treatment Time Hours	Heat Treatment Temperature °F	Heat Treatment Temperature °K	Stress KSI	Stress MN/M²	Test Temperature °F	Test Temperature °K	1% Creep Life Hours	Termination of Test Time, Hours	Termination of Test Percent Creep	1% Creep Larson-Miller Parameter T_{θ_R} (15+logt) x10⁻³
B-39A	B-1962	1	1832	1273	13.6	93.7	1100	866	31	32	1.020	25.8
B-39B	B-1962	1/4	1832	1273	11.6	79.9	1100	866	603*	264	0.542	27.8
B-39C	B-1962	1/4	1832	1273	10.1	69.5	1183	912	463*	282	0.635	29.0
B-40A	B-1962	1	1832	1273	7.0	48.3	1350	1005	9	9	1.000	28.9
B-40B	B-1962	1/4	1832	1273	4.9	33.8	1350	1005	6600*	1386	0.300	34.0
B-41	B-1962	1	1832	1273	11.1	76.5	1100	866	144	160	1.078	26.7
B-42A	B-1962	1	1832	1273	4.0	27.5	1350	1005	170	186	1.015	31.2
B-42B	B-1962	1/4	1832	1273	4.0	27.5	1350	1005	2070	1775	0.892	33.1
B-45	60249	0.1	2290	1528	4.0	27.5	1350	1005	***	69.6	0.002	***
B-45B	60249	0.1	2290	1528	8.0	55.0	1350	1005	520	1800	1.823	32.0
B-46	60249	0.1	2290	1528	6.5	44.8	1350	1005	5600*	155.8	0.215	34.0
B-47++	60249	0.1	2290	1528	16 PSI/HOUR		1350	1005	544	548.3	1.050	--
B-47A	60249	-	--	--	8.0	55.0	1350	1005	714	907	1.190	32.3
B-48A+	60249	0.1	2290	1528	6.5	44.8	1450	1061	252	2371	2.885	33.2

*Exptrapolated
***Insufficient creep to extrapolate
+welded
++Linearly increasing stress

TABLE II-14. Summary of Pure Ta Ultra-High Vacuum Creep Test Results

Test No.	Heat No.	Heat Treatment Time Hours	Heat Treatment Temperature °F	Heat Treatment Temperature °K	Stress KSI	Stress MN/M²	Test Temperature °F	Test Temperature °K	1% Creep Life Hours	Termination of Test Time, Hours	Termination of Test Percent Creep	1% Creep Larson-Miller Parameter $T_{\circ R}$ (15+logt) x10⁻³
B-48B+	60249	-	--	--	7.5	52.3	1450	1061	150	1177.2	3.212	32.8
B-49	60249	0.1	2290	1528	6.5	44.8	1450	1061	92	2175.4	3.372	32.4
B-49A	60249	-	--	--	7.5	52.3	1450	1061	180	1363.9	3.282	33.0
B-49B	60249	-	--	--	9.0	62.1	1450	1061	24	497.8	5.698	31.3
B-51	60379	0.1	2290	1528	6.5	44.8	1350	1005	26	2712.0	4.412	29.8
B-52	60065	0.1	2290	1528	6.5	44.8	1350	1005	17,000*	2062	0.115	34.8
B-53	60381	0.1	2290	1528	6.5	44.8	1350	1005	12,000*	6930.9	0.858	34.5
P-2	818072	++	++	++	6.5	44.8	1350	1005	1.6	649.7	4.685	27.5
P-3	B-1960	++	++	++	6.5	44.8	1350	1005	60	6096.2	3.168	30.4
P-4	B-1960	++	++	++	6.5	44.8	1350	1005	30	5689.4	4.230	29.8
P-5	B-1960	++	++	++	6.5	44.8	1350	1005	110,000*	4900.5	0.155	36.3

*Extrapolated
**Pre-strained 30% in tension prior to testing
+Welded
++Not available

TABLE II-15. Summary of Ta-10W Ultra-High Vacuum Creep Test Results

Test No.	Heat No.	Heat Treatment Time Hours	Heat Treatment Temperature °F	Heat Treatment Temperature °K	Stress KSI	Stress MN/M²	Test Temperature °F	Test Temperature °K	1% Creep Life Hours	Termination of Test Time, Hours	Termination of Test Percent Creep	1% Creep Larson-Miller Parameter $T_{\bullet_R}$ (15+logt) x10⁻³
S-58A	630002	1	3000	1922	20	38.0	2100	1422	285	308	1.125	44.7
S-58B	630002	1/4	3000	1922	11.5	79.3	2210	1483	770*	410	0.572	47.7
S-58C	630002	1/4	3000	1922	6.2	42.7	2320	1544	2200*	700	0.330	51.0
S-58D	630002	1/4	3000	1922	3.5	24.1	2430	1605	10,200*	1290	0.202	54.9
S-64	630002	1	3000	1922	16	111.0	2000	1366	250	266	1.060	42.8
S-66	630002	1	3000	1922	16	111.0	2000	1366	135	550	5.150	42.1
S-67	630002	1	3000	1922	12	82.9	2000	1366	5227	6098	1.270	46.0

*Extrapolated

TABLE II-16. Summary of T-111 Linearly Decreasing Temperature Ultra-High Vacuum Creep Test Results

Test No.	Heat No.	Heat Treatment Time Hours	Heat Treatment Temperature °F	Heat Treatment Temperature °K	Stress KSI	Stress MN/M²	Starting Test Temperature °F	Starting Test Temperature °K	1% Creep Life Hours	Termination of Test Time, Hours	Termination of Test Percent Creep	Rate of Temperature Decrease F°/hr
S-65	65079	1	3000	1922	7	48.2	2400	1589	--	1850	0.105	0.6
S-72	650028	1	3000	1922	7	48.2	2400	1589	370	1322.1	1.282	0.3
S-82	650028	1	3000	1922	31	214.0	1900	1311	235	2013.8	1.180	0.5

TABLE II-17. Summary of T-111 Exponentially Varying Stress and Temperature Ultra-High Vacuum Creep Test Results

Test No.	Heat No.	Heat Treatment Time Hours	Heat Treatment Temperature °F	Heat Treatment Temperature °K	Stress Level (Dimensionless)	Starting Temperature °F	Starting Temperature °K	Half Life (Hours)	Stall* Strain Percent	Termination of Test Time, Hours	Termination of Test Percent Creep
S-130	650028	1	3000	1922	.65	2800	1811	100	0.271	166.5	-0.220
S-133	650028	1	3000	1922	.65	2800	1811	170	0.610	173.6	0.318
S-137	650028	1	3000	1922	.65	2800	1811	400	1.327	310.0	1.145
S-140	650028	1	3000	1922	.65	2600	1700	400	0.209	454.0	-0.112
S-151	650028	1	3000	1922	.65	2600	1700	1000	0.643	1030.0	0.380
S-153	650028	1	3000	1922	.65	2600	1700	2000	0.987	3571.0	0.560
S-110	650028	1	3000	1922	1.0	2600	1700	100	1.195	192.2	0.795
S-111	650028	1	3000	1922	1.0	2600	1700	170	1.464	333.0	1.060
S-109	650028	1	3000	1922	1.0	2600	1700	400	3.012	600.0	2.702
S-145	650028	1	3000	1922	1.0	2400	1589	400	1.719	653.4	1.445
S-152	650028	1	3000	1922	1.0	2400	1589	1000	2.484	1507.9	3.210
S-154	650028	1	3000	1922	1.0	2400	1589	2000	5.177	3940.0	6.135

* Adjusted for Elastic Strain at Stall

TABLE II-18. Summary of Ultra-High Vacuum Creep Test Results on T-111 Heat 650050 Annealed 1 Hour at 3000°F (1922°K) Plus 1 Hour 2400°F (1589°K) and Exposed for Various Times and Temperatures to Liquid Lithium or to 10^{-9} TORR Vacuum in G. E. Alkali Metal Exposure Program.

Test No.	G.E. Specimen No.	Environment	Exposure Time Hours	Exposure Temperature °F	Exposure Temperature °K	Stress KSI	Stress MN/M²	Test Temperature °F	Test Temperature °K	1% Creep Life Hours	Termination of Test Time, Hours	Termination of Test Percent Creep	1% Creep Larson-Miller Parameter ($T_{\circ R}$ (15+logt) x10^{-3}
S-166	04-62	VACUUM	1000	1800	1255	50	344.0	1650	1172	4	48+	30.0*	32.9
			4000	1900	1310								
S-158	04-59	VACUUM	1000	1800	1255	35	241.0	1800	1255	10	185	7.205	36.2
			4000	1900	1310								
S-159	04-60	VACUUM	1000	1800	1255	24	165.0	2000	1366	55	585	5.400	41.2
			4000	1900	1310								
S-172	04-64	VACUUM	1000	1800	1255	16	110.0	2000	1366	2780	4242	1.780	45.4
			4000	1900	1310								
S-165	04-61	VACUUM	1000	1800	1255	16	110.0	2200	1478	155	548	6.280	45.7
			4000	1900	1310								
S-171	04-63	VACUUM	1000	1800	1255	10.5	72.3	2200	1478	1475	2712	2.375	48.3
			4000	1900	1310								
S-184	04-65	VACUUM	1000	1800	1255	5	34.4	2400	1589	570	965	1.895	50.8
			4000	1900	1310								

+ Rupture Time
* Rupture Elongation

TABLE II-18. Summary of Ultra-High Vacuum Creep Test Results on T-111 Heat 650050 Annealed 1 Hour at 3000°F (1922°K) Plus 1 Hour 2400°F (1589°K) and Exposed for Various Times and Temperatures to Liquid Lithium or to 10^{-9} TORR Vacuum in G. E. Alkali Metal Exposure Program.

Test No.	G.E. Specimen No.	Environment	Exposure Time Hours	Exposure Temperature °F	Exposure Temperature °K	Stress KSI	Stress MN/M²	Test Temperature °F	Test Temperature °K	1% Creep Life Hours	Termination of Test Time, Hours	Termination of Test Percent Creep	1% Creep Larson-Miller Parameter (T_R (15+logt) x 1^{-3}
S-161	04-18	LITHIUM	1000	1800	1255	50	344.0	1650	1172	2	34+	26.6*	32.3
			4000	1900	1310								
S-167	04-19	LITHIUM	1000	1800	1255	35	241.0	1800	1255	5	49	6.085	35.5
			4000	1900	1310								
S-168	04-20	LITHIUM	1000	1800	1255	24	165.0	2000	1366	10	187	5.300	39.4
			4000	1900	1310								
S-179	04-23	LITHIUM	1000	1800	1255	16	110.0	2000	1366	1530	5873	5.410	44.7
			4000	1900	1310								
S-169	04-21	LITHIUM	1000	1800	1255	16	110.0	2200	1478	73	313	4.880	44.9
			4000	1900	1310								
S-170	04-22	LITHIUM	1000	1800	1255	10.5	72.3	2200	1478	732	2017	3.095	47.5
			4000	1900	1310								
S-182	04-24	LITHIUM	1000	1800	1255	5	34.4	2400	1589	463	1344	2.740	50.5
			4000	1900	1310								

+ Rupture Time
* Rupture Elongation

TABLE II-18. Summary of Ultra-High Vacuum Creep Test Results on T-111 Heat 650050 Annealed 1 Hour at 3000°F (1922°K) Plus 1 Hour 2400°F (1589°K) and Exposed for Various Times and Temperatures to Liquid Lithium or to 10^{-9} TORR Vacuum in G. E. Alkali Metal Exposure Program.

Test No.	G.E. Specimen No.	Environment	Exposure Time Hours	Exposure Temperature °F	Exposure Temperature °K	Stress KSI	Stress MN/M²	Test Temperature °F	Test Temperature °K	1% Creep Life Hours	Termination of Test Time, Hours	Termination of Test Percent Creep	1% Creep Larson-Miller Parameter ($T_{°R}$ (15+logt) x 1^{-3}
S-122	04-36	VACUUM	1000	2400	1589	50	344.0	1650	1172	1278	1886+	27.0*	38.2
S-121	04-37	VACUUM	1000	2400	1589	40	276.0	1650	1172	4500	4823	1.380	39.4
S-200	04-42	VACUUM	1000	2400	1589	35	241.0	1800	1255	465	889	7.935	39.9
S-209	04-43	VACUUM	1000	2400	1589	24	165.0	2000	1366	215	1009	10.040	42.6
S-124	04-41	VACUUM	1000	2400	1589	16	110.0	2000	1366	7532	8731	1.260	46.4
S-132	04-33	VACUUM	1000	2400	1589	16	110.0	2200	1478	546	673	1.490	47.2
S-201	04-2	LITHIUM	1000	2400	1589	50	344.0	1650	1172	448	700+	17.9*	37.2
S-206	01-1	LITHIUM	1000	2400	1589	35	241.0	1800	1255	323	650	10.095	39.6
S-208	01-3	LITHIUM	1000	2400	1589	24	165.0	2000	1366	91	435	8.240	41.7
S-127	04-1	LITHIUM	1000	2400	1589	16	110.0	2200	1478	440	505	1.290	46.9
S-205	01-16	VACUUM	1000	1800	1255	50	344.0	1650	1172	262	420+	25.8*	36.8
S-190	01-15	VACUUM	1000	1800	1255	35	241.0	1800	1255	227	571	13.025	39.2
S-173	01-14	VACUUM	1000	1800	1255	24	165.0	2000	1366	123	577	9.015	42.0
S-199	04-38	VACUUM	1000	1800	1255	16	110.0	2200	1478	429	1252	8.415	46.9

+ Rupture Time
* Rupture Elongation

TABLE II-18. Summary of Ultra-High Vacuum Creep Test Results on T-111 Heat 650050 Annealed 1 Hour at 3000°F (1922°K) Plus 1 Hour 2400°F (1589°K) and Exposed for Various Times and Temperatures to Liquid Lithium or to 10^{-9} TORR Vacuum in G. E. Alkali Metal Exposure Program.

Test No.	G.E. Specimen No.	Exposure Environment	Exposure Time Hours	Exposure Temperature °F	Exposure Temperature °K	Stress KSI	Stress MN/M²	Test Temperature °F	Test Temperature °K	1% Creep Life Hours	Termination of Test Time, Hours	Termination of Test Percent Creep	1% Creep Larson-Miller Parameter ($T_{\bullet_R}$ (15+logt) x 1^{-3}
S-196	04-31	LITHIUM	1000	1800	1255	50	344.0	1650	1172	43	165+	25.3*	35.1
S-189	01-10	LITHIUM	1000	1800	1255	35	241.0	1800	1255	87	379	9.750	38.3
S-178	04-27	LITHIUM	1000	1800	1255	24	165.0	2000	1366	65	559	9.310	41.4
S-207	04-25	LITHIUM	1000	1800	1255	16	110.0	2200	1478	110	554	9.770	45.3

+ Rupture Time
* Rupture Elongation

TABLE II-18. Summary of Ultra-High Vacuum Creep Test Results on T-111 Heat 650050 Annealed 1 Hour at 3000°F (1922°K) Plus 1 Hour 2400°F (1589°K) and Exposed for Various Times and Temperatures to Liquid Lithium or to 10^{-9} TORR Vacuum in G. E. Alkali Metal Exposure Program.

Test No.	G.E. Specimen No.	Exposure Environment	Exposure Time Hours	Exposure Temperature °F	Exposure Temperature °K	Stress KSI	Stress MN/M²	Test Temperature °F	Test Temperature °K	1% Creep Life Hours	Termination of Test Time, Hours	Termination of Test Percent Creep	1% Creep Larson-Miller Parameter ($T_{°R}$ (15+logt) x 1^{-3}
S-141	04-49	VACUUM	5000	2400	1589	50	344.0	1650	1172	340	655+	13.8*	37.0
S-146	04-50	VACUUM	5000	2400	1589	35	241.0	1800	1255	745	906	1.705	40.4
S-148	04-51	VACUUM	5000	2400	1589	24	165.0	2000	1366	205	673	4.430	42.6
S-139	04-48	VACUUM	5000	2400	1589	16	110.0	2200	1478	885	1275	2.265	47.7
S-156	04-12	LITHIUM	5000	2400	1589	50	344.0	1650	1172	180	204+	19.6*	36.4
S-149	04-10	LITHIUM	5000	2400	1589	35	241.0	1800	1255	350	507	3.525	39.6
S-155	04-11	LITHIUM	5000	2400	1589	24	165.0	2000	1366	200	692	6.550	42.6
S-157	04-13	LITHIUM	5000	2400	1589	16	110.0	2200	1478	1100	2971	7.945	48.0

+Rupture Time
*Rupture Elongation

TABLE II-18. Summary of Ultra-High Vacuum Creep Test Results on T-111 Heat 650050 Annealed 1 Hour at 3000°F (1922°K) Plus 1 Hour 2400°F (1589°K) and Exposed for Various Times and Temperatures to Liquid Lithium or to 10^{-9} TORR Vacuum in G. E. Alkali Metal Exposure Program.

Test No.	G.E. Specimen No.	Exposure Environment	Exposure Time Hours	Exposure Temperature °F	Exposure Temperature °K	Stress KSI	Stress MN/M²	Test Temperature °F	Test Temperature °K	1% Creep Life Hours	Termination of Test Time, Hours	Termination of Test Percent Creep	1% Creep Larson-Miller Parameter ($T_{°R}$ (15+logt) x10^{-3}
S-186	PRE-EXPOSURE				50	344.0	1650	1172	938	1242+	20.8*	37.9
S-162	PRE-EXPOSURE				35	241.0	1800	1255	528	811	4.220	40.1
S-163	PRE-EXPOSURE				24	165.0	2000	1366	410	457	1.195	43.3
S-164	PRE-EXPOSURE				16	110.0	2200	1478	435	1193	6.710	46.9
S-187	PRE-EXPOSURE				10.5	72.3	2200	1478	2330	4361	3.320	48.9
S-181	PRE-EXPOSURE				5	34.4	2400	1589	600	1177	2.025	50.8

+ Rupture Time
* Rupture Elongation

1. Report No.	2. Government Accession No.	3. Recipient's Catalog No.
NASA-CR-134481		

4. Title and Subtitle	5. Report Date
GENERATION OF LONG TIME CREEP DATA ON REFRACTORY ALLOYS AT ELEVATED TEMPERATURES	September 1973
	6. Performing Organization Code
7. Author(s)	8. Performing Organization Report No.
K. D. Sheffler and R. R. Ebert	TRW-ER-7648
	10. Work Unit No.
9. Performing Organization Name and Address	11. Contract or Grant No.
TRW Inc. Materials Technology Laboratory 23555 Euclid Avenue Cleveland, Ohio 44117	NAS-3-15554
	13. Type of Report and Period Covered
12. Sponsoring Agency Name and Address	Contractor Report (Final)
National Aeronautics and Space Administration Washington, D.C. 20546	14. Sponsoring Agency Code

15. Supplementary Notes

Project Managers, P. E. Moorhead and R. H. Titran - Materials and Structures Division
NASA Lewis Research Center
Cleveland, Ohio 44135

16. Abstract

Four separate studies of various aspects of the vacuum creep behavior of two tantalum alloys (T-111 and ASTAR 811C) and of pure CVD tungsten are reported. The first part of the program involved a study of the influence of high temperature pre-exposure to vacuum or to liquid lithium on the subsequent creep behavior T-111 alloy. Results of this study revealed significant effects of pre-exposure on the 1% creep life of T-111, with life reductions of about 3 orders of magnitude being observed in extreme cases. These effects are interpreted in terms of variations in the grain size and residual oxygen in solid solution caused by the exposures. The second part of this study involved an investigation of the creep behavior of T-111 under conditions of continuously increasing stress and decreasing temperature which simulated the conditions anticipated in radioisotope capsule service. Results of this study showed that such test conditions produced a creep curve having a very unusual shape, and led to the identification of a new creep design parameter for this type of service. Methods were also investigated for the prediction of long time variable stress and temperature creep behavior from short time results. The third area of investigation was a study of the influence of heat treatment on the microstructure and creep behavior of ASTAR 811C. Results of this study established tentative design data for ASTAR 811C annealed for 1/2 hour at 3600°F (2255°K) and for 1 hour at 3000°F (1922°K) and led to a hypothesis concerning the role of the carbide in strengthening this alloy. A third heat treatment cycle, 100 hours at 3000°F (1922°K) was defined for this alloy which maximized the advantages and minimized the disadvantages associated with the other two treatments. The fourth part of the program was directed toward a preliminary characterization of the 1% creep life of CVD tungsten as obtained from two different sources. The creep data obtained in this study was insufficient to define a significant difference between materials from these two sources.

17. Key Words (Suggested by Author(s))		18. Distribution Statement
Creep	Tungsten	Unclassified - Unlimited
Microstructures	Tantalum	
Vacuum	T-111	
Lithium	ASTAR 811C	
Radioisotope Capsule		

19. Security Classif. (of this report)	20. Security Classif. (of this page)	21. No. of Pages	22. Price*
Unclassified	Unclassified		

* For sale by the National Technical Information Service, Springfield, Virginia 22151